

AMERICAN UNIVERSITY OF BEIRUT

TIME-DEPENDENT AND POST-ELEVATED
TEMPERATURE PERFORMANCE OF WELDED STEEL
CONNECTIONS SUBJECTED TO FIRE

by
AHMAD HOUSNI EL GHOR

A dissertation
submitted in partial fulfillment of the requirements
for the degree of Doctor of Philosophy
to the Department of Civil and Environmental Engineering
of Maroun Semaan Faculty of Engineering and Architecture
at the American University of Beirut

Beirut, Lebanon
April 2021

AMERICAN UNIVERSITY OF BEIRUT

TIME-DEPENDENT AND POST-ELEVATED
TEMPERATURE PERFORMANCE OF WELDED STEEL
CONNECTIONS SUBJECTED TO FIRE

by
AHMAD HOUSNI EL GHOR

Approved by:

Elie G. Hantouche

Dr. Elie G. Hantouche, Associate Professor
Department of Civil and Environmental Engineering

Advisor

Mounir Mabsout

Dr. Mounir E. Mabsout, Professor
Department of Civil and Environmental Engineering

Chair of Committee

George Saad

Dr. George A. Saad, Associate Professor
Department of Civil and Environmental Engineering

Member of Committee

Adnan Masri

Dr. Adnan C. Masri, Professor
Department of Civil and Environmental Engineering
Beirut Arab University (BAU)

Member of Committee

Michael D. Engelhardt

Dr. Michael D. Engelhardt, Professor
Department of Civil and Environmental Engineering
The University of Texas at Austin (UT-Austin)

Member of Committee

Date of dissertation defense: April 6, 2021


AMERICAN UNIVERSITY OF BEIRUT

DISSERTATION RELEASE FORM

Student Name: EL Ghor Ahmad Housni
Last First Middle

I authorize the American University of Beirut, to: (a) reproduce hard or electronic copies of my dissertation; (b) include such copies in the archives and digital repositories of the University; and (c) make freely available such copies to third parties for research or educational purposes:

- As of the date of submission
- One year from the date of submission of my dissertation.
- Two years from the date of submission of my dissertation.
- Three years from the date of submission of my dissertation.

Signature  Date April, 29, 2021

ACKNOWLEDGEMENTS

I do not believe any expression of gratitude is fit enough to describe my appreciation for all the support, patience, guidance, education, and all time I was granted from my advisor Dr. Elie G. Hantouche. His expertise and dedication were essential in the successful development of this research work. I appreciate his constant support and valuable critics which helped me develop my research skills, and knowledge throughout the time spent at the American University of Beirut.

My recognition and gratitude are also extended to Dr. Mounir E. Mabsout (Chair-AUB), Dr. George A. Saad (AUB), Dr. Adnan C. Masri (BAU), and Dr. Michael D. Engelhardt (UT-Austin) for serving on my dissertation committee.

I would like to thank Dr. Michael D. Engelhardt for giving me the outstanding opportunity to perform part of my PhD experimental work at the Ferguson Structural Engineering Laboratory at the University of Texas at Austin. Also, I would like to thank Dr. Mohamad Ali Morovat, an associate at Thornton Tomasetti, for his valuable efforts, time, and helpful discussions throughout our collaborative research work.

Special thanks are also for the lab managers and technical staffs at Riad Kamal Structural Engineering Laboratory at AUB and Ferguson Structural Engineering Laboratory-UT Austin for their extensive assistance in the experimental testing programs.

Furthermore, I would like to gratefully acknowledge the financial support provided by the American University of Beirut Research Board under grant No.103604-24705. Also, I would like to thank the National Council for Scientific Research in Lebanon and the American University of Beirut, CNRS-L/AUB, PhD award program 2019-2020 for the support of my PhD studies.

Finally, I would like to express gratitude to my family, friends and Dr. Adnan C. Masri (BAU) for their constant and endless support in the pursuit of my degree. Thank you all for being part of my life and it is a great honor to be part of yours.

ABSTRACT OF THE DISSERTATION OF

Ahmad Housni El Ghor

for

Doctor of Philosophy

Major: Civil and Environmental Engineering

Title: Time-Dependent and Post-Elevated Temperature Performance of Welded Steel Connections Subjected to Fire

The objective of this research work is to investigate the time-dependent and the post-elevated temperature behavior of welded lap joints under elevated temperatures. Weld is a metal joining material that is commonly used in steel connections and can affect their governing failure modes during fire and post-fire events. Despite their importance, very limited studies are conducted to examine the time-dependent or the creep behavior of welds and welded connections subjected to elevated temperatures. To address this issue, an experimental program is first conducted to examine the implicit and explicit time-dependent thermal creep behavior of weld material in transverse welded lap joints. In order to investigate implicitly the creep behavior of transverse welded lap joints in fire, two different loading rate scenarios (fast and slow) are used. Peak loads and retention factors for the weld material under both fast and slow loading rates are computed for all temperatures. However, for the explicit time-dependent behavior, the transverse welded lap joints are subjected to a constant load at a specific temperature for 120 min or until failure. Critical times, loads, and temperatures at which weld material fails due to creep are examined. Then, the creep curves resulted from the experimental tests are used to develop a *Norton-Bailey* creep power law equation for the welded lap joints. Then, two creep models for the welds and steel base material are proposed by introducing temperature-dependent scaling factors to the creep power law equation of the welded lap joints. Further, the two creep models are then used in the material properties of the welded lap joint in ABAQUS and then calibrated in order to predict with reasonable accuracy the experimental results. Also, another experimental program is conducted to investigate the effect of load angles on the thermal behavior of welds in welded lap joints while considering different loading rates. The lap joints used in this analysis are classified as longitudinal, inclined, and transverse where the angle between the axis of the fillet weld and the direction of the applied load is 0°, 45°, and 90°, respectively. Retention factors for the weld material under different loading rate scenarios and load

angles are calculated and compared with those available in the literature. Finally, the post-fire behavior of welded specimens subjected to different load angles is also studied experimentally. More specifically, in the post-fire analysis, the test specimen is heated up to a target temperature and then cooled back to ambient and then loaded until failure. The results of this analysis are presented as residual strength capacities for the weld material after being exposed to elevated temperatures. Effect of load angles on the ductility of weld material under time-dependent thermal conditions and post-fire analysis are also studied and presented. Design equations that consider the rate-dependent and post-fire effects on fillet welds subjected to different loading angles are also provided. This research work will help providing deep understanding into the influence of different major parameters that affect the behavior of weld material in fire and post-fire conditions. Consequently, considering these parameters can provide essential data that will be intended to support the development of design guidelines of welded connections for structural-fire engineering application.

TABLE OF CONTENTS

ACKNOWLEDGEMENTS	1
ABSTRACT	2
ILLUSTRATIONS	7
TABLES	11
I. INTRODUCTION AND LITRATURE REVIEW	13
A. Introduction.....	13
B. Literature Review.....	17
II. GOALS AND OBJECTIVES.....	25
III. IMPLICIT AND EXPLICIT CREEP BEHAVIOR OF TRANSVERSE WELDED LAP JOINTS AS EXPOSED TO ELEVATED TEMPERATURES.....	30
A. Experimental Program	30
1. Test Specimens	30
2. Test Procedure	31
B. Implicit Thermal Creep Behavior of Transverse Welded Lap Joints	33
1. Loading Protocol.....	33
2. Experimental Tests Observations	34
3. Effect of Temperature on Load-Deformation Response.....	40
4. Effect of Loading Rates on Load-Deflection Response	44
5. Effect of Loading Rate and Temperature on the Ductility of the Transverse Welded Lap Joint	48

6. Retention Factors	50
C. Explicit Thermal Creep Behavior of Transverse Welded Lap Joints	53
1. Load Protocol.....	53
2. Experimental Tests Observation	54
3. Effect of Thermal Creep on Transverse Welded Lap Joint	56
4. Effect of Temperature on Load-Deformation Response.....	58
5. Connection Creep Curve Response	61
6. Isochronous Behavior of Transverse Welded Lap Joint.....	63
IV. CREEP MODELING OF TRANSVERSE WELDED LAP JOINTS EXPOSED TO FIRE TEMPERATURES	66
A. Methodology	66
B. Proposed Creep Model.....	67
1. Power Law Equation Constant Estimation	67
2. Power Law Regression Application	69
C. FE Modeling.....	76
1. Boundary Conditions	77
2. Model Discretization.....	77
3. Material Properties and Modeling Considerations	78
4. Creep Modeling	78
5. Creep Models Calibration.....	81
6. FE Results	82
V. EXPERIMENTAL INVESTIGATION ON THE EFFECT OF LOAD ANGLES ON WELD BEHAVIOR AT ELEVATED AND POST-ELEVATED TEMPERATURE CONDITIONS	90
A. Experimental Program	90
1. Test Specimens	90
2. Setup and Instrumentation	92

B. Rate-dependent Thermal Behavior of Fillet Welds Subjected to Various Load Angles	94
1. Load Protocol.....	94
2. Experimental Test Observation	96
3. Effect of Temperatures on the Fillet Weld Behavior.....	104
4. Effect of Loading Rate and Load Angle on the Fillet Weld Behavior	106
5. Effect of Loading Rate on the Fillet Weld Orientation	110
6. Effect of Loading Rate, Angles, and Temperature on the Ductility of Welded Lap Joints.....	111
7. Retention Factors	114
8. Fire Design Equation for Weld Material	116
C. Post-Elevated Temperature Tests.....	118
1. Load Protocol.....	118
2. Experimental Test Observations.....	121
3. Residual Load-Displacement Response.....	125
4. Effect of Load Angle on the Residual Behavior of Fillet Welds.....	129
5. Residual Ductility of the Welded Lap Joints	132
6. Residual Response of the Weld Material versus the Steel Base Material	135
VI. SUMMARY AND CONCLUSIONS	137
VII. SIGNIFICANCE, LIMITATIONS, AND FUTURE WORK	143
A. Significance.....	143
B. Limitations	144
C. Future Work	145
BIBLIOGRAPHY	148

ILLUSTRATIONS

Figure

1. Classical creep curve	16
2. Eurocode 3 retention factors for fillet weld [10]	18
3. Transverse welded lap joints configuration	31
4. Experimental test equipment	32
5. Thermocouples and foils implementation.....	33
6. Failure at the throat of the weld for all test specimens at ambient and elevated temperatures: (a) Fast tests (0.254 mm/min), (b) Slow tests (0.0254 mm/min).....	36
7. Failure modes for welded specimens subjected to fast and slow loading rates at: (a) 20 °C, (b) 400 °C, (c) 425 °C, (d) 450 °C, (e) 475 °C	37
8. Failure modes for welded specimens subjected to fast and slow loading rates at: (a) 500 °C, (b) 550 °C, (c) 600 °C, (d) 650 °C, (e) 700 °C	38
9. Fracture surface at the weld region for the welded specimens at: (a) 400 °C, (b) 425 °C, (c) 450 °C, (d) 475 °C, (e) 500 °C.....	39
10. Fracture surface at the weld region for the welded specimens at: (a) 550 °C, (b) 600 °C, (c) 650 °C, (d) 700 °C.....	40
11. Force-displacement characteristics of transverse welded lap joints at ambient and elevated temperatures under: (a) Fast loading rate scenario, (b) Slow loading rate scenario	42
12. Force-displacement characteristics of transverse welded lap joints at temperatures ranging between 400°C and 500°C under: (a) Fast loading rate scenario, (b) Slow loading rate scenario	43
13. Effect of loading rate on the behavior of transverse welded lap joints at: (a) 20 °C, (b) 400°C, (c) 425°C, (d) 450°C	45
14. Effect of loading rate on the behavior of transverse welded lap joints at: (a) 475°C (b) 500°C, (c) 550°C, (d) 600°C, (e) 650°C, (f) 700°C	46
15. . Results from tests performed at 500 °C and 600 °C under fast and slow loading rates	48
16. Normalized ductility verses temperature under fast and slow loading rates	50
17. Retention factors for weld specimens	52
18. Time-dependent deformation or failure for transverse welded lap joints at: (a) Temperatures below 475 °C, (b) 500 °C, (c) 600 °C, (d) 700 °C.....	55

19. Creep fracture at the throat of the weld for transverse welded lap joints subjected to 0.90P at: (a) 475 °C, (b) 500 °C, (c) 600 °C, (d) 700 °C	56
20. Effect of peak load ratio on thermal creep response of transverse welded lap joints at: (a) 500 °C, (b) 600 °C, (c) 700 °C	58
21. Effect of temperature on thermal creep response of transverse welded lap joints.	60
22. Creep curves at different load and temperature conditions	62
23. Isochronous axial load-creep displacement curves for transverse welded lap joint at 600°C	64
24. Isochronous creep displacement-temperature response at 0.50P.....	65
25. Assumptions used for creep model of the transverse welded lap joint	70
26. Creep model versus experimental results at: (a) 400°C, (b) 450 °C, (c) 475 °C	73
27. Creep model versus experimental results at 500°C for: (a) 0.50P, (b) 0.80P, (c) 0.90P	74
28. . Creep model versus experimental results at 600°C for: (a) 0.50P, (b) 0.60P, (c) 0.75P, (d) 0.90P	75
29. Creep model versus experimental results at 700°C for: (a) 0.50P, (b) 0.60P, (c) 0.75P, (d) 0.90P	76
30. Transverse welded lap joint model used in ABAQUS [42] simulations	78
31. FE results versus experimental results for the fast tests	83
32. FE versus experimental failure mode for fast test analysis at: (a) 500°C (b) 700°C	84
33. Time-dependent results for FE and creep models versus experimental results for: (a) 400°C, (b) 450 °C, (c) 475 °C	86
34. Time-dependent results for FE and creep models versus experimental results at 500°C for: (a) 0.50P, (b) 0.80P, (c) 0.90P	87
35. Time-dependent results for FE and creep models versus experimental results at 600°C for: (a) 0.50P, (b) 0.60P, (c) 0.75P, (d) 0.90P	88
36. Time-dependent results for FE and creep models versus experimental results at 700°C for: (a) 0.50P, (b) 0.60P, (c) 0.75P, (d) 0.90P	89
37. Welded lap joints configuration: (a) Transverse, (b) Inclined, (c) Longitudinal	91
38. Welded lap joint specimens	92

39. Tinius-Olsen Universal Testing Machine coupled with the electric furnace.....	93
40. Thermocouple implementation for elevated temperature tests: (a) Transverse (90°), (b) Inclined (45°), (c) Longitudinal (0°).....	93
41. Thermocouple implementation for post-fire analysis: (a) Transverse (90°), (b) Inclined (45°), (c) Longitudinal (0°).....	94
42. Failure at the throat of the weld for all test specimens at ambient and elevated temperatures: (a) Transverse-fast tests, (b) Transverse-slow tests, (c) Inclined-fast tests, (d) Inclined-slow tests, (e) Longitudinal-fast tests, (f) Longitudinal-slow tests.....	97
43. Failure modes for the transverse welded lap joints subjected to fast and slow loading rates	98
44. Failure modes for the inclined welded lap joints subjected to fast and slow loading rates	99
45. Irregular fracture mode for the inclined welded lap joints subjected to fast and slow loading rates	100
46. Failure modes for the longitudinal welded lap joints subjected to fast and slow loading rates	102
47. Excessive deformation for the longitudinal welded lap joints at 700°C: (a) Fast loading rate, (b) Slow loading rate.....	102
48. Fracture surfaces: Texture and color for the welded configuration at ambient and elevated temperatures	104
49. Axial load-displacement characteristics of the welded lap joints at ambient and elevated temperatures: (a) Transverse-fast tests, (b) Transverse-slow tests, (c) Inclined-fast tests, (d) Inclined-slow tests, (e) Longitudinal-fast tests, (f) Longitudinal-slow tests.....	105
50. Effect of loading rate on the behavior of the welded lap joints at: (a) 20°C, (b) 400°C, (c) 500°C, (d) 600°C, (e) 700°C.....	108
51. Effect of loading rate on fillet weld orientation.....	111
52. Effect of temperature on the normalized ductility of weld materials under fast and slow loading rates.....	113
53. Retention factors for the three different welded lap joint configurations.....	115
54. Slow to fast loading rate capacity ratio versus temperature	117
55. Strength capacity model calculation versus temperature.....	118
56. Tinius-Olsen Universal Testing Machine coupled with the electric furnace: The cooling phase	119

57. Temperature profile for post-fire temperature profile	120
58. Failure at the throat of the weld for all test specimens at ambient and post-elevated temperatures: (a) Transverse (b) Inclined, (c) Longitudinal	122
59. Failure modes for the transverse welded lap joints after exposed to elevated temperatures.....	123
60. Failure modes for the inclined welded lap joints after exposed to elevated temperatures.....	124
61. Failure modes for the longitudinal welded lap joints after exposed to elevated temperatures.....	125
62. Residual load-displacement response of welded lap joint: (a) Transverse, (b) inclined, (c) Longitudinal	126
63. Percentage decrease for the three welded lap joints after exposed to elevated temperatures.....	128
64. Residual load-displacement response of the three welded lap joint after exposed to elevated temperatures	130
65. Load angle effectiveness ratio versus post-temperature	132
66. Post-fire normalized ductility of fillet weld after subjected to different load angles	134
67. Residual peak load agianst post-fire normalized ductility	134
68. Residual behavior of fillet material versus steel base material: (a) Normalized residual strength, (b) Ultimate residual strength	136

TABLES

Table

1. Test matrix of transverse welded lap joints at ambient and elevated temperatures	34
2. Effect of loading rate on the strength capacity of transverse welded lap joints under ambient and elevated temperatures.....	47
3. Retention factors estimated for transverse welded lap joints at ambient and elevated temperatures	51
4. Test matrix for creep tests at elevated temperatures.....	54
5. Test matrix of creep tests conducted on transverse welded lap joints at elevated temperatures	60
6. Power law creep constants for the transverse welded lap joint	71
7. Calibrated power law creep constants for the fillet weld material	82
8. Calibrated power law creep constants for the steel base material	82
9. Test matrix of the welded lap joints subjected to different load angles and rates	95
10. Retention factors for the strength of fillet welds exposed to elevated temperatures and their percentage decrease in capacities due effect of loading rate	109
11. Test matrix of the welded lap joints after exposed to fire temperatures.....	120
12. Weld strength reduction after exposed to elevated temperatures	128

*“Allah Himself bears witness that there is no God but He;
and likewise do the angels and the men possessed of knowledge
bear witness in truth and justice that there is no God but He,
the All-Mighty, the All-Wise.”*

(18-Al Imran-Quran)

To the memory of my beloved Father, Housni El Ghor
To my beloved Mother and Sister, Inaya and Sara El Ghor
To Whom Else It May Concern

CHAPTER I

INTRODUCTION AND LITRATURE REVIEW

A. Introduction

The current building fire safety regulations and codes in the U.S. follow the *prescriptive* approach. In this approach, engineers or architects rely on codes to determine the fire-resistance rating in order to meet the required fire protection on the structural components of the building. This fire design approach is performed either through standard fire tests on the individual building components or empirical approaches [1]. That is, this approach cannot predict accurately the structural performance of the entire structure when subjected to fire. Following the *World Trade Center collapse in 2001*, prescriptive approach has been further studied by many professionals, calling for a change to performance-based fire-resistance design and for the structural engineers to take over the responsibility of the fire-resistance design of the structure through conducting fire analysis [1, 2]. However, many reports [3, 4, 5, 6] have indicated that performance-based fire design codes requires several key elements that are not fully developed or understood. These key elements mainly include better understanding of materials performance in case of fire and a development of advanced engineering tools for alternative fire protection design. Therefore, the performance-based fire design is an alternative approach that permits engineers to design accurately for the structural and thermal responses of steel structures when exposed to wide range of fire temperatures.

Welded connections are commonly used in steel structures and play a crucial role in transferring the loads between connection components. The large deformation

and force demands due to the applied gravity loads and the thermal expansion and contraction of structural members combined with material strength degradation can potentially result in the failure of welded connections during the heating or cooling stages of a fire. Failure of welded connections during a fire event depends not only on the applied load and temperature but also on the rate and time duration at which loads are applied. Although the applied gravity loads may remain relatively constant during a fire, the loading developed by thermally induced deformations can vary significantly during a fire event. Therefore, accurate knowledge of time-dependent mechanical properties of weld materials is an important part of predicting the real response of welded steel connections in fire.

Steel materials and structures, when exposed to fire temperatures, experience increasing permanent deformation with time, even when the applied load level is below the yield stress [7]. The time-dependent inelastic deformation under constant stress and temperature is referred to isothermal creep phenomenon. Creep of steel occurs when the steel material is subjected to a constant load at a temperature slightly above its recrystallization temperature [8]. At this temperature, the atoms become quite mobile at which time-dependent alterations of steel materials or structures occur. Creep of steel in steel connections is a thermally activated process that is highly dependent on the type of the steel base materials, bolts, and welds used.

Modeling of thermal creep of steel in structural-fire engineering analysis can be classified into two approaches: explicit and implicit thermal creep models. Explicit creep model is when the steel material is subjected to constant load and temperature conditions, and the only variable is time. In this case, the creep strains are added directly into the strain profile of the cross section of the steel material [9]. Therefore, the

explicit creep model can directly compute the creep strains, and then these strains are added to thermal and mechanical strains as follows [9]:

$$\varepsilon_{Total} = \varepsilon_{Thermal}(T) + \varepsilon_{Mechanical}(\sigma, T) + \varepsilon_{creep}(\sigma, T, t) \quad (1)$$

Where ε_{Total} is the total strain, $\varepsilon_{Thermal}(T)$ is the thermal strain (function of temperature (T)), $\varepsilon_{Mechanical}(\sigma, T)$ is the stress related strain (function of both the applied stress (σ) and the temperature (T)) and $\varepsilon_{creep}(\sigma, T, t)$ is the creep strain (stress (σ), temperature (T) and time (t) dependent strain).

The explicit creep strain for a steel material can be computed through a one-dimensional tensile elevated temperature test where constant load and temperature are applied. Therefore, for a specific constant tensile load and targeted elevated temperature, a displacement-time plot defined as a creep curve can be presented in Fig. 1. This creep curve shows three distinct stages. At time equal zero, instantaneous displacement is resulted due to the fast loading application. Note that, this displacement can be either elastic or plastic depends on the applied load. In the first interval of time (primary creep stage), the curve is non-linear and exhibits a decreasing creep strain rate. For the next interval of time, the secondary stage of a creep curve, the creep strain is almost constant and is maintained until it reaches the tertiary stage. In the tertiary stage, the creep strain rate increases rapidly with time until failure. At the start of the tertiary stage, damage is initiated by the formation of internal voids resulting in reduction in the material cross-sectional area and consequently failure or fracture.

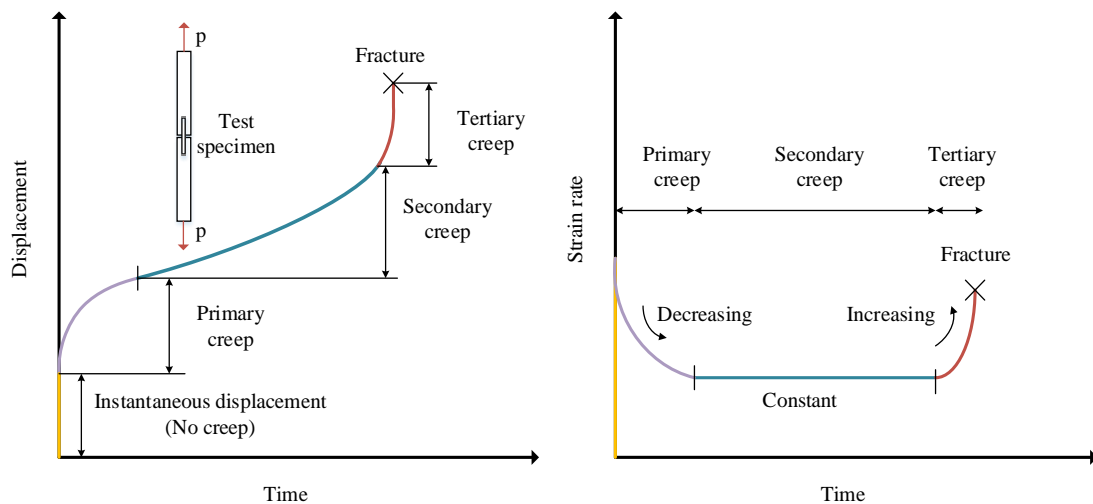


Fig. 1. Classical creep curve

Implicit creep model is considered when the steel material is subjected either to a variable stress or temperature or both parameters together. In this case, the creep strains are included indirectly into the stress-strain curves of the material and cannot be explicitly computed [9]. Creep of steel is considered implicitly in the stress-strain curves for structural steel at elevated temperatures in Eurocode 3 [10]. The retention factors proposed by Eurocode 3 [10] were based on transient coupon tests conducted by Kirby and Preston [11] and Cooke [12] with heating rate of $10^{\circ}\text{C}/\text{min}$ [13, 14]. Kirby and Preston [11] considered in their research different heating rates and then adjusted the material properties of steel materials for different heating rates relative to those at $10^{\circ}\text{C}/\text{min}$. Based on their adjustment, the retention factors obtained from stress-strain curves predicted at $10^{\circ}\text{C}/\text{min}$ heating rate are conservative for heating rates greater than $10^{\circ}\text{C}/\text{min}$. However, for heating rates below $10^{\circ}\text{C}/\text{min}$, the retention factors proposed are not applicable due to the effect of implicit creep [14].

Steel structures experience loss of strength and stiffness as exposed to fire temperatures that might lead to a total collapse of the structure. However, in some cases

steel structures can withstand the induced fire loads and can retain their integrity after the fire event ends. In these cases and after the steel material cools down to ambient temperature, the mechanical material properties of the structural steel might change. This change in material properties is referred to residual mechanical properties of steel material. Therefore, residual mechanical properties of steel base material, bolt, and welds are the key factors for evaluating the connections fire-resistance design capacities to maintain the integrity and stability of steel structures during and after fire exposure.

B. Literature Review

Weld is a metal joining material that is commonly used in steel connections and can affect their governing failure modes in fire. Previous research studies investigated the behavior of welded and simple bolted (shear tab) connections at elevated temperatures [15, 16, 17]. These studies indicated that when welds are subjected to elevated temperatures they can lead to poor performance and unexpected failure of steel connections. Therefore, studying the mechanical and thermal properties of welds when exposed to high temperatures is of great importance to ensure safe design of steel connections in fire.

A significant amount of previous research has examined the elevated temperature properties of structural steel and bolts. However, very limited data are available on the elevated temperature properties of weld materials. Latham and Kirby [18] performed an extensive experimental tests on the behavior of longitudinal and transverse butt weld joints as well as cruciform fillet welded connections when exposed to elevated temperatures. This study includes different welding process (manual metal arc welding (MMA), submerged arc welding (SAW), and gas shielded welding

(GMAW)), steady-state and transient thermal analysis, and different steel base material grades and thicknesses. For evaluating the material properties of fillet welds at elevated temperatures, the cruciform fillet weld connections were tested under steady-state elevated temperature tensile tests. The tests were carried out at a rate of 0.02/min up to a 5% plastic strain and then the rate altered to a nominal strain rate of 0.1/min. This loading protocol differs from the conventional one where high strain rates are used as per Latham and Kirby [18]. Also, it was emphasized that it is important to examine the significance of strain rates on steel plates and weld metal behavior when exposed to high temperatures. Based on the work performed by Latham and Kirby [18], Annex D of Eurocode 3 (Part 1-2) [10] specifies the retention factors for welds at elevated temperatures as discussed by Twilt [19]. The retention factors for fillet welds proposed by the Eurocode 3 Part 1-2 [10] are illustrated in Fig. 2.

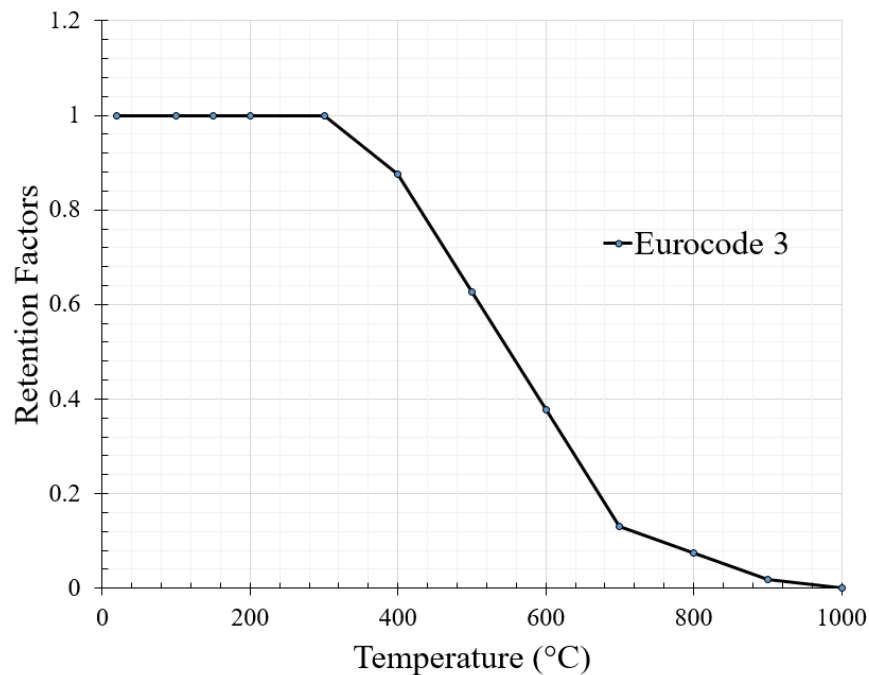


Fig. 2. Eurocode 3 retention factors for fillet weld [10]

Another investigation was also conducted by Ufuah and Ikhayere [20] to estimate the elevated temperature mechanical properties of butt-welded joints and compared the results with Eurocode 3 retention factors [10]. Transient test method was used in modeling and calibrating the elevated temperature reduction factors for the butt welded connections. The results showed that the welded connections made of S460M (ASTM A572 Gr.65) started to lose their strength at temperatures greater than 100 °C, whereas the Eurocode 3 [10] indicated that welded connections lose their strength for temperatures greater than 400 °C. Also, the results indicated that Eurocode 3 [10] design guidelines can be used to model butt-welded connections made with S355 (ASTM A572 Gr.50) steel material. Also, an experimental investigation on high-temperature mechanical properties of all welded specimens (only welds) under steady state tension test was conducted by Rezaeian et al. [21]. Two weld electrodes, E6013 and E7018, were incorporated in the analysis. Results were used to evaluate the stress-strain response, tensile strength, ultimate strength and the modulus of elasticity at each temperature for the weld materials. The experimental results showed a rapid reduction in weld strength at temperatures larger than 400°C reaching to 50% and 8% of its initial ultimate strength at 600°C and 800°C, respectively. Furthermore, the influence of electrode type using SMAW process on the behavior and microstructure of steel welds was investigated. The results showed that the electrode type has a great effect on strength characteristics of steel welds at elevated temperatures.

Furthermore, an experimental testing was performed by Conlon [22] to identify the strength of the transverse fillet welds subjected to tensile loading at elevated and post-elevated temperatures. For the elevated temperature tests, all specimens were heated up to a desired temperature, then a tension load with a rate of 0.10 in./min (0.254

mm/min) was applied until failure. While for post-fire conditions, the specimens were heated up to 870 °C (1600 °F) and then cooled back to a desired temperature before testing. The results showed that the weld material began to undergo significant reduction in strength at a temperature equal to 430 °C (800 °F) when subjected to fire. However, during the post-fire scenario, tests had a smaller reduction in the weld strength than those tested during the elevated temperature tests. Another experimental investigation was conducted to study the post-fire behavior of welded connections after they were subjected to elevated temperatures [23]. Three different configurations of weld specimens (butt welds, longitudinal fillet welds, and transverse fillet welds) having Q345 (ASTM A572 Gr.50) steel material were studied. The three different welded specimens were first heated to a specified temperature and then cooled back to ambient temperature using two different cooling processes (natural cooling and water cooling) and then loaded till failure. Note that, all test specimens were designed to fail in the base material at ambient temperature. Also, the test specimens were heated up to a targeted temperature and kept constant for 60 min duration before loading to ensure uniform temperature distribution around the weld regions. The results showed that for the butt welded connections, the fracture location changed from base metal to the butt weld at temperature equals to 500°C and 600°C for natural air cooling and water cooling regimes, respectively. This indicates that for temperatures greater than or equal 500°C and 600°C and after the butt weld is cooled back to ambient temperature, the butt weld experienced tensile strength degradation more than the base metal. Also, for temperatures beyond 700°C, an increase in residual strength of the butt weld was noted. Whereas the transverse and longitudinal fillet welded connections failed in the base material at temperatures ranging from 20 °C to 800 °C. In addition, another

experimental investigation was conducted on S355JR (ASTM A572 Gr.50) butt-welded joints to characterize the resistance of butt welds under shear stresses during a natural fire [24]. The results showed that for temperatures lower than or equal to 600 °C, welds recovered their initial ultimate strength after cooling, whereas for temperatures equal to 800 °C and 900 °C, the reduction of the ultimate strength after a complete heating-cooling cycle was around 20% of the initial one. Another experimental study was conducted to examine further the post-fire residual mechanical behavior of steel Q235 (ASTM A36) and Q345 (ASTM A572 Gr.50) butt welds [25]. The butt weld specimens were heated to various temperatures ranging between 400 °C and 800 °C and then cooled back to ambient temperature. The results showed that the post-fire mechanical properties of butt welds were affected by the material grade and heating temperature, and strength began to decrease after temperature exceeded 600 °C. More specifically, at 800 °C, the yield and ultimate strength decreased to 87% and 91% for Q235 (ASTM A36 (ASTM 2014a)), respectively, and to 83% and 87% for Q345 (ASTM A572 Gr.50 (ASTM 2018)), respectively.

All these previous studies on welded specimens did not consider the effect of creep implicitly or explicitly on the behavior of weld materials when exposed to fire temperatures. However, limited research studies have been conducted on the effect of heating rate or strain rate on the steel base material when exposed to elevated temperatures [11, 12, 26-28]. All these studies indicated that the strength of the steel material increases with the increase of heating or strain rate. These experimental studies recognized the importance of heating/loading rate (implicit creep) on the elevated temperature properties of the steel base material when exposed to fire. Moreover, the effect of explicit creep on steel base materials has been studied by many researchers [7,

29-36]. All these studies indicated that the creep deformation in steel base material becomes significant for temperatures above 40% of the steel melting temperature and creep strains are highly dependent on stress levels, temperatures, and time durations for which building structures can undergo in case of fire. Based on these creep tests, limited number of creep models were developed to predict the time-dependent creep behavior of steel base materials. Among these studies, the most popular ones are those developed by Harmathy [37] and Fields and Fields [38]. Harmathy proposed a creep model based on testing several structural and prestressing steels [29, 37]. The Harmathy creep model [37] is capable of predicting the creep strains in both the primary and secondary stages of creep using the concept of activation energy for creep. However, Fields and Fields [38] used the power law creep model and represented creep strain in the form of a *Norton-Bailey* equation [39]. The model developed by Fields and Fields [38] is capable of predicting the primary and secondary stages of creep in temperatures ranging from 350 °C to 650 °C and for creep strains up to 6-percent. The creep model developed by Fields and Fields [38] was based on the creep tests conducted by Knight et al. [30] on AS 149 steel. Also, it was used to predict the creep strain behavior of SS 41 steel creep tests conducted by Fujimoto et al. [32]. Since the chemical composition and yield strengths of AS A149 and SS 41 are similar to those of ASTM A36 steel, Fields and Fields [38] creep model can be used to model the thermal creep of ASTM A36 steel. However, for different steel materials, a scaling factor can be added to the original power law equation of ASTM A36 steel material as per [40]. Furthermore, long-term creep modelling for welds is very limited and previous studies focus more on butt welds [41] that are heavily used for main stream pipes, headers, boilers, or other component in power plants. However, no creep model (short-term) is developed for fillet weld for

structural engineering application. Previous creep models were based on experimental tests conducted to predict the time-dependent creep behavior of the structural materials solely. However, the creep of steel becomes more complex in case of connections, where different material types and interactions between components are included. Therefore, it is of a great importance to develop creep models for welds, bolts, and steel materials based on experimental investigations conducted on creep behavior of steel connections.

Performance-based fire design approach is gaining more interest from the fire engineering community, especially that this approach can assess, with reasonable accuracy, the real fire resistance of steel structures. However, following such approach requires thorough understanding of the time- and temperature-dependent material properties of steel under various fire loading conditions. Therefore, this research outlines ongoing efforts to study the major parameters that affect the behavior of weld material in fire and post-fire conditions. These efforts are addressed through an extensive experimental program to provide unique results that represent an important contribution to the field of structural fire engineering. That is, quantifying the load developed in the welded connections due to different fire-time exposures is complex. This is due to creep effects that can dominate the response of welded steel connections when subjected to fire temperatures. Therefore, one of the main contributions of this research work is to study implicitly and explicitly the effect of creep or time on the behavior of welded connections in fire. Also, creep models for the fillet welds and steel base material were proposed and calibrated using ABAQUS [42] to best fit the experimental results of the explicit creep tests. These creep models for fillet welds and steel base materials can be used for future studies to predict the creep behavior of

welded connections. Further, it is well known that weld behavior depends highly on the load angles. This research also aims at providing a deep understanding on the behavior of welded lap joints subjected to different load angles while taking into account implicitly the creep effect. Therefore, the outcome of this research is to generate retention factors for fillet weld materials while considering the effect of different loading rates and load angles. Finally, steel in general loses its strength after a heating and cooling cycle of a real fire. In some cases, steel structures can be reused after fire events. Therefore, another contribution of this research is to study the residual mechanical properties of fillet welds after exposed to fire while considering different geometrical properties (load angles). A deep understanding of the time-dependent and post-fire behaviors of welded connections will ensure safe design of these connection during and after fire exposure.

CHAPTER II

GOALS AND OBJECTIVES

The overarching goal of this research study is to establish a deep understanding of the time-dependent and the post-elevated temperature performance of steel welded connections subjected to fire. Several objectives were implemented in order to accomplish the aforementioned goal:

1. Implicit creep behavior of transverse welded lap joints when subjected to elevated temperatures.
 - a. A series of experimental tests on transverse welded lap joints were conducted at different elevated temperatures and different loading rates under steady-state thermal analysis. More specifically, the transverse welded lap joint was first heated up to a targeted temperature and then loaded until failure with a specified loading rate.
 - b. Two loading rates were chosen, with a factor of ten difference between the fast (0.254 mm/min) and the slow (0.0254 mm/min) rates, to allow the examination of loading rate effects.
 - c. These tests were conducted under a wide range of temperatures ranging between 400°C and 700°C.
 - d. The results are presented as axial load-displacement characterizations at each temperature and for each loading rate.
 - e. Failure modes of the welded connections showing fracture surfaces, texture, and colors are also presented.

- f. Rate- and temperature- retention factors for the weld material under both fast and slow loading rates were calculated and compared with other research available in the literature.
 - g. Effect of loading rate on the ductility of transverse welded lap joints was also studied and presented.
2. Explicit creep behavior of transverse welded lap joints when subjected to elevated temperatures.
- a. A series of tests were performed to investigate explicitly the time-dependent or creep behavior of the transverse welded lap joints under constant load at different elevated temperatures. That is, at each specific temperature, a load, equal to a fraction of the ultimate load predicted in the fast tests, was applied in a very fast manner (within 1 sec.) and kept constant throughout the test. Tests were conducted for 120 minutes or until failure.
 - b. Creep curves are presented as creep displacement-time relations at constant load and temperature.
 - c. Failure modes of the welded connections showing fracture surfaces, texture, and colors due to creep are presented.
 - d. Isochronous representation are also presented to further understand the creep behavior of transverse welded lap joints under combined loading and temperature conditions.
 - e. Critical times, loads, and temperatures at which welds can fail due to creep during a fire event are also specified.

3. Creep modeling of transverse welded lap joints exposed to fire temperatures.
 - a. The creep curves resulted from the explicit creep tests were used to develop a *Norton-Bailey* power law creep equation for the transverse welded lap joints.
 - b. Tertiary part of creep curves was also predicted by introducing a damage parameter to the power law equation of the transverse welded lap joint.
 - c. The *Norton-Bailey* power law creep model for the welded lap joint was scaled using reasonable assumptions to develop the creep models for the welds and the steel base material.
 - d. FE models were developed using ABAQUS [42] and validated first against the experimental tests conducted on the transverse welded lap joints under fast loading rate. Temperature-retention factors for the weld material estimated in the implicit creep tests under fast loading rate were used for validation purposes.
 - e. Then, the proposed thermal creep models for the welds and steel base material were used and calibrated using ABAQUS [42] to predict the creep behavior of the transverse welded lap joint subjected to elevated temperatures.
 - f. Fields and Fields [38] creep model for the steel base material was also used for comparison purposes.
4. Effect of load angle on the rate-dependent behavior of fillet welds exposed to fire temperatures.

- a. Steady-state thermal analysis was used to investigate experimentally the implicit thermal creep behavior of welded lap joints under different loading rates while considering different load angles (0° , 45° , and 90°).
 - b. The loading rates were chosen with a factor of fifteen difference between the fast (1.5 mm/min) and the slow (0.1 mm/min) rates, to allow a better examination of loading rate effects.
 - c. These tests were conducted under a wide range of temperatures ranging between 400°C and 700°C with 100°C increment.
 - d. The results are presented as load-displacement characterizations at each temperature and each loading rate for each load angle.
 - e. Failure modes of the welded connections showing fracture surfaces, texture, and colors are presented.
 - f. Retention factors for each loading rate scenario and loading angle application at ambient and elevated temperatures were generated and compared with other research available in the literature.
 - g. Effect of loading rate and load angle on the ductility of welded lap joints were also studied and presented.
5. Post-fire behavior of the welded lap joints after exposed to fire temperatures.
- a. A series of experimental tests on three welded lap joint configurations having three different load angles (0° , 45° , and 90°) were conducted after exposed to elevated temperatures. More specifically, the welded lap joint was heated up to a targeted temperature and then kept constant for 60 min to ensure uniform temperature distribution around the weld region.

After that, the specimen cooled back to ambient and then loaded until failure.

- b. Different elevated temperatures ranging from 500°C to 900°C with 100°C increment were used in this analysis. Also, ambient tests for all welded lap joint configurations were conducted for comparison purposes.
- c. Results are presented as residual load-displacement characterizations for each lap joint configuration after being exposed to target temperature.
- d. Percentage decrease in weld strength capacities due to post-fire analysis were computed.
- e. Failure modes of the welded connection showing fracture surfaces, texture, and colors are presented.
- f. Effect of loading angle on the residual ductility of fillet welds in welded lap joints was also studied and presented.

CHAPTER III

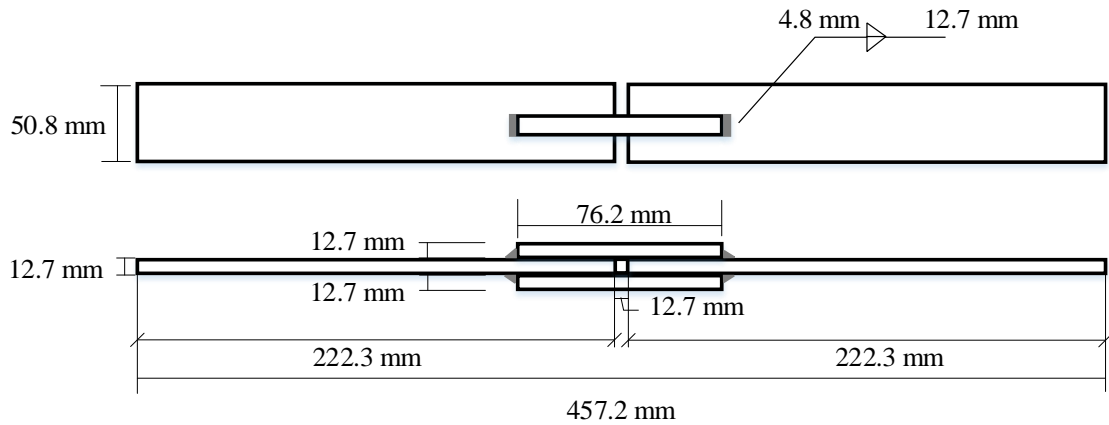
IMPLICIT AND EXPLICIT CREEP BEHAVIOR OF TRANSVERSE WELDED LAP JOINTS AS EXPOSED TO ELEVATED TEMPERATURES

A. Experimental Program

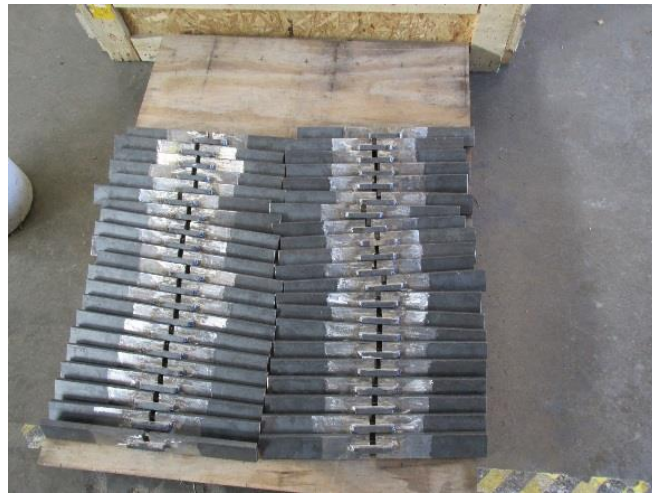
The first two parts of the experimental program mainly emphasis on the implicit and explicit creep behavior of transverse welded lap joints when subjected to elevated temperatures. These two parts were performed at Ferguson Structural Engineering Laboratory at The University of Texas at Austin-USA.

1. Test Specimens

For the first two parts of the experimental program, details of the transverse welded lap joint specimens are shown in Fig. 3. The specimens consisted of two large plates (222.3 mm × 50.8 mm × 12.7 mm) connected to each other through two smaller plates (76.2mm × 12.7 mm × 12.7 mm) with equal-leg fillet welds of leg sizes of 4.8 mm. The fillet welds were designed such that failure will occur in the fillet welds at both ambient and elevated temperatures. The weld strength retention factors proposed by Eurocode 3 [10] were used in the calculations of the capacity of the transverse welded lap joints at elevated temperatures. All plate material was ASTM A529 Gr.50 with measured yield and tensile strengths of 372 MPa (54 ksi) and 510 MPa (74 ksi), respectively. The welding process adopted was shielded metal arc welding (SMAW) using E7018 electrodes [43].



(a)



(b)

Fig. 3. Transverse welded lap joints configuration

2. Test Procedure

A 98-kN capacity MTS-810 test frame with water cooled grips was used to perform the direct tension tests for the transverse welded lap joints at ambient and elevated temperatures as shown in Fig. 4. An MTS Model-653 furnace was used as the heating device for the elevated temperature tests. The furnace generates heat using electrical coils, and is separated into upper, middle and lower heating zones that can be individually controlled using an MTS Model-409.83 temperature controller system. To

investigate the thermal behavior of transverse welded lap joints at a target temperature, a uniform temperature distribution over the length of the welded lap joint was applied. To control the uniform temperature distribution, three thermocouples (Type K) were used to measure the surface temperature of the specimen at different locations throughout the length of the specimen as shown in Fig. 5. Also, the specimens were wrapped by stainless steel foils (SSF) to protect the thermocouples from direct exposure to thermal radiation from heating coils of the furnace. During the heating phase, the test machine was controlled so that no load was applied to the specimen as the specimen expanded. Note that before loading was applied the temperature was held constant for 30 minutes.

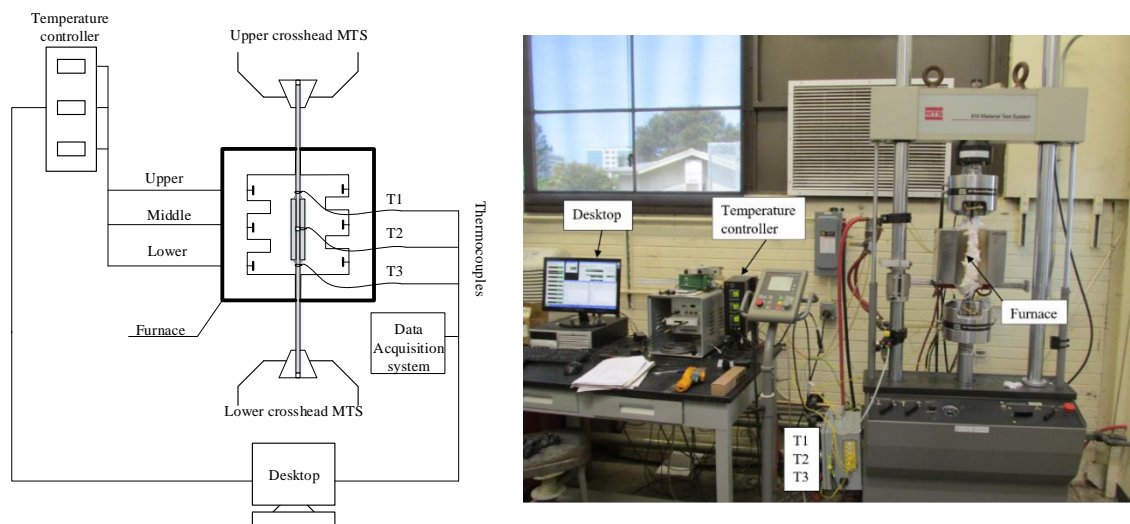


Fig. 4. Experimental test equipment

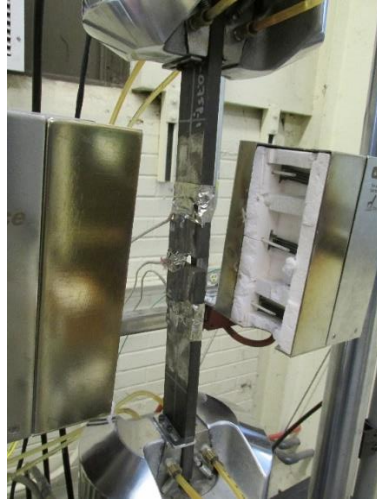


Fig. 5. Thermocouples and foils implementation

B. Implicit Thermal Creep Behavior of Transverse Welded Lap Joints

1. Loading Protocol

To investigate the effect of loading rates on the behavior of transverse welded lap joint specimens, steady-state thermal testing was used in this study. The transverse welded lap joint specimens were first heated up to a target temperature with no load. The temperature was then held constant as load was applied to the specimen and increased until fracture occurs. Loading was applied using a constant test machine cross-head displacement rate. Specimens were tested at two cross-head displacement rates of 0.254 mm/min (fast) and 0.0254 mm/min (slow). These rates were chosen somewhat arbitrarily, with a factor of ten difference between the “fast” and the “slow” rates, to allow the examination of loading rate effects. Steady-state thermal testing, rather than transient-state thermal testing was used in this research since transient-state thermal testing calls for a constant load on the specimen as the temperature is increased, and is therefore not amenable to studying loading rate effects. The test matrix of

transverse welded lap joints at ambient and elevated temperatures under fast and slow loading conditions is in Table 1.

Table 1. Test matrix of transverse welded lap joints at ambient and elevated temperatures

Test Name	Temperature (°C)	Loading Rate (mm/min.)	Test Name	Temperature (°C)	Loading Rate (mm/min.)
20°C-Fast	20	0.2540	20°C-Slow	20	0.0254
400°C-Fast	400	0.2540	400°C-Slow	400	0.0254
425°C-Fast	425	0.2540	425°C-Slow	425	0.0254
450°C-Fast	450	0.2540	450°C-Slow	450	0.0254
475°C-Fast	475	0.2540	475°C-Slow	475	0.0254
500°C-Fast	500	0.2540	500°C-Slow	500	0.0254
550°C-Fast	550	0.2540	550°C-Slow	550	0.0254
600°C-Fast	600	0.2540	600°C-Slow	600	0.0254
650°C-Fast	650	0.2540	650°C-Slow	650	0.0254
700°C-Fast	700	0.2540	700°C-Slow	700	0.0254

2. Experimental Tests Observations

For implicit creep tests, all specimens failed due to fracture of the weld as shown in Fig. 6. More specifically, Figs. 7 and 8 show the failure modes for the welded specimens at ambient and elevated temperatures under fast and slow loading rates. It can be seen that at ambient temperature (Fig. 7 (a)), the welded specimen fractured through the weld at an angle around 40° to 45° with respect to 50.8 mm wide plate. However, as temperature increased, the weld fracture angle decreased and the fracture

plane slightly deviated towards the toe of the weld. Also, it can be seen from Figs. 7 and 8 that the effect of loading rates on the weld fracture angle is not significant. These observations were done visually without any measurements for the angle of weld fracture for all tests. This is due to the fact that the throat size and length of the welds are small and is difficult to measure their fracture angle after failure. As the test specimens were exposed to different elevated temperatures, the steel surfaces exhibited changes in color and texture.

Figures 9 and 10 show the fracture surfaces at the weld region for all specimens at different elevated temperatures. It can be seen in Fig. 9 that for tests conducted at elevated temperatures up to 500 °C, the fracture surfaces are smooth and their color is different from that of the exposed steel surface. Large deformations and necking were observed at the fracture surface in the weld region when the welded specimens were exposed to 650 °C and 700 °C as shown in Fig. 10(c) and Fig. 10(d), respectively. These observations suggest for temperatures greater than 500 °C, the weld exhibits increasing ductility prior to complete failure.

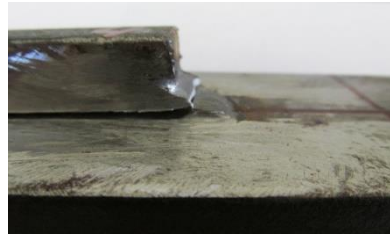


(a)

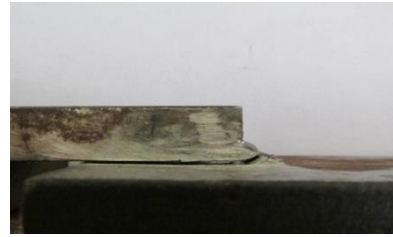


(b)

Fig. 6. Failure at the throat of the weld for all test specimens at ambient and elevated temperatures: (a) Fast tests (0.254 mm/min), (b) Slow tests (0.0254 mm/min)

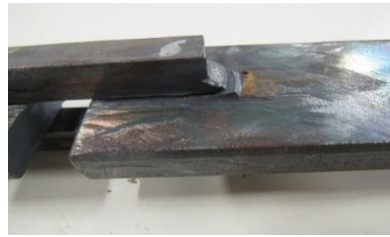


20 °C-Fast

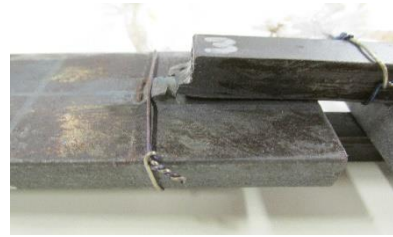


20 °C-Slow

(a)



400 °C-Fast

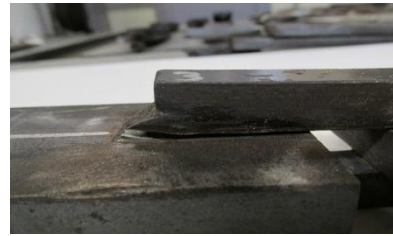


400 °C-Slow

(b)



425 °C-Fast



425 °C-Slow

(c)

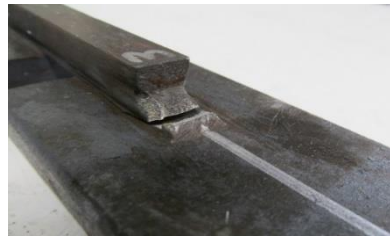


450 °C-Fast

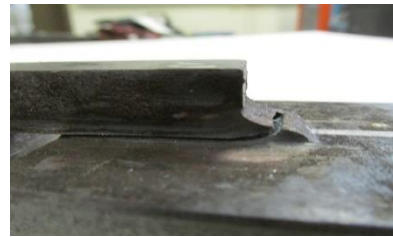


450 °C-Slow

(d)



475 °C-Fast



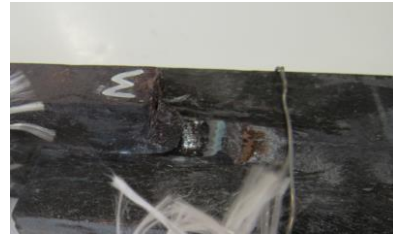
475 °C-Slow

(e)

Fig. 7. Failure modes for welded specimens subjected to fast and slow loading rates at: (a) 20 °C, (b) 400 °C, (c) 425 °C, (d) 450 °C, (e) 475 °C



500 °C-Fast



500 °C-Slow

(a)



550 °C-Fast



550 °C-Slow

(b)



600 °C-Fast



600 °C-Slow

(c)



650 °C-Fast



650 °C-Slow

(d)



700 °C-Fast



700 °C-Slow

(e)

Fig. 8. Failure modes for welded specimens subjected to fast and slow loading rates at: (a) 500 °C, (b) 550 °C, (c) 600 °C, (d) 650 °C, (e) 700 °C

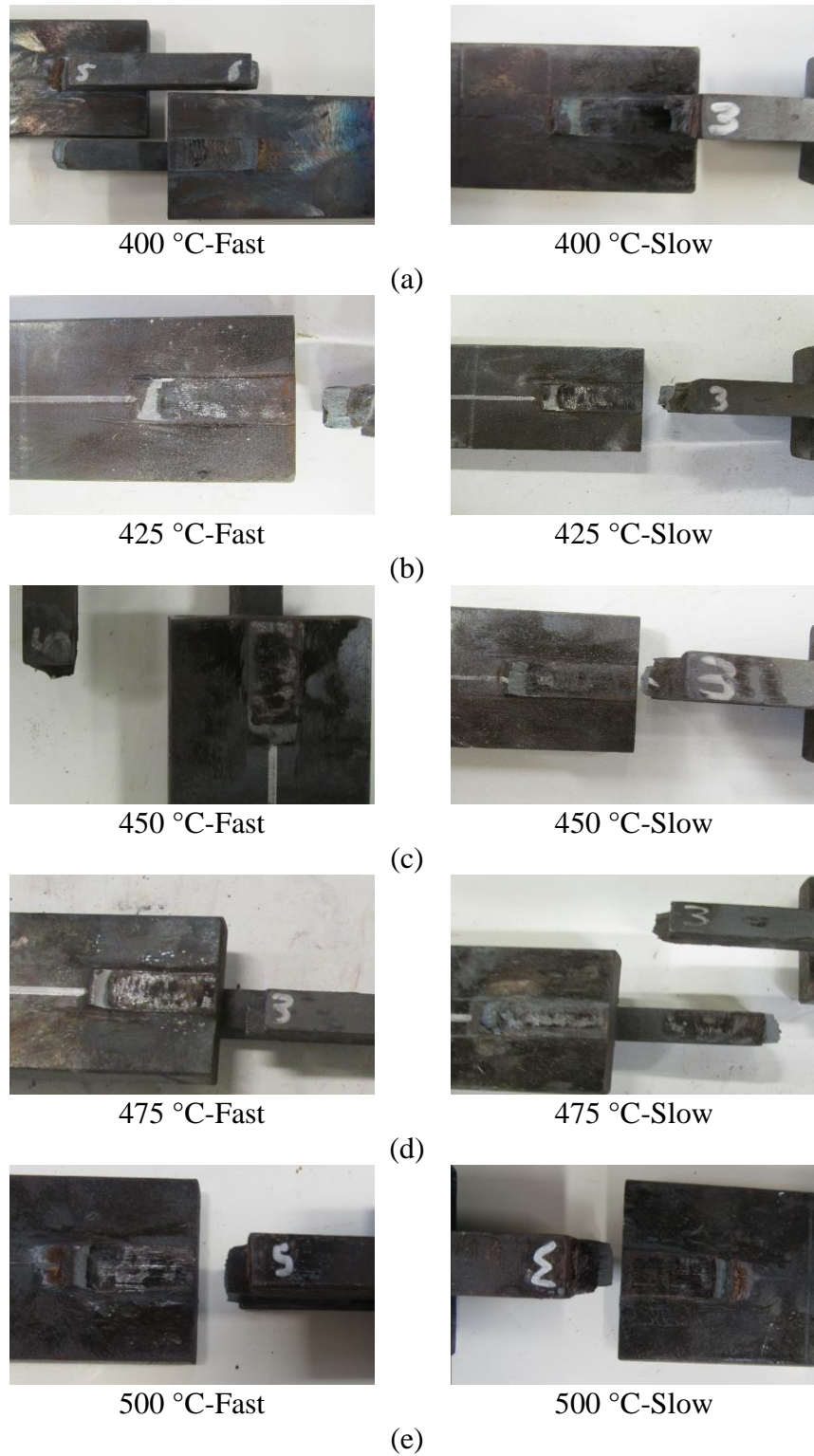


Fig. 9. Fracture surface at the weld region for the welded specimens at: (a) 400 °C, (b) 425 °C, (c) 450 °C, (d) 475 °C, (e) 500 °C

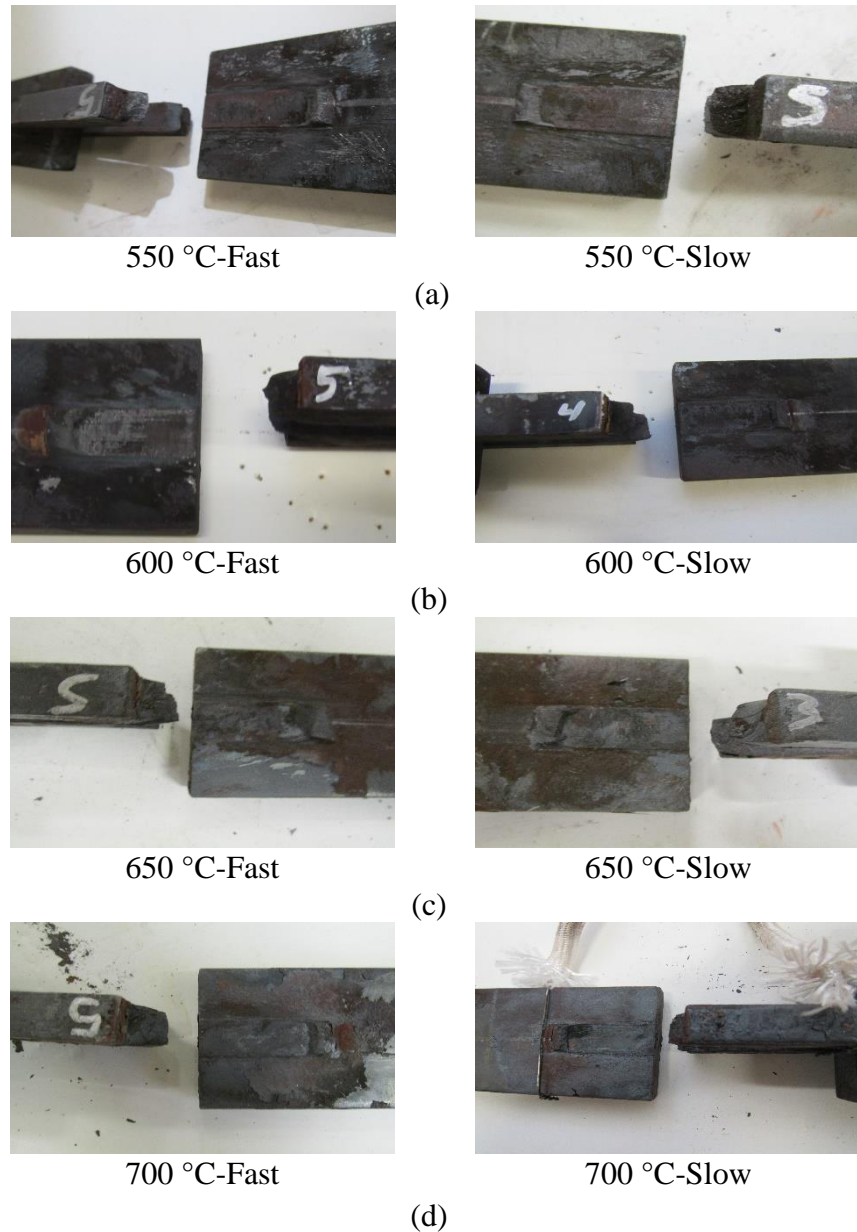
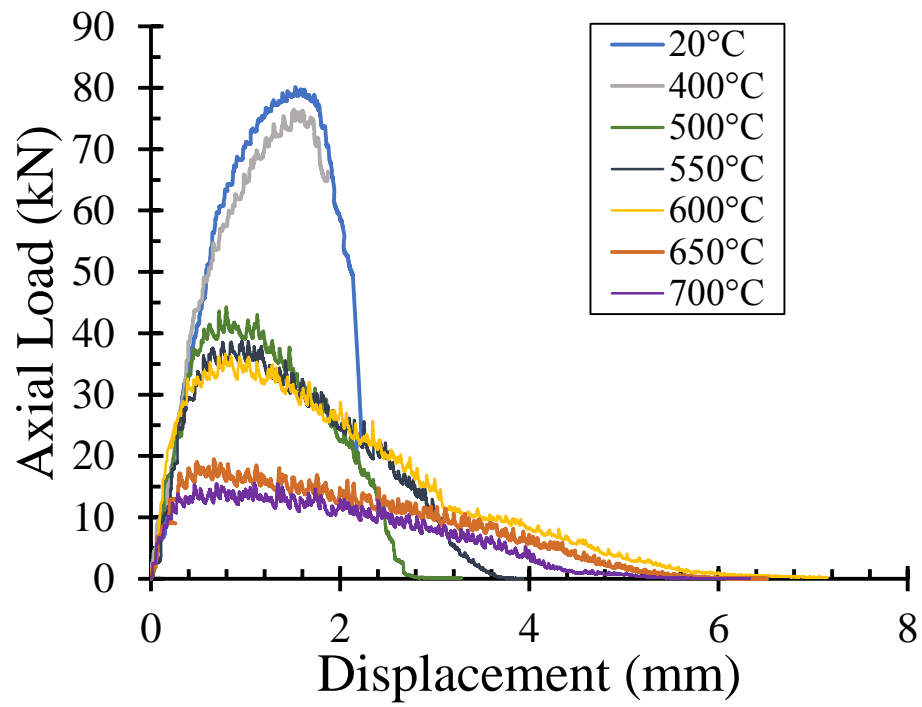


Fig. 10. Fracture surface at the weld region for the welded specimens at: (a) 550 °C, (b) 600 °C, (c) 650 °C, (d) 700 °C

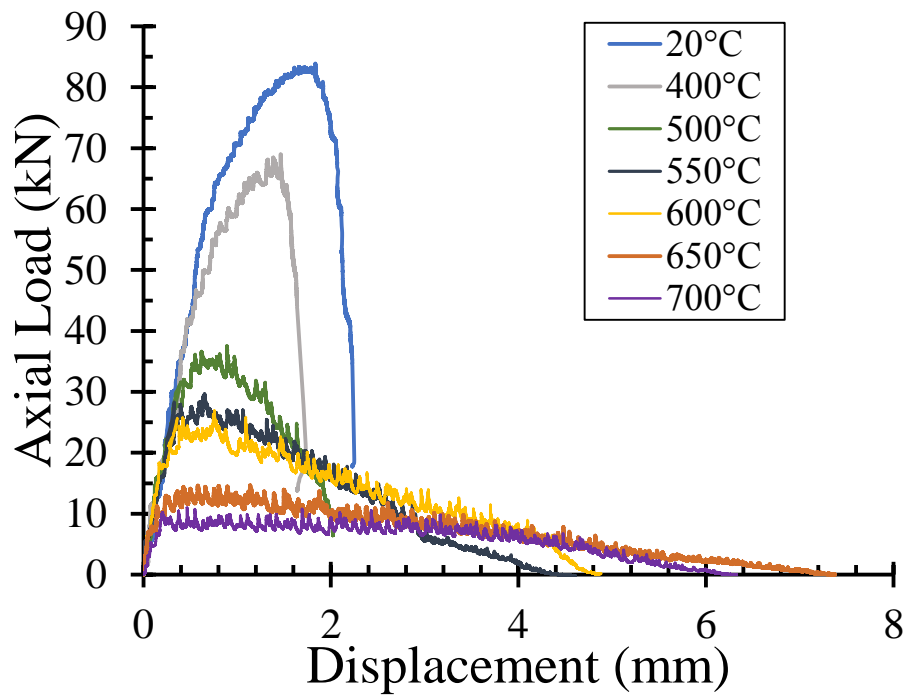
3. Effect of Temperature on Load-Deformation Response

To study the effect of temperature on the load-deformation response, representative results from the tension tests on transverse welded lap joints subjected to different elevated temperatures under slow and fast loading rates are shown in Figs. 11(a) and 11(b), respectively. The capacity of the welded specimen decreases as

temperature increases, and for a given temperature the capacity is smaller at the lower loading rate. A large difference can be seen between the test results performed at 400°C and 500 °C and between 600°C and 700°C for both fast and slow test scenarios. Therefore, Figs. 12(a) and 12(b) illustrate the force-displacement characteristics of the welded specimen at temperatures ranging between 400°C and 500°C for 25°C increments. Figure 12(a) indicates that the results obtained from the fast tests performed at 425°C and 475°C are very close to those obtained at 400°C and 450 °C, respectively. However, for slow test scenarios, as shown in Fig. 12(b), only the tests that were performed at 400°C and 425°C yield the same stiffness and strength capacity. This might be due to the uncertainty associated with weld quality, material strength, and dimensional tolerance that influence the thermal and mechanical behavior of weld material and welded specimens in fire.

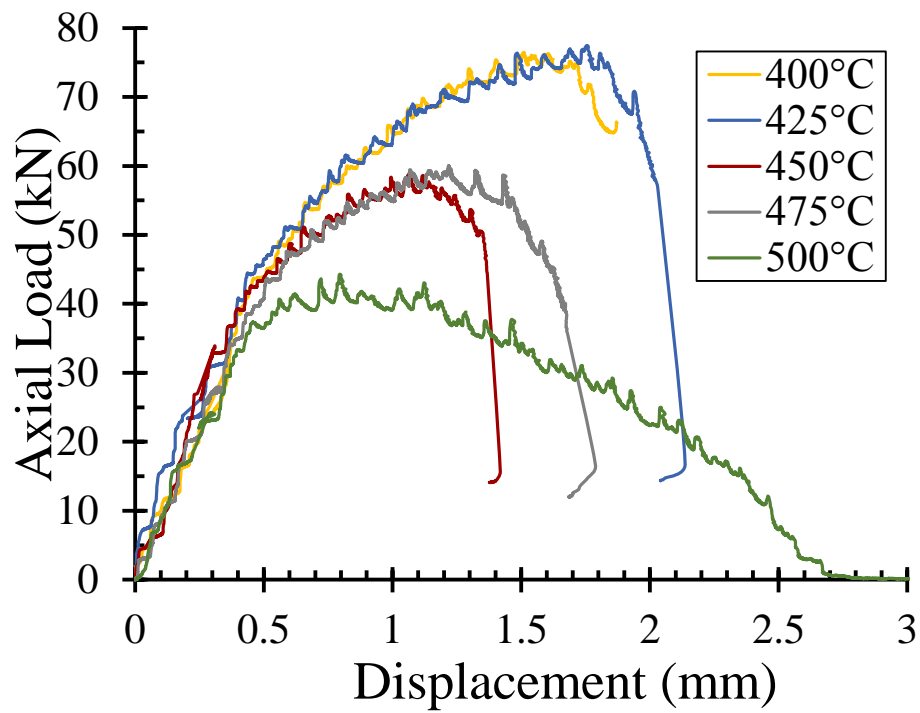


(a)

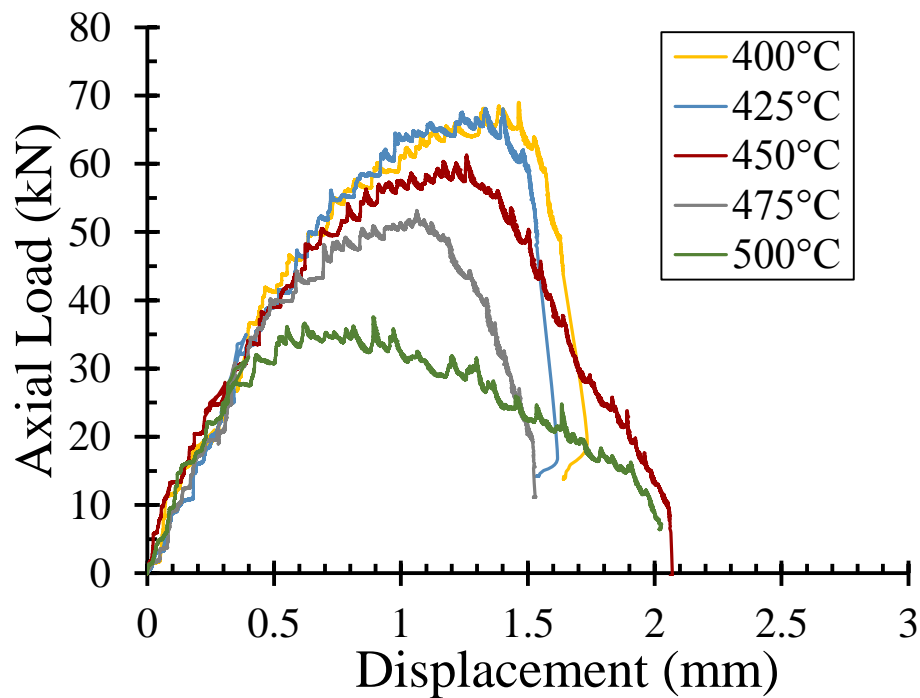


(b)

Fig. 11. Force-displacement characteristics of transverse welded lap joints at ambient and elevated temperatures under: (a) Fast loading rate scenario, (b) Slow loading rate scenario



(a)



(b)

Fig. 12. Force-displacement characteristics of transverse welded lap joints at temperatures ranging between 400°C and 500°C under: (a) Fast loading rate scenario, (b) Slow loading rate scenario

4. Effect of Loading Rates on Load-Deflection Response

To investigate the effect of loading rate on the behavior of transverse welded lap joints under ambient and elevated temperatures, illustrative plots are shown in Figs. 13 and 14. Figures 13 and 14 demonstrate a comparison between the strength capacities of test results obtained at temperatures ranging from 20°C to 450°C and from 475°C to 700°C, respectively, under both fast and slow loading rate scenarios. It can be seen that at 20 °C (Fig. 13(a)) there is no effect of loading rate on the load-deformation response or strength. The effect of loading rate on the strength of the welded test specimens at 400°C and 425°C is more noticeable as shown in Figs. 13(b) and 13(c), respectively. Interestingly, Fig. 13(d) shows little difference for the stiffness, strength, and ductility between the tests performed at 450°C under both fast and slow loading rates. This indicates that the small difference in the strength capacity of the weld material when exposed to temperatures less than or equal to 450°C might be due to the variations in material and geometric properties more than the loading rate conditions. In Fig. 14, the different loading rates have a noticeable impact on the behavior of transverse welded lap joints as temperature reaches 475 °C and becomes more significant as it reaches 700°C.

Table 2 illustrates the decrease in strength capacity of the specimens as loading changes from fast loading rate (0.245 mm/min) to slower one (0.0254 mm/min). It can be seen that the slow loading rate results in 11% to 29% decrease in strength capacity compared with the fast loading rate, as temperature increases from 475°C to 700°C. Also, as shown in Fig. 14, the welded specimen undergoes larger displacements as temperature increases and the load rate becomes slower. This indicates that the welded specimen gains more ductility when exposed to higher temperature and creep strains are

more pronounced in the axial load-displacement characteristics of the weld specimens when subjected to slow loading rates.

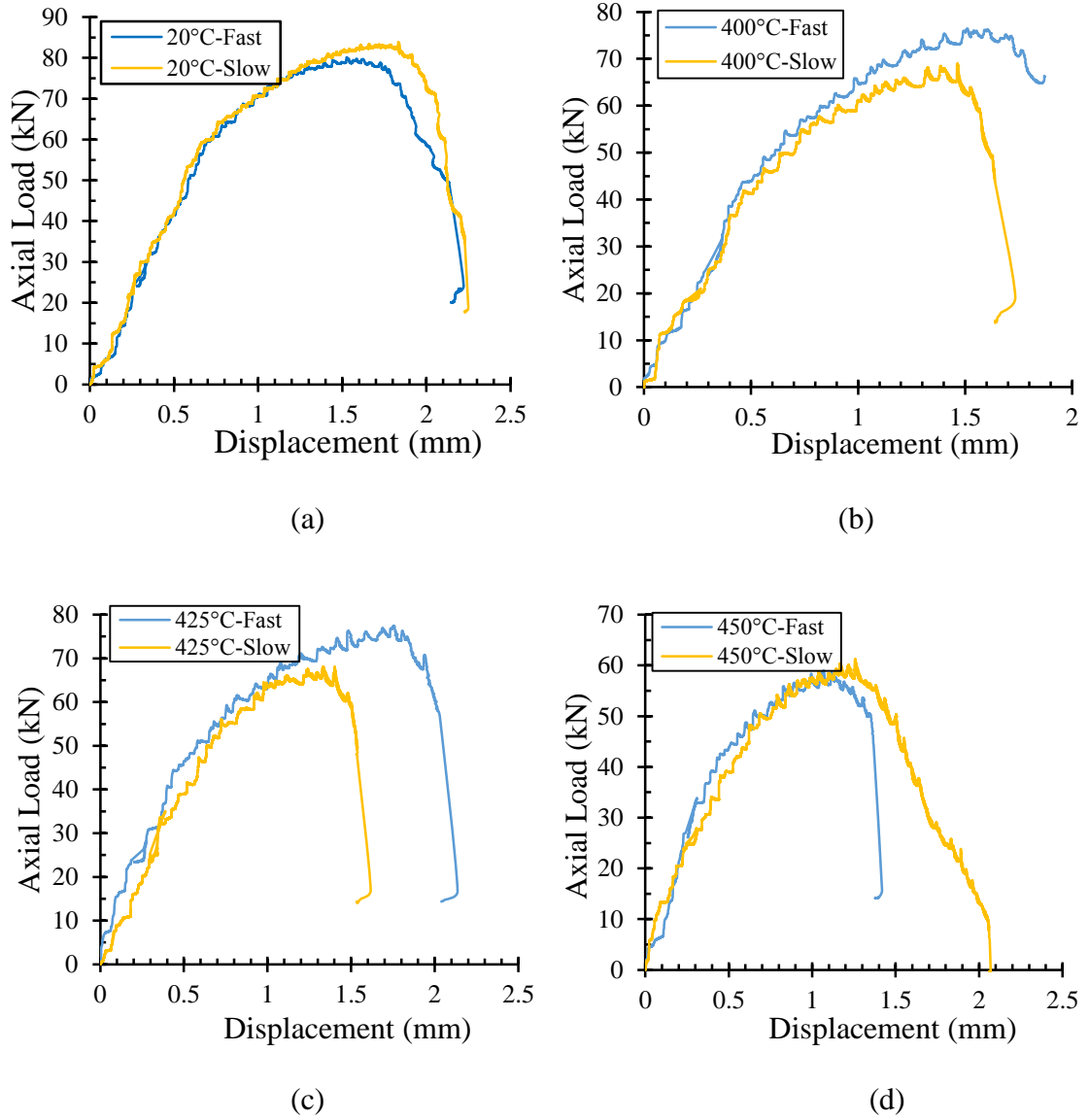


Fig. 13. Effect of loading rate on the behavior of transverse welded lap joints at: (a) 20 °C, (b) 400°C, (c) 425°C, (d) 450°C

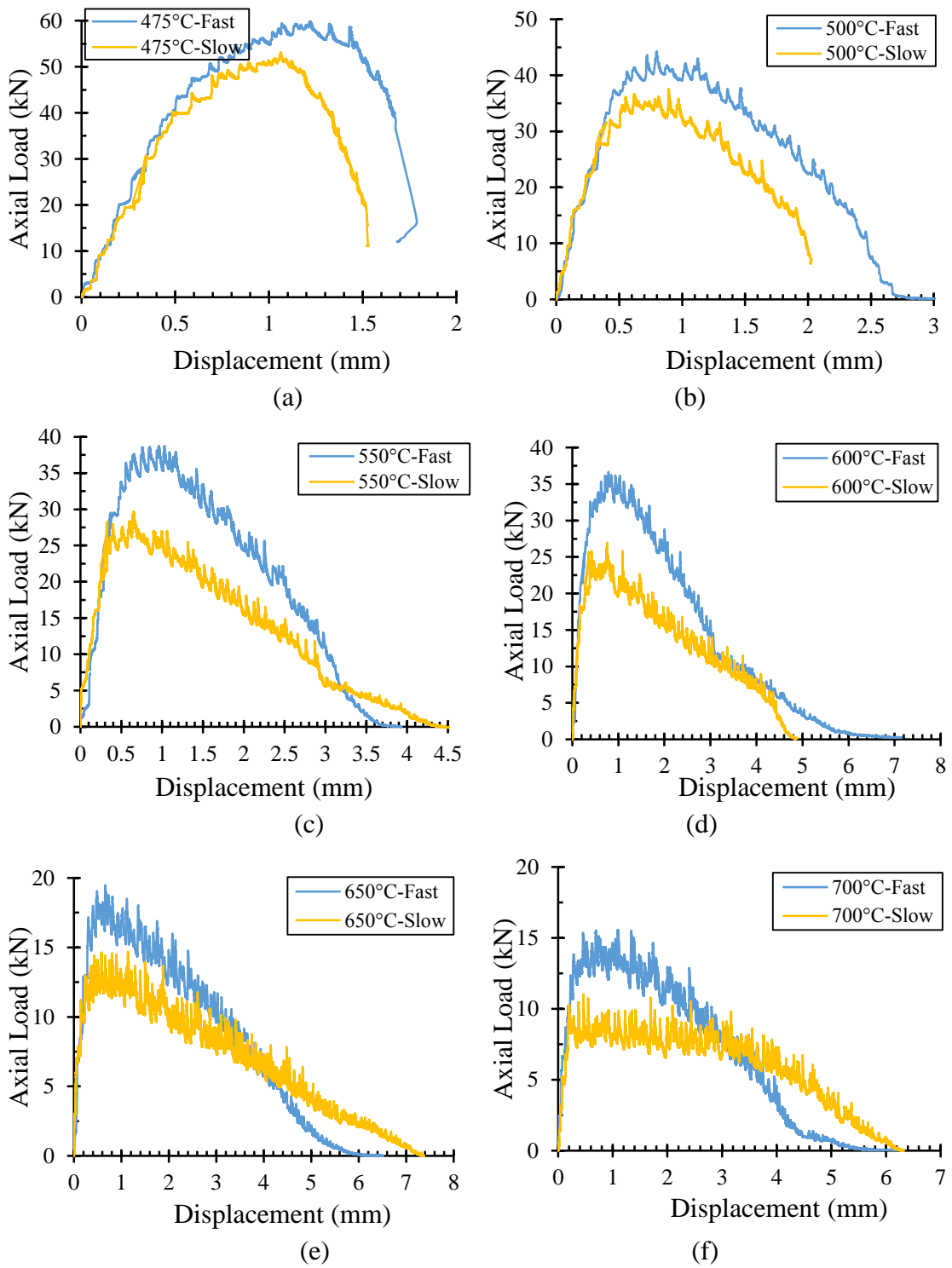


Fig. 14. Effect of loading rate on the behavior of transverse welded lap joints at: (a) 475°C (b) 500°C, (c) 550°C, (d) 600°C, (e) 650°C, (f) 700°C

Table 2. Effect of loading rate on the strength capacity of transverse welded lap joints under ambient and elevated temperatures

Fast test name	Maximum axial load (kN)	Slow test name	Maximum axial load (kN)	Decrease in capacity (%)
20 °C-Fast	80.12	20 °C-Slow	83.90	-4.71
400 °C-Fast	76.45	400 °C-Slow	69.01	9.73
425 °C-Fast	77.43	425 °C-Slow	68.13	12.01
450 °C-Fast	59.01	450 °C-Slow	61.32	-3.92
475 °C-Fast	60.03	475 °C-Slow	53.17	11.42
500 °C-Fast	44.29	500 °C-Slow	37.58	15.15
550 °C-Fast	38.72	550 °C-Slow	29.65	23.42
600 °C-Fast	36.66	600 °C-Slow	26.99	26.40
650 °C-Fast	19.48	650 °C-Slow	14.70	24.55
700 °C-Fast	15.55	700 °C-Slow	11.02	29.12

Figure 15 shows the axial load-displacement characteristics of test specimens at different elevated temperatures (500 °C and 600 °C) under different loading rates (0.254 mm/min and 0.0254 mm/min). When the welded specimen is heated up to 600 °C and subjected to a fast loading rate (0.254 mm/min), it gives approximately the same capacity as when it is subjected to 500 °C with a slow loading rate (0.0254 mm/min). This indicates that failure of welded connections due to fire temperatures depends not only on the applied load and temperature but also on the rate at which the load is applied.

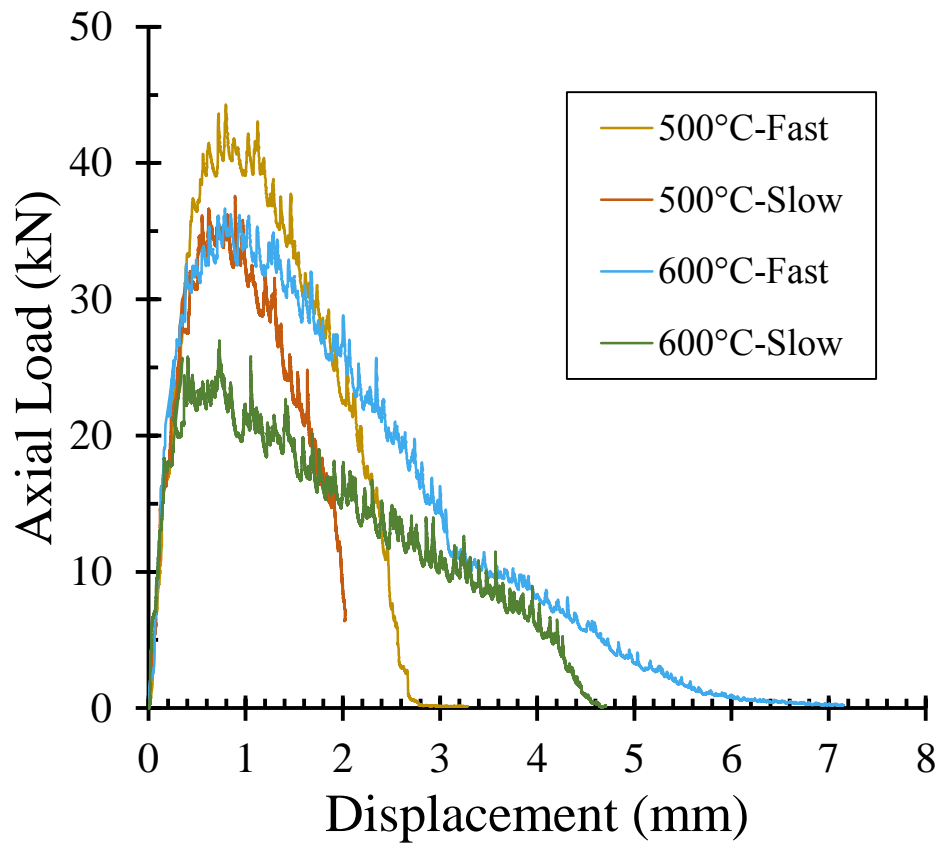


Fig. 15. Results from tests performed at 500 °C and 600 °C under fast and slow loading rates

5. Effect of Loading Rate and Temperature on the Ductility of the Transverse Welded Lap Joint

The ductility of the transverse welded lap joint refers to the ability of the lap joint to undergo a significant plastic deformation before the welds fracture. Since the inelastic creep strains are added implicitly to the axial load-displacement curves, the ductility of the lap joints can be computed as follows:

$$\phi = \frac{A}{PL} \tag{2}$$

Where ϕ is the normalized ductility, A is the area under the axial load-displacement curve, P is the peak load predicted at a specified temperature and loading

rate, and L is the total length of the specimen. In this approach, all axial load-displacement curves are normalized to one peak load of value of 1. The change in the joint displacements indicates the extent of which the specimen is experiencing high or low ductility in terms of temperature and loading rate. Figure 16 shows the variation of normalized ductility versus temperatures for both fast and slow tests. It can be seen for temperatures less than 500 °C, the ductility of the specimen is not changing for both fast and slow loading rates. However, as temperature increases (greater than 500 °C), the ductility of the welded lap joint increases with the increase of temperature. These results confirm with the observations presented in Fig. 9 where fracture surfaces become rough for temperatures greater than 500 °C. Also, the effect of loading rates on the ductility of welded lap joint is not significant for temperatures up to 625 °C. However, beyond 625 °C, the behavior of the weld specimen under slow loading rate shows larger ductility than that of the fast loading rate.

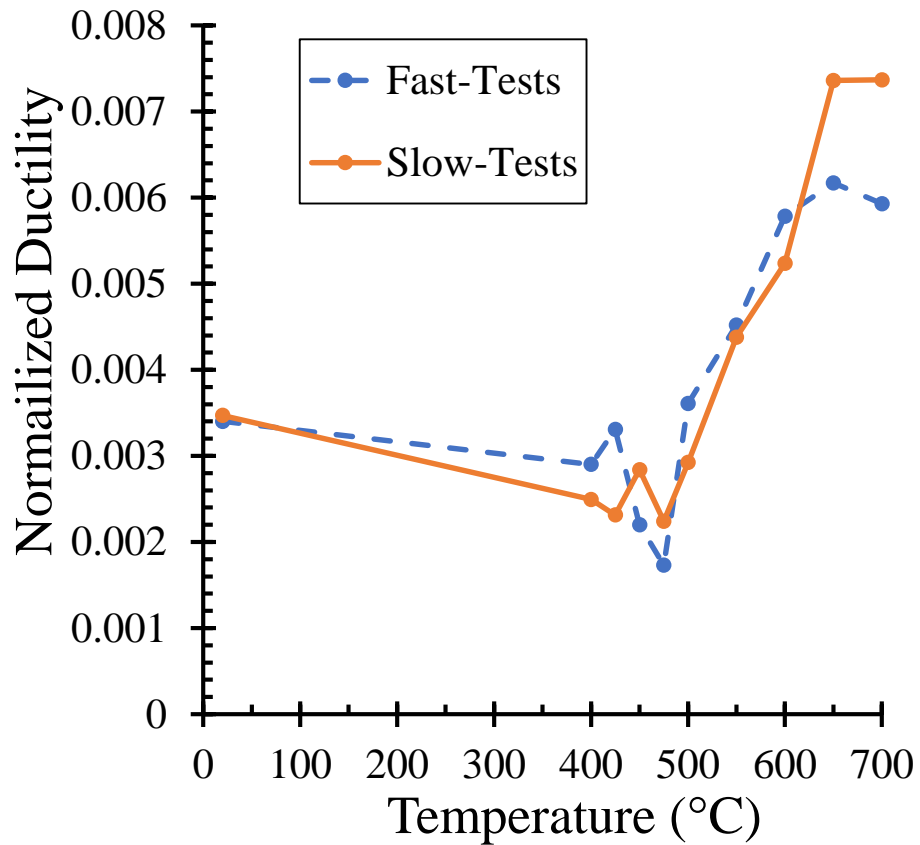


Fig. 16. Normalized ductility versus temperature under fast and slow loading rates

6. Retention Factors

The experimental results were used to compute the retention factors for the transverse welded lap joints when subjected to tension loading. The retention factors can be calculated by dividing the maximum strength capacity of the welded specimen at each temperature to that obtained from ambient temperature tests for each loading rate. The retention factors for transverse welded lap joints subjected to fast and slow test scenarios are listed in Table 3. Figure 17 shows a comparison between the retention factors obtained from these tests with those specified in Eurocode 3 [10] and those reported by Conlon [22]. The specimens conducted by Conlon [22] were subjected to a 0.1in./min (2.54 mm/min) loading rate, which is ten times higher than the fast loading

rate used in this study. It can be seen that, for temperatures greater than 430°C, the retention factors proposed by Conlon [22] are higher than those proposed by Eurocode 3 [10] and the ones from this study. However, the retention factors proposed by Eurocode 3 [10] are close to those resulted from the fast loading tests conducted in this study. Based on the experimental results, the effect of loading rate on the retention factors and strength capacities of transverse welded lap joints is significant for temperatures greater than 400°C. In general, the faster the load is applied the higher the retention factors are obtained. This indicates that ignoring the effect of loading rate in fire design of welded connections can potentially lead to unsafe predictions.

Table 3. Retention factors estimated for transverse welded lap joints at ambient and elevated temperatures

Test name	Temperature (°C)	Loading rate (mm/min.)	Maximum axial load (kN)	Retention factors
20 °C-Fast	20	0.2540	80.12	1.00
400 °C-Fast	400	0.2540	76.45	0.95
425 °C-Fast	425	0.2540	77.43	0.97
450 °C-Fast	450	0.2540	59.01	0.74
475 °C-Fast	475	0.2540	60.03	0.75
500 °C-Fast	500	0.2540	44.29	0.55
550 °C-Fast	550	0.2540	38.72	0.48
600 °C-Fast	600	0.2540	36.66	0.46
650 °C-Fast	650	0.2540	19.48	0.24
700 °C-Fast	700	0.2540	15.55	0.19
20 °C-Slow	20	0.0254	83.90	1.00
400 °C-Slow	400	0.0254	69.01	0.82
425 °C-Slow	425	0.0254	68.13	0.81

450 °C-Slow	450	0.0254	61.32	0.73
475 °C-Slow	475	0.0254	53.17	0.63
500 °C-Slow	500	0.0254	37.58	0.45
550 °C-Slow	550	0.0254	29.65	0.35
600 °C-Slow	600	0.0254	26.99	0.32
650 °C-Slow	650	0.0254	14.70	0.18
700 °C-Slow	700	0.0254	11.02	0.13

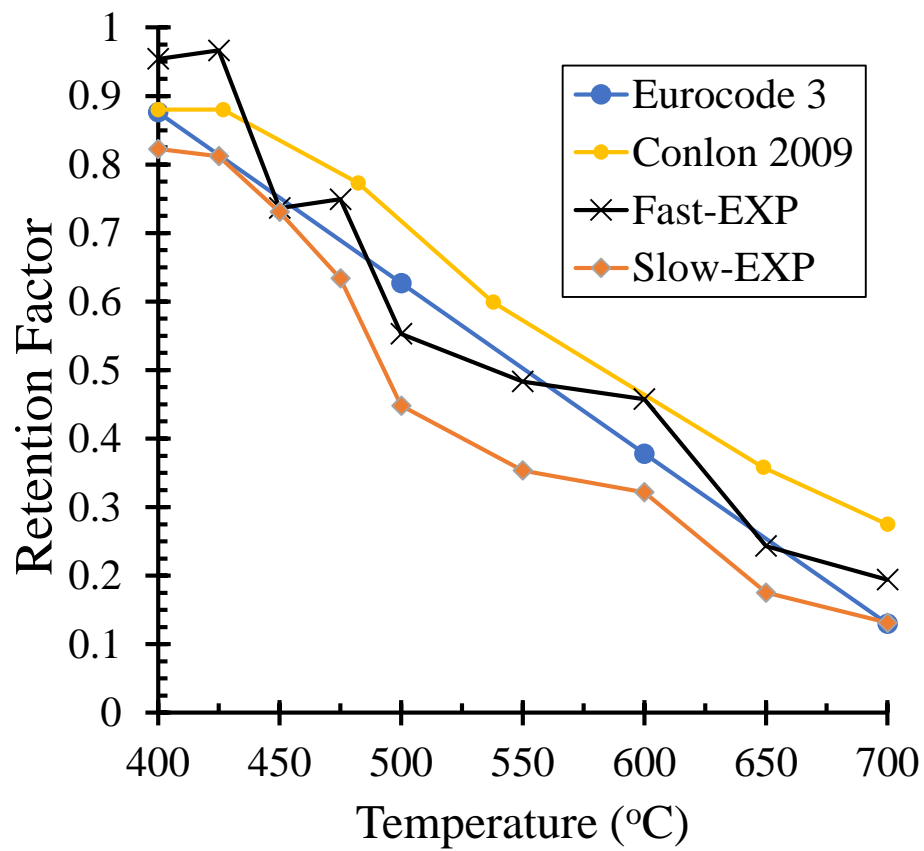


Fig. 17. Retention factors for the transverse welded specimens

C. Explicit Thermal Creep Behavior of Transverse Welded Lap Joints

1. Load Protocol

This research work aims at developing a fundamental understanding of the creep behavior of transverse welded lap joints exposed to fire temperatures. This approach requires to conduct two series of experimental test analysis: fast temperature tests and creep tests. In the fast temperature tests, the test specimen was heated up to a target temperature without applying any load. Once the test specimen reached the targeted temperature, a displacement-control load was applied until failure with a fast loading rate (0.254 mm/min) to estimate the peak load that the test specimen can withstand at each temperature. In this series, the peak loads are assumed to be the maximum time-independent loads that the specimen can resist excluding the effect of time on the strength and stiffness of the tested specimens. Note that, this series of analysis is a part of the implicit creep tests that were conducted under the fast loading rate. Also, some tests were repeated and the lower peak load values were used for the creep tests. In the creep tests, and after the specimen was heated up to a specified temperature, a force-controlled load equals to a fraction of the peak load predicted in the first series of analysis was applied in a very fast manner (within 1 sec.) and kept constant throughout the test. In this case, the only variable is time in order to study its effect solely on the welded lap joint behavior as temperature and loading conditions are kept constant. Note that, the creep tests were conducted for 120 min time duration or until the test specimen failed.

The way of selecting the load ratios applied on the test specimens was as follows. For temperatures below 500°C where the thermal creep is not significant or unlikely to occur, the test specimen was subjected to a load equals to 90% of the peak

loads predicted from the fast loading tests. For temperatures greater than 500°C, a range of peak load ratios (0.90, 0.75, 0.60, and 0.50) was applied to the welded specimen. At 500°C, 0.80 peak load ratio was used instead of 0.60 to see the effectiveness of higher load ratios on the explicit time-dependent behavior of welded lap joints at a temperature where creep of steel is slightly significant. The test matrix of creep tests conducted on the transverse welded lap joints is tabulated in Table 4.

Table 4. Test matrix for creep tests at elevated temperatures

Test Name	Temperature (°C)	Peak Load Ratio	Test Name	Temperature (°C)	Peak Load Ratio
400°C-0.90P	400	0.90	600°C-0.60P	600	0.60
450°C-0.90P	450	0.90	600°C-0.75P	600	0.75
475°C-0.90P	475	0.90	600°C-0.90P	600	0.90
500°C-0.50P	500	0.50	700°C-0.50P	700	0.50
500°C-0.75P	500	0.75	700°C-0.60P	700	0.60
500°C-0.80P	500	0.80	700°C-0.75P	700	0.75
500°C-0.90P	500	0.90	700°C-0.90P	700	0.90
600°C-0.50P	600	0.50	-	-	-

2. Experimental Tests Observation

The time-dependent deformation and failure for the transverse welded lap joints when subjected to various sustained loads at constant temperature conditions are presented in Fig. 18. As it can be seen from Fig. 18 (a), no failures occurred in the specimens for temperatures equal or below 450°C although 90% of the peak loads were applied. However, for the 475°C creep test with 90% peak load, the specimen failed in the weld region. For the test conducted at 500°C (Fig. 18(b)), fracture occurred at the

throat of the weld when subjected to load ratios greater than 0.80P. However, for those conducted at higher temperatures, 600 °C and 700°C, fracture occurred at a load ratio greater or equal to 0.60P. Figure 19 shows the fracture mode that occurred at the throat of the welds for temperatures equal and larger than 475°C with 0.90P load application. It can be seen from Fig. 19 that the sign of necking starts to be noticeable at 500°C and become more significant for 600°C and 700°C. This is due to the fact that the damage starts by the formation of cavities or voids in the microstructure of the weld material resulting in the reduction of the material cross section and consequently fracture. In the following section, factors that influence the creep behavior of welded joints, along with representative results, are presented and briefly discussed.

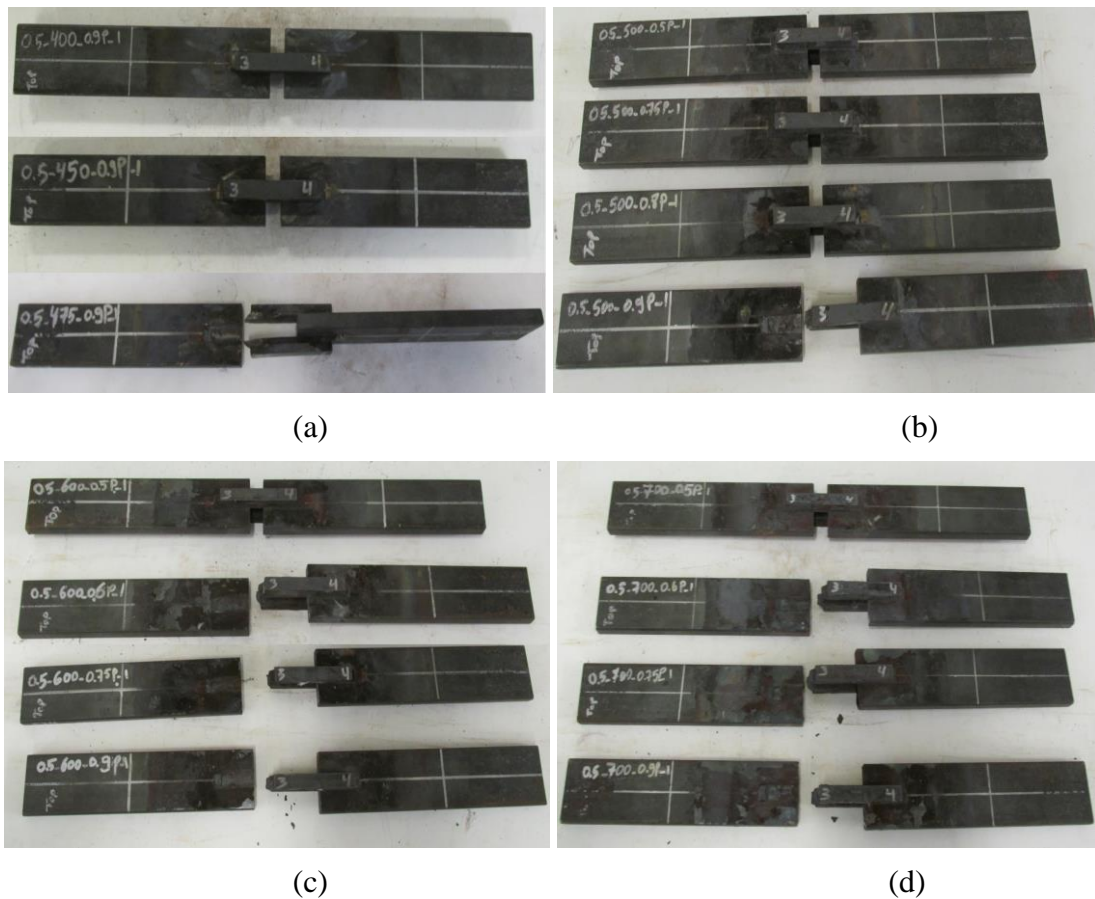


Fig. 18. Time-dependent deformation or failure for transverse welded lap joints at: (a) Temperatures below 475 °C, (b) 500 °C, (c) 600 °C, (d) 700 °C

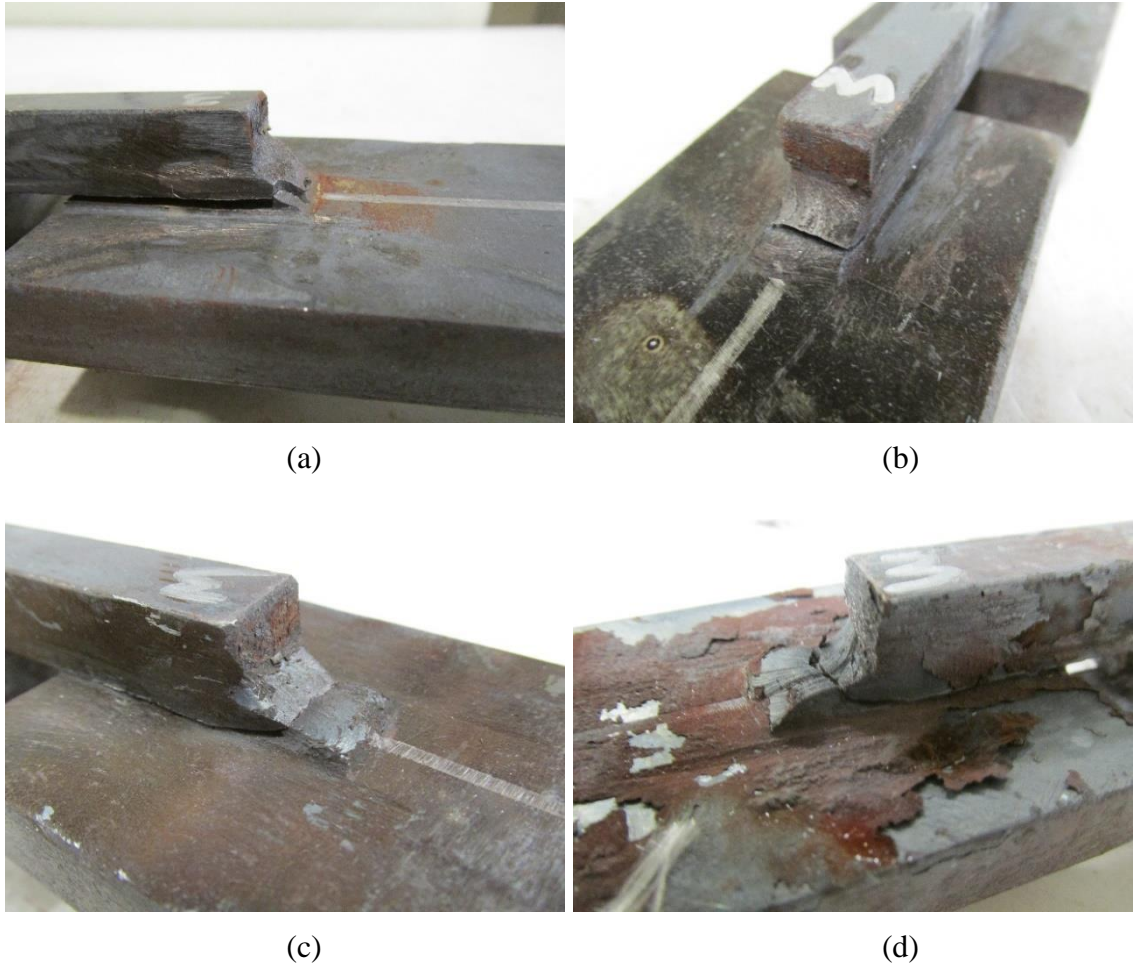
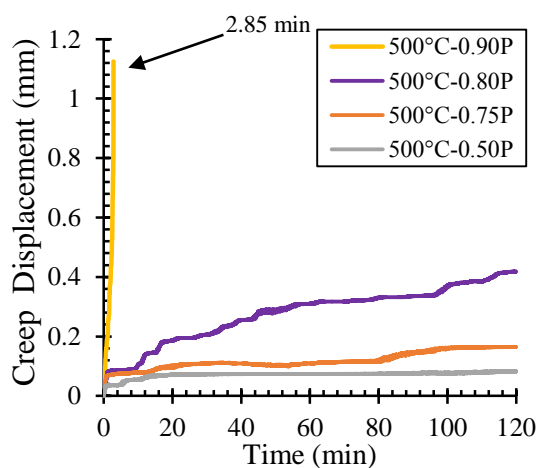


Fig. 19. Creep fracture at the throat of the weld for transverse welded lap joints subjected to 0.90P at: (a) 475 °C, (b) 500 °C, (c) 600 °C, (d) 700 °C

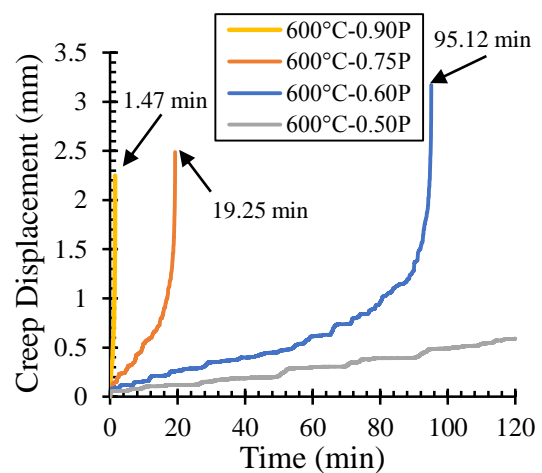
3. Effect of Thermal Creep on Transverse Welded Lap Joint

The thermal creep of steel is highly dependent on the stress or load level [8]. Figure 20 shows the thermal creep curves representation for transverse welded lap joints subjected to different peak load ratios at different temperatures. Figure 20(a) shows that the welded specimen can sustain loads up to 80% of the peak load predicted in the fast temperature test at 500°C for 120 min time duration. However, for 90% of the peak load, the welded specimen was rapidly failed after *2 min and 51 sec* from conducting the creep test. Another observation can be concluded from Fig. 20(a) is that the creep displacement-time behavior of the welded specimen at 0.75P is close to that response

conducted at 0.50P more than that at 0.80P. Also, it can be seen that there is a large gap between the tests conducted at 0.80P and 0.90P. This indicates that for temperatures at which creep is slightly significant (500°C), load or stress level dominates the thermal creep behavior of transverse welded connections in fire. For creep tests conducted at 600°C and 700°C, the results show that the welded specimen cannot resist loads greater than 0.50P for a 120 min time duration as shown in Figs. 20(b) and 20(c), respectively. However, the specimen cannot resist the 0.60P for a duration more than 95 min and 7 sec, and 8 min and 51 sec when subjected to 600°C and 700°C, respectively. Further, as the load ratio increases up to 0.90P, the welded lap joints rapidly failed after 1 min and 28 sec, and 1 min and 32 sec from conducting the creep tests at 600°C and 700°C, respectively. Also, it can be seen from Fig. 20(c) that there is a large gap between the tests conducted at 700°C with peak load ratios of 0.50P and 0.60P. This indicates that at higher elevated temperatures, the temperature dominates significantly the thermal creep behavior of the welded connection more than the peak load ratio.



(a)



(b)

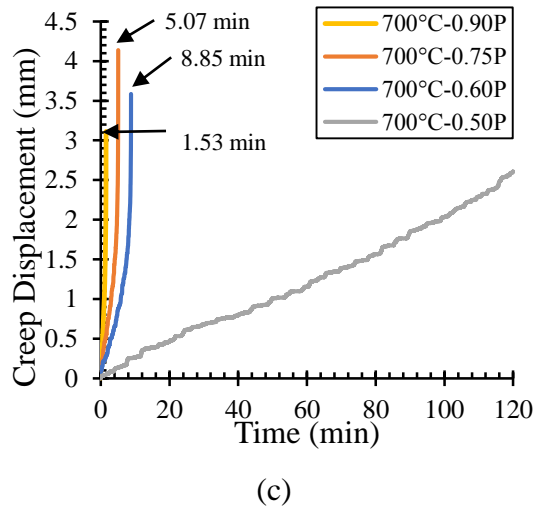
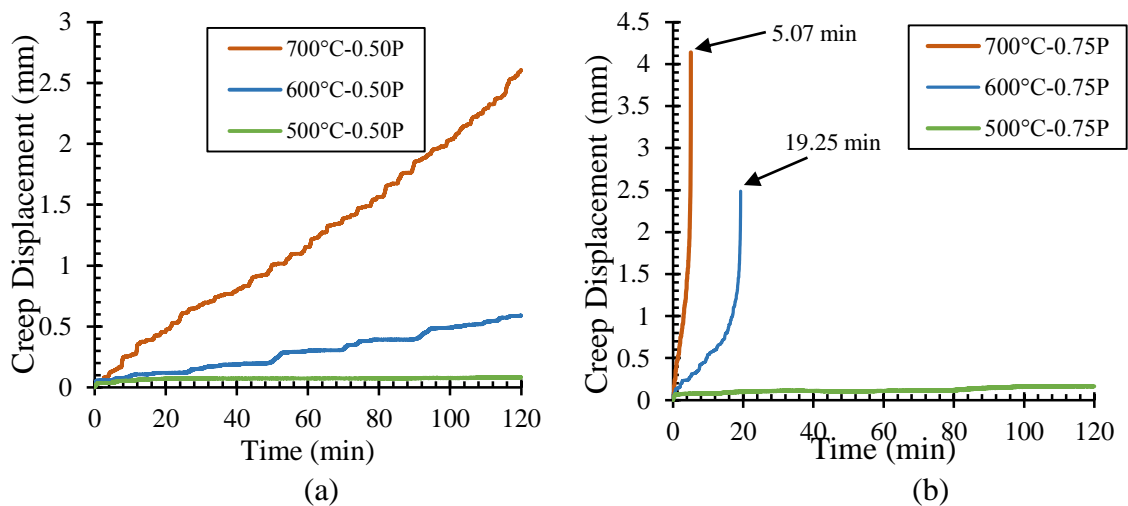


Fig. 20. Effect of peak load ratio on thermal creep response of transverse welded lap joints at: (a) 500 °C, (b) 600 °C, (c) 700 °C

4. Effect of Temperature on Load-Deformation Response

Thermal creep of steel material occurs when the temperature of steel exceeds one-third to one half of its melting temperature [44]. To investigate the effect of temperature on thermal creep response of transverse welded lap joints, a representative results of creep curves are illustrated in Fig. 21. Figures 21(a) and 21(b) show displacement-time creep curves for tests conducted at temperatures equal to or greater than 500°C having low (0.50P) and moderate (0.75P) constant loading conditions, respectively. It can be seen that at a low constant loading conditions (0.50P), all specimens survived the creep tests, however, the specimens undergo larger displacement for higher temperatures. For tests conducted with moderate constant loading conditions (0.75P), fracture occurred in the weld region after *19 min and 15 sec*, and *5 min and 4 sec* from the beginning of the creep tests conducted at 600°C and 700°C, respectively. However, at temperature equals to 500°C no failure occurred in the welds. Also, Figs. 21(c) and 21(d) present the thermal creep behavior of transverse welded lap joints subjected to 0.90P for all temperatures above and below 475°C,

respectively. It can be seen that for tests conducted at 475°C and above (Fig. 21(c)), the transverse welded lap joint failed in welds at early stages where maximum time recorded to resist the 0.90P is 5 min and 6 sec at 475°C. However, for those conducted below 475°C, the welded specimen resists the 0.90P for 120 time duration. Note that both the creep tests conducted at 450°C and 475°C were subjected approximately to the same constant load (Table 3). This indicates that the thermal creep of weld material becomes significant for temperatures slightly greater than 450°C and becomes more prominent for larger temperatures. Further, Fig. 21(d) shows that the creep test conducted at 400°C results in higher creep displacement than that conducted at 450°C. This is because the peak load predicted from the fast temperature test at 400°C is higher than that at 450°C and creep effect at these temperatures is not significant. Note that, all the critical times at which the welded specimen fractured due to creep are illustrated in Table 5.



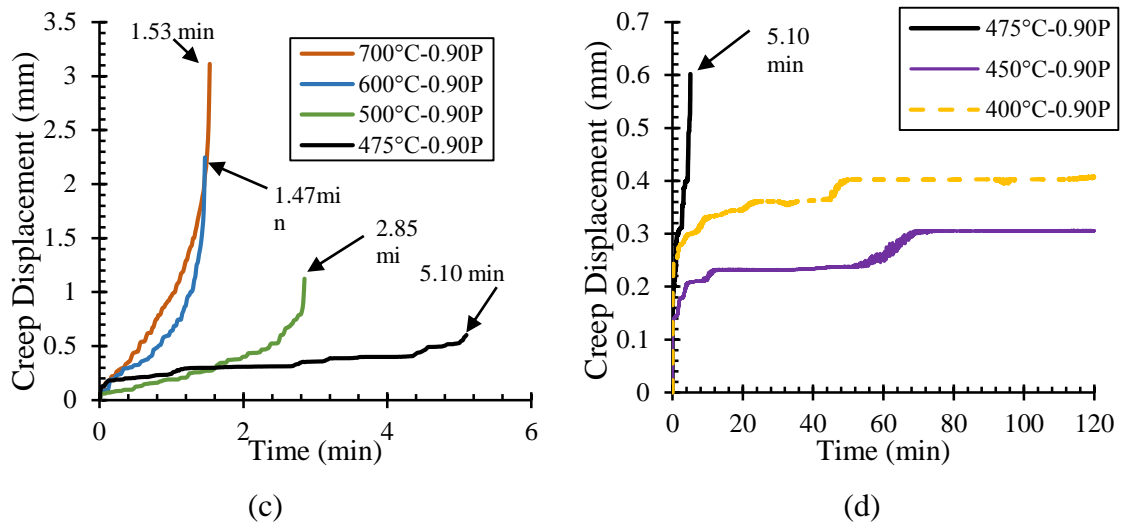


Fig. 21. Effect of temperature on thermal creep response of transverse welded lap joints

Table 5. Test matrix of creep tests conducted on transverse welded lap joints at elevated temperatures

Test Name	Temperature °C	Peak load (kN)	Applied load (kN)	Peak load ratio	Failure time (min)
400°C-0.90P	400	71.32	64.40	0.90	-
450°C-0.90P	450	59.01	53.20	0.90	-
475°C-0.90P	475	60.03	54.02	0.90	5.10
500°C-0.50P	500	44.29	23.13	0.52	-
500°C-0.75P	500	44.29	33.20	0.75	-
500°C-0.80P	500	44.29	35.42	0.80	-
500°C-0.90P	500	44.29	39.80	0.90	2.85
600°C-0.50P	600	31.59	15.80	0.50	-
600°C-0.60P	600	31.59	18.34	0.58	95.12
600°C-0.75P	600	31.59	23.70	0.75	19.25
600°C-0.90P	600	31.59	27.44	0.87	1.47

700°C-0.50P	700	15.55	7.77	0.50	-
700°C-0.60P	700	15.55	9.31	0.60	8.85
700°C-0.75P	700	15.55	11.62	0.75	5.07
700°C-0.90P	700	15.55	13.85	0.89	1.53

5. Connection Creep Curve Response

The classical creep curve presented in Fig. 1 is typically resulted from a tensile coupon test of steel base material under constant load and temperature. However, the creep of steel becomes more complex in case of connections, where different material types and interactions between components are included. Figure 22 shows different shapes of creep curves for transverse welded lap joints resulted from the experimental work. Figure 22 (a) presents the creep curves for cases where creep is not significant or unlikely to happen. It can be seen that the creep curve in Fig. 22(a) is a summation of a consecutive *minor* creep curves combined together. These *minor* creep curves are only consisted of primary and secondary stages of a classical creep curve (Fig. 1). This phenomenon is due to the fact that when creep is not that significant, the mobility of atoms is *low* and each connection component is said to creep alone *in a low rate*. Moreover, since the creep deformation is irreversible, component creep displacements will accumulate until failure occurs at a particular point in time. Figure 22(b) shows a creep curves for a case where temperature can dominate the creep behavior of the welded specimen (700°C) as subjected to low stress level (0.50P). In this curve, the primary stage can barely be noticeable, however, the welded specimen undergoes a perfect steady state creep-displacement (secondary stage) where creep-displacement rate is constant. Figure 22(c) represents a creep curve that set between the two previous

cases presented in Figs. 22(a) and 22(b). More specifically, the creep curve in Fig. 22(c) comprises of *minor* creep curves combined together to form a classical creep curve of primary and secondary stages. Finally, Fig. 22(d) represents a creep curve for a case where both temperature and stress level significantly control the thermal creep behavior of transverse welded lap joints (700°C-0.90P). In this case, the curve shows a classical creep curve with primary, secondary, and tertiary stages. This is due to the fact that at high temperature and load level the lap joint acts as a single unit subjected to a constant tensile stress.

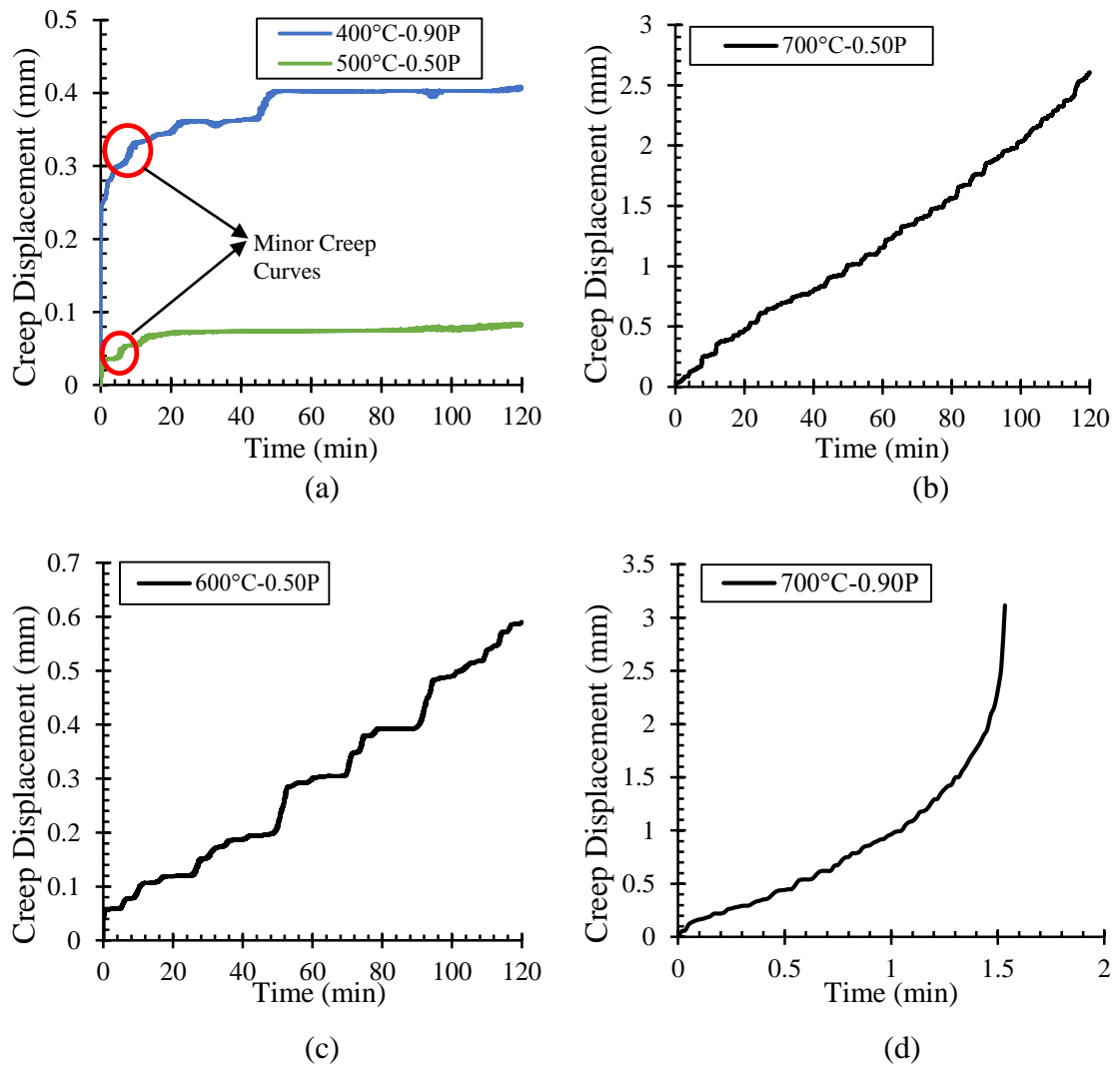


Fig. 22. Creep curves at different load and temperature conditions

6. Isochronous Behavior of Transverse Welded Lap Joint

In order to deeply understand the creep behavior of transverse welded lap joints at elevated temperature, inter-relations among stresses, creep displacements, temperatures, and time are required. To address this issue, the creep curves obtained at a specified load and temperature can be presented in a way to depict the variation of stress or temperature with creep displacement at any specific time. This type of depiction is referred to isochronous representations.

a. Isochronous Behavior under Constant Temperature and Variable Loads

The results obtained from the tests conducted at a constant temperature with different peak load ratios (Fig. 20) can be presented in the so-called isochronous axial load-creep displacement curves. This isochronous representation is defined as the axial load-creep displacement characteristics of transverse welded lap joint at different time values for a given temperature. Figure 23 represents the isochronous axial load- creep displacement behavior of the transverse welded lap joint at 600°C with peak load ratios ranging from 0.50P to 0.90P. It indicates that at a specific time, larger connection creep displacement can be obtained for larger applied loads. Also, it can be seen that for tests subjected to loads greater than 0.60P, the creep displacement rate increases rapidly with time to fail at *19 min and 15 sec* after 0.75P is applied, and becomes very fast (*1min and 28 sec*) for 0.90P load application. This indicates that for temperatures that set between 500°C and 700°C, both stress and temperature levels combined can dominate the creep behavior of the transverse welded lap joint.

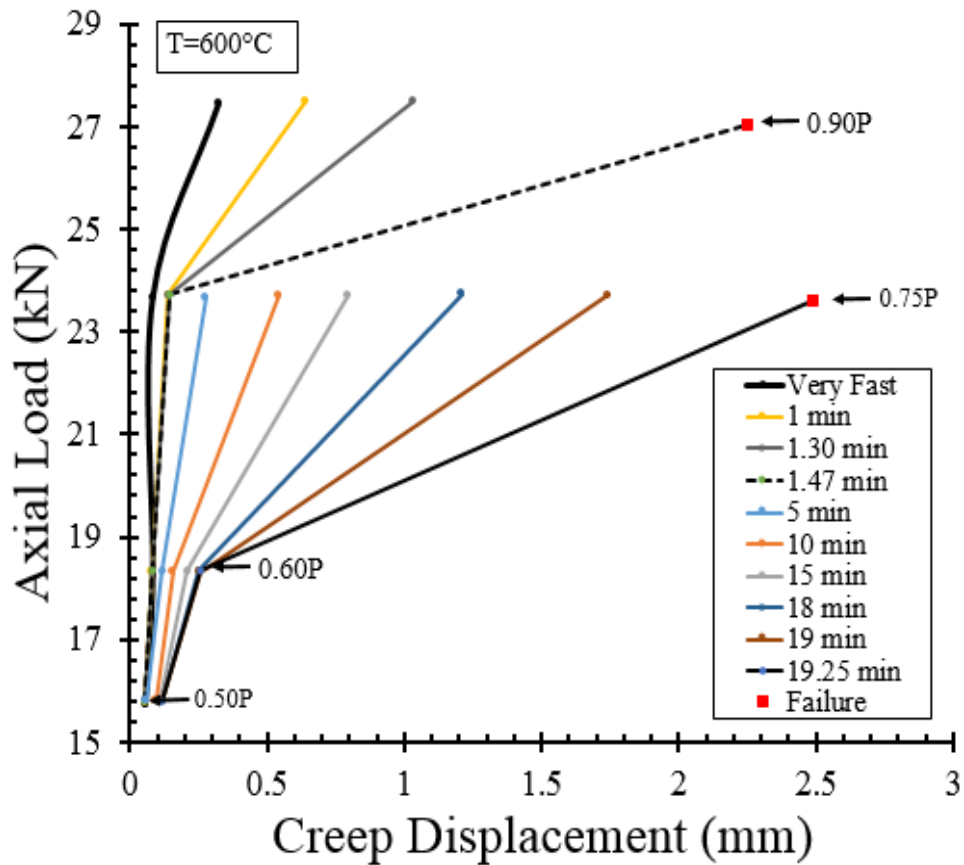


Fig. 23. Isochronous axial load- creep displacement curves for transverse welded lap joint at 600°C

b. Isochronous Behavior under Constant Load Ratio and Variable Temperature

The results shown in Fig. 21 can be represented in the form of isochronous creep displacement-temperature curves. This representation is defined as the creep displacement-temperature curves at different specified times for a given peak load ratio. To construct such type of isochronous response, a wide range of time plots is needed. Therefore, all tests conducted at 0.50P were used, since no creep fracture occurred during the 120 min time duration. Fig. 24 represents the isochronous creep displacement versus temperature response at 0.50P. Recall that, although the curves in Fig. 24 correspond to 0.50P at each temperature, the actual applied load is different from one temperature to another. When the transverse welded lap joint is subjected to a constant

applied load of 0.50P, it undergoes larger creep displacements for higher temperatures (Fig. 24). Also, it can be seen that the effect of temperature on the thermal creep response is not that significant for temperatures below 600°C. More specifically, the difference in creep displacement (Δ_c) resulted from 60 and 120 min time plots at 500°C is almost zero ($\Delta_c=0.009$ mm). As temperature increases to 600°C, Δ_c increases in a slow rate to 0.29 mm. At temperatures where creep starts slightly to occur, atoms become quite mobile resulting in the occurrence of creep at a slow rate. However, for larger temperatures (700°C) the welded specimen tends to creep in a fast rate due to the high activation of atoms mobility where Δ_c increases rapidly from 0.29 mm at 600°C to 1.45 mm at 700°C.

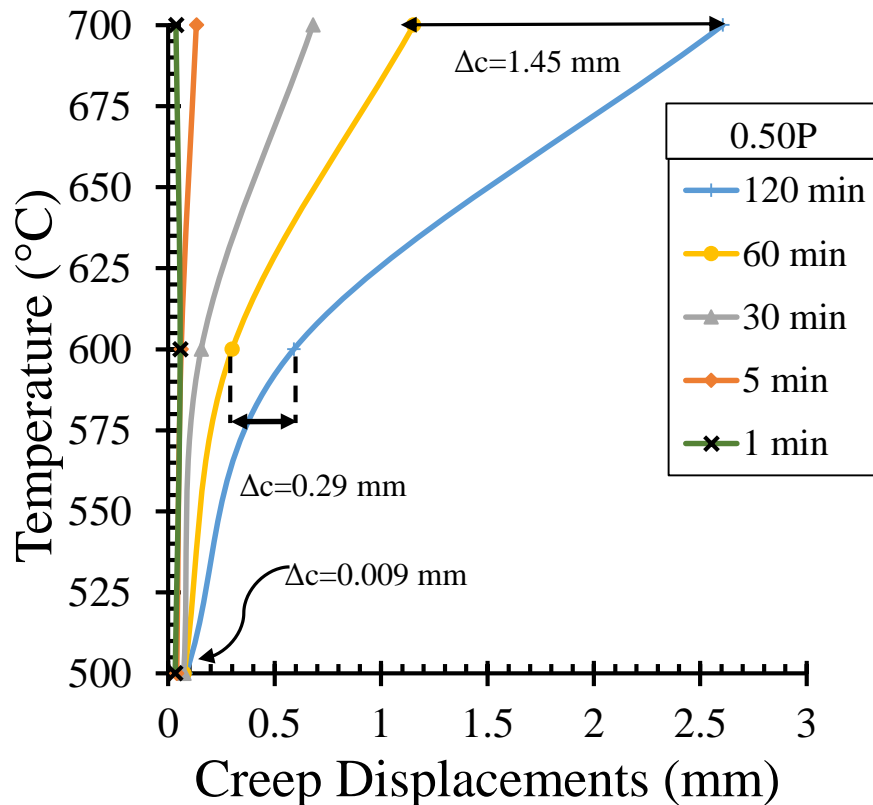


Fig. 24. Isochronous creep displacement-temperature response at 0.50P

CHAPTER IV

CREEP MODELING OF TRANSVERSE WELDED LAP JOINTS EXPOSED TO FIRE TEMPERATURES

A. Methodology

In this section a methodology is presented for the development of two creep models for the welds and the steel base material that are capable of predicting the thermal creep behavior of transverse welded lap joints. This methodology is based on the experimental program of the explicit thermal creep effect on transverse welded lap joints conducted as a part of this research work. The creep curves presented previously were first used to develop a *Norton-Bailey* power law creep equation for the welded lap joints. Then, two creep models for the welds and steel base material were proposed by introducing temperature-dependent scaling factors to the *Norton-Bailey* power law creep equation of the welded lap joints. Finite element (FE) simulations were then developed in ABAQUS [42] to predict the thermal creep behavior of the welded lap joint using the two proposed creep models for the welds and the steel base material. The two creep models were then calibrated by changing the power law creep constants in order to predict the experimental creep curves with reasonable accuracy. Also, another series of FE simulations was conducted using Fields and Fields creep model [38] for the steel base material instead of the proposed one for comparison purposes. The fillet weld and structural steel creep models will be intended to support the development of modeling the creep behavior of large-scale welded connections for structural-fire engineering application.

B. Proposed Creep Model

1. Power Law Equation Constant Estimation

Two creep models for the fillet welds and steel base material used in the transverse welded lap joints were developed. Through a regression analysis, the power law creep constants for the welded lap joint creep model were first estimated to best fit the experimental creep curves (Fig. 20 and 21). A *Norton-Baily* power law equation [39] was used as a given function in the regression analysis and is presented as follows:

$$\varepsilon_{cr} = A\sigma^n t^m \quad (3)$$

Where ε_{cr} is the creep strain, σ is the applied stress, t is time, and A, m , and n are the temperature-dependent constants for the creep model of the transverse welded lap joint. The regression analysis was developed by considering the time-hardening approach as per [45]. The general power law regression curve fitting can be written as per [45]:

$$y = Bx^c \quad (4)$$

Where y can be ε_{cr} , x can be either the σ or t , and B and C can be calculated through regression equations as follows where k is the number of points selected from the creep curve:

$$c = \frac{k \sum_{i=1}^k (\ln x_i \ln y_i) - \sum_{i=1}^k (\ln x_i) \sum_{i=1}^k (\ln y_i)}{k \sum_{i=1}^k (\ln x_i)^2 - (\sum_{i=1}^k \ln x_i)^2} \quad (5)$$

$$B = e^{\frac{\sum_{i=1}^k (\ln y_i) - c \sum_{i=1}^k (\ln x_i)}{k}} \quad (6)$$

To get the power law constants, the *Norton-Baily* power law equation [39] can be written as:

$$\varepsilon_{cr} = (A\sigma^n)t^m \quad (7)$$

Then by comparing Eq. 7 to Eq. 4, the results will be:

$$B = A\sigma^n \quad (8)$$

$$t^m = x^c \quad (9)$$

Therefore, m is equal to C , and by replacing x and y by t and ε_{cr} , respectively, m will be as follows:

$$m = \frac{k \sum_{i=1}^k (\ln t_i \ln \varepsilon_{cr_i}) - \sum_{i=1}^k (\ln t_i) \sum_{i=1}^k (\ln \varepsilon_{cr_i})}{k \sum_{i=1}^k (\ln t_i)^2 - (\sum_{i=1}^k \ln t_i)^2} \quad (10)$$

To compute n in Eq. 3, the *Norton-Baily* equation [39] can be also written as follows:

$$\varepsilon_{cr} = (At^m)\sigma^n \quad (11)$$

Thus, by comparing Eq. 11 to Eq. 4, the results will be,

$$B = At^m \quad (12)$$

$$x^c = \sigma^n \quad (13)$$

Therefore, in this case, n is equal to C (Eq. 5) and by replacing x and y by σ and ε_{cr} , respectively, n will be as follows:

$$n = \frac{k \sum_{i=1}^k (\ln \sigma_i \ln \varepsilon_{cr_i}) - \sum_{i=1}^k (\ln \sigma_i) \sum_{i=1}^k (\ln \varepsilon_{cr_i})}{k \sum_{i=1}^k (\ln \sigma_i)^2 - (\sum_{i=1}^k \ln \sigma_i)^2} \quad (14)$$

To get n in Eq. 14, at least two creep curves having different constant load applied should be used so that the dominator in Eq. 14 is not equal to zero. Finally, to get A , the *Norton-Baily* equation [39] can be written in another way as follows:

$$\varepsilon_{cr} = A(\sigma^n t^m) \quad (15)$$

In this case, the findings will be:

$$A = B \quad (16)$$

$$(\sigma^n t^m)^1 = x^c \quad (17)$$

Therefore, Eq. 6 can be applied and by replacing y by ε_{cr} , x by $(\sigma^n t^m)$ and C by 1, the constant A will be:

$$A = e^{\frac{\sum_{i=1}^k (\ln \varepsilon_{cr_i}) - 1 \sum_{i=1}^k (\ln(\sigma^n t^m)_i)}{k}} \quad (18)$$

2. Power Law Regression Application

This proposed method was applied first to predict the temperature-dependent constants A , m , and n for the *Norton-Baily* power law creep equation of the transverse welded lap joints. To estimate n in Eq. 14, it is required to have at least two different creep tests at a same temperature with two different peak load ratios. However, for tests conducted at a specified temperature with only one peak load ratio (0.90P-400°C, 0.90P-450°C, 0.90P-475°C), n in Eq. 14 is not valid with zero denominator. Therefore, n in these cases can be assumed to be any number and accordingly A in Eq. 18 is calculated. Further, some assumptions were considered in this power law regression analysis. The stress σ in Eq. 3 was assumed to be the stress applied by the *MTS-810*

machine on one side of the welded specimen as shown in Fig. 25. Also, the creep strain, ε_{cr} , was computed by dividing the creep displacement measured from the crossheads of the *MTS-810* machine to the total length of the welded specimen.

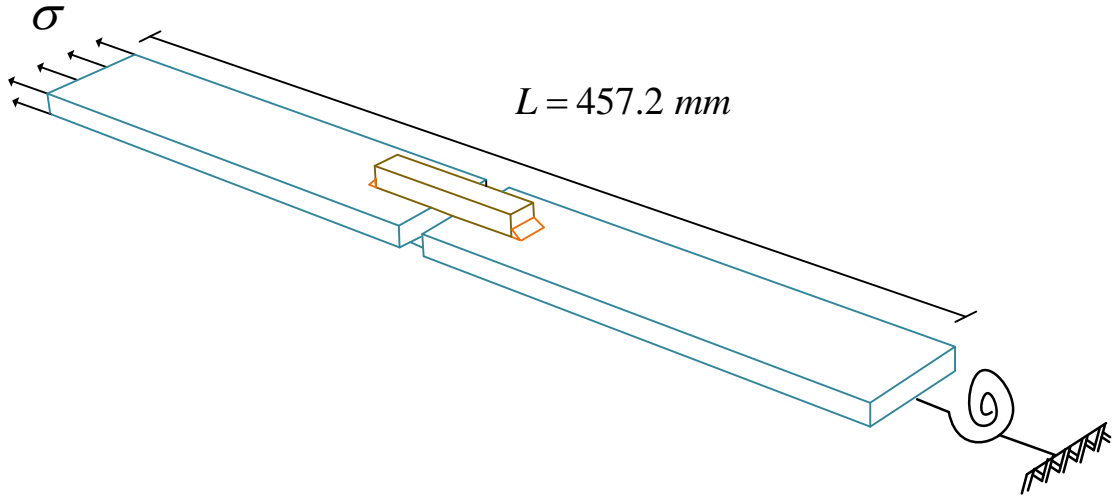


Fig. 25. Assumptions used for creep model of the transverse welded lap joint

After doing all the power law regression analysis (Eqs. 10, 14, and 18), the *Norton-Baily* constants for the transverse welded lap joint are tabulated in Table 6, where A is in $Gpa^{-n} \min^{-m}$, and n and m are unitless. These constants of the power law equation were used to predict only the primary and secondary stages of a typical creep curve of the welded lap joint. Therefore, in order to predict the tertiary part of the creep curve, an additional damage parameter, W , was introduced to the original creep power law equation of the welded lap joint (Eq. 3) as per [41] and it is as follows:

$$\varepsilon_{cr} = A \left(\frac{\sigma}{1-w} \right)^n t^m \quad (19)$$

The damage parameter, W , can be also calculated as :

$$w(t) = 1 - \left(1 - \frac{t}{t_f + e}\right)^l \quad (20)$$

Where w is approximately zero or an ineffective value in estimating the creep displacement at the primary and secondary stages. However, it starts rapidly to increase at time at which failure initiates “ t_f ”. That means, w is equal to 1 immediately after t_f and consequently ϵ_{cr} is infinity. Therefore, a finite time value, e , equals to 1 msec is added to t_f in Eq. 20 to get a valid number of $\epsilon_{cr}(t_f)$ with $w(t_f)$ less than 1. Also, l is a temperature-dependent constant that can be calculated as follows:

$$l = \frac{\log\left(1 - \left(1 - \frac{\sigma}{\left(\frac{\epsilon_{cr}(t_f)}{At_f^m}\right)^{\frac{1}{n}}}\right)\right)}{\log\left(1 - \frac{t_f}{t_f + e}\right)} \quad (21)$$

The value of l was selected within the range of values that were calculated at each temperature using Eq. 21 with different load ratios to best fit the tertiary part of the creep tests and is tabulated in Table 6.

Table 6. Power law creep constants for the transverse welded lap joint

Temperature (°C)	A	n	m	l
400	0.365991	2.80	0.094256	N/A
450	0.302329	2.73	0.143422	N/A
475	1.270727	3.10	0.249102	0.010471835
500	3.012700	3.1408	0.188200	0.03809
600	47870.00	5.557	0.611500	0.014501

700	25138590	5.99445	0.864753	0.016
-----	----------	---------	----------	-------

By substituting A , m , n and W in Eq. 19 and multiplying with the total length of the specimen L , the creep displacement of transverse welded lap joints, Δ_{cr} , can be calculated as follows:

$$\Delta_{cr} = \varepsilon_{cr} \times L = A\varepsilon_{cr} = A\left(\frac{\sigma}{1-w}\right)^n t^m L \quad (22)$$

Therefore, by plotting Δ_{cr} with time, creep curves based on time-hardening *Norton-Baily* power law regression analysis for the transverse welded lap joint are presented in Figs. 26 to 29. It can be seen from Figs. 26 to 29, the proposed creep model matches with reasonable accuracy the experimental creep curves. For Fig. 26, it can be shown that the creep model predicts the experimental results more precisely than those shown in Figs. 27 to 29. This is because, for temperatures equal or below 475°C, only one load ratio is applied at each temperature. In other words, the power law creep constants proposed for temperatures equal or below 475°C (Table 6) are considered to be a stress- and temperature-dependent creep constants. However, since creep of steel at temperature below 475°C is not likely to occur, these constant can be used for peak load ratios other than that of 0.90P. Nevertheless, in some cases like Figs. 28(c) and 29(b) there is a difference between the creep model predictions and the experimental results. This is due to the fact that creep tests are very sensitive, and the creep model constants are temperature-dependent only. Also, the prediction of the tertiary part is highly dependent on the failure time and due to the lack of data, it is still complex to get exactly the tertiary part of the creep curves under different load ratios. Further, 0.75P-500°C is neglected in the creep model predictions because the creep model is highly

dependent on stress level. Therefore, 0.80P was chosen instead, since stress level of 0.75P and 0.80P are close to each other.

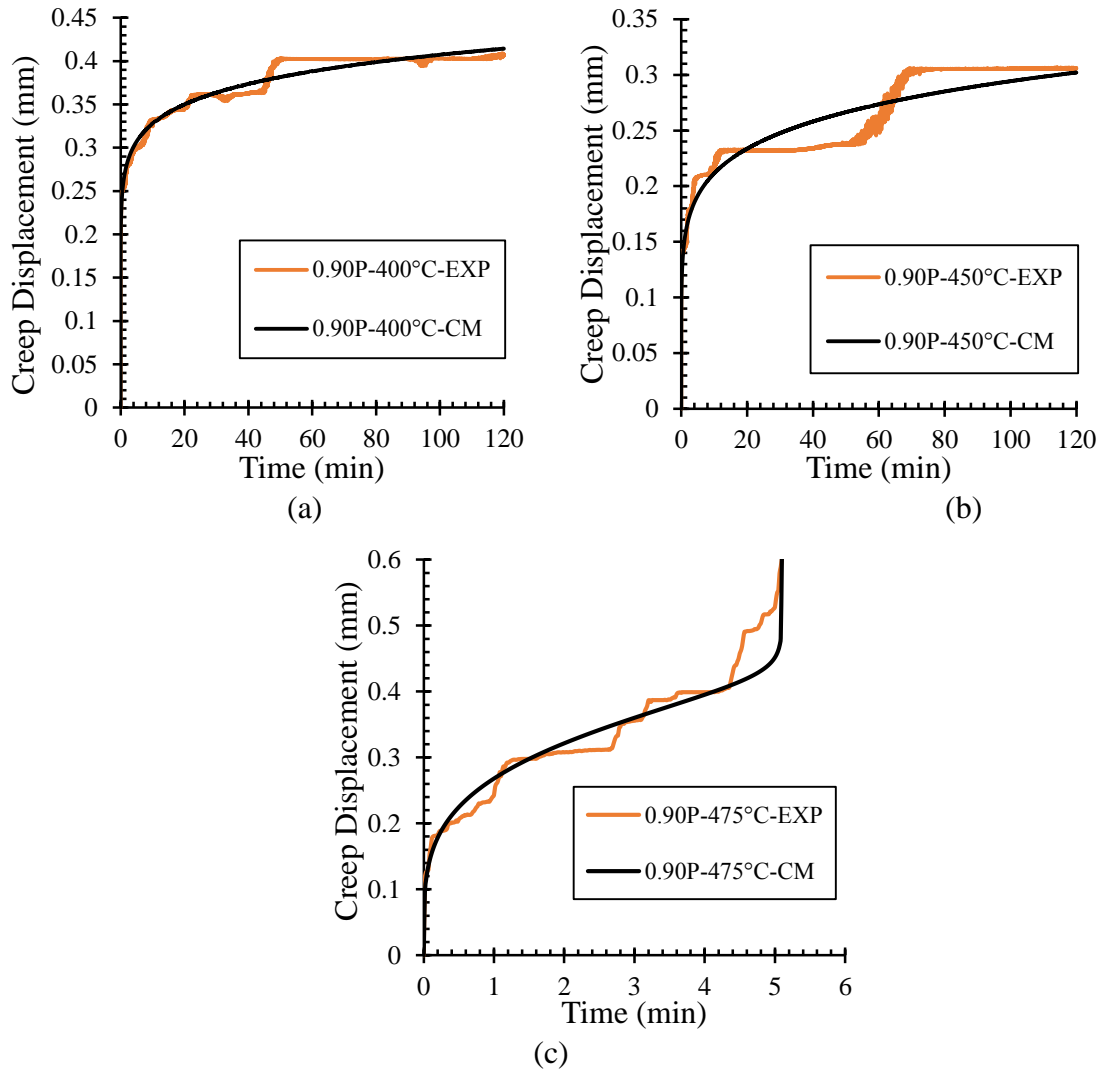
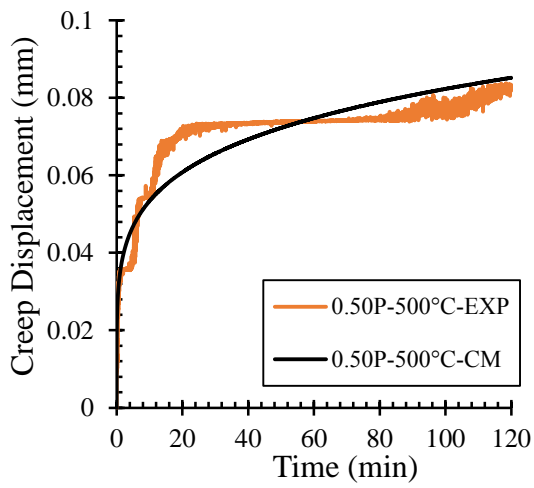
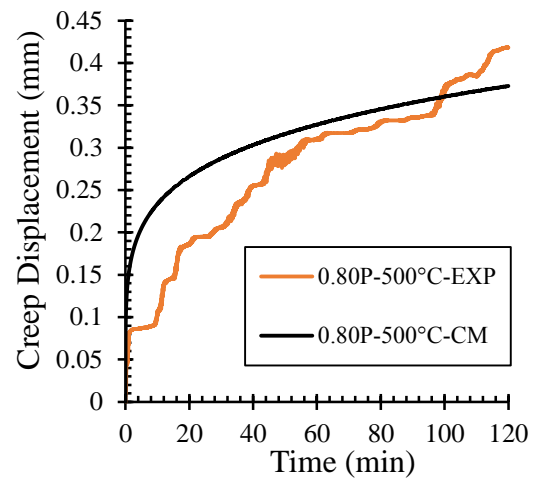


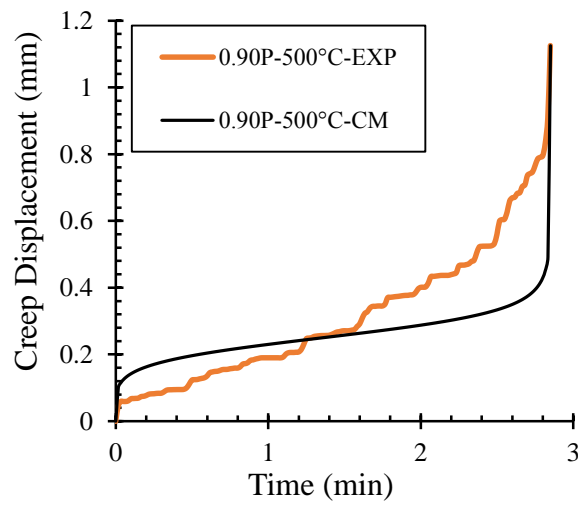
Fig. 26. Creep model versus experimental results at: (a) 400°C, (b) 450 °C, (c) 475 °C



(a)

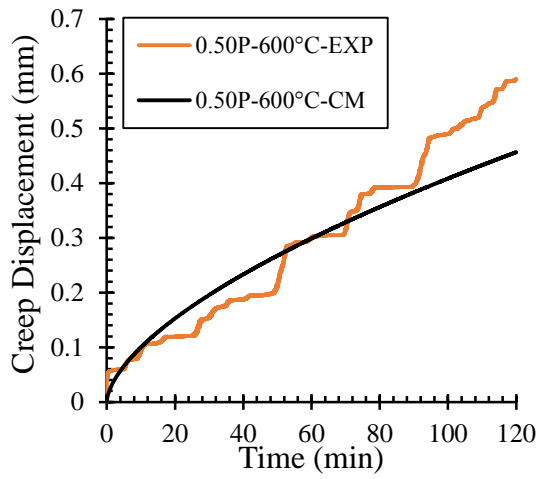


(b)

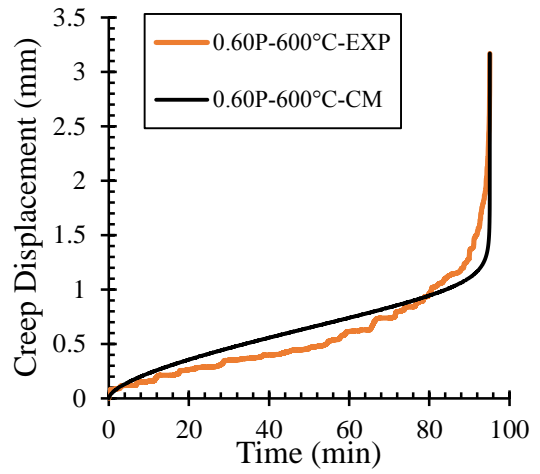


(c)

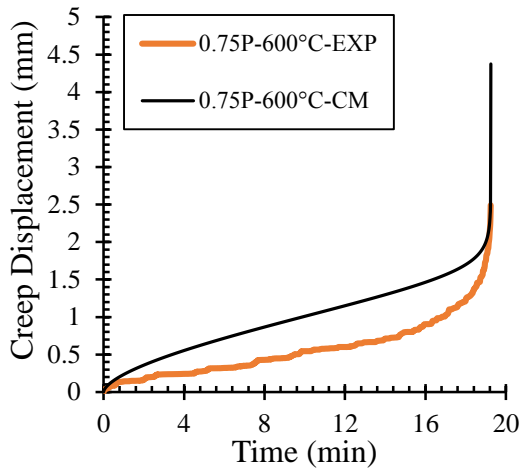
Fig. 27. Creep model versus experimental results at 500°C for: (a) 0.50P, (b) 0.80P, (c) 0.90P



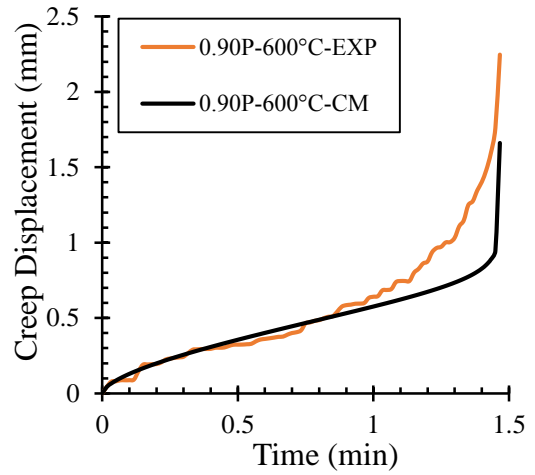
(a)



(b)



(c)



(d)

Fig. 28. Creep model versus experimental results at 600°C for: (a) 0.50P, (b) 0.60P, (c) 0.75P, (d) 0.90P

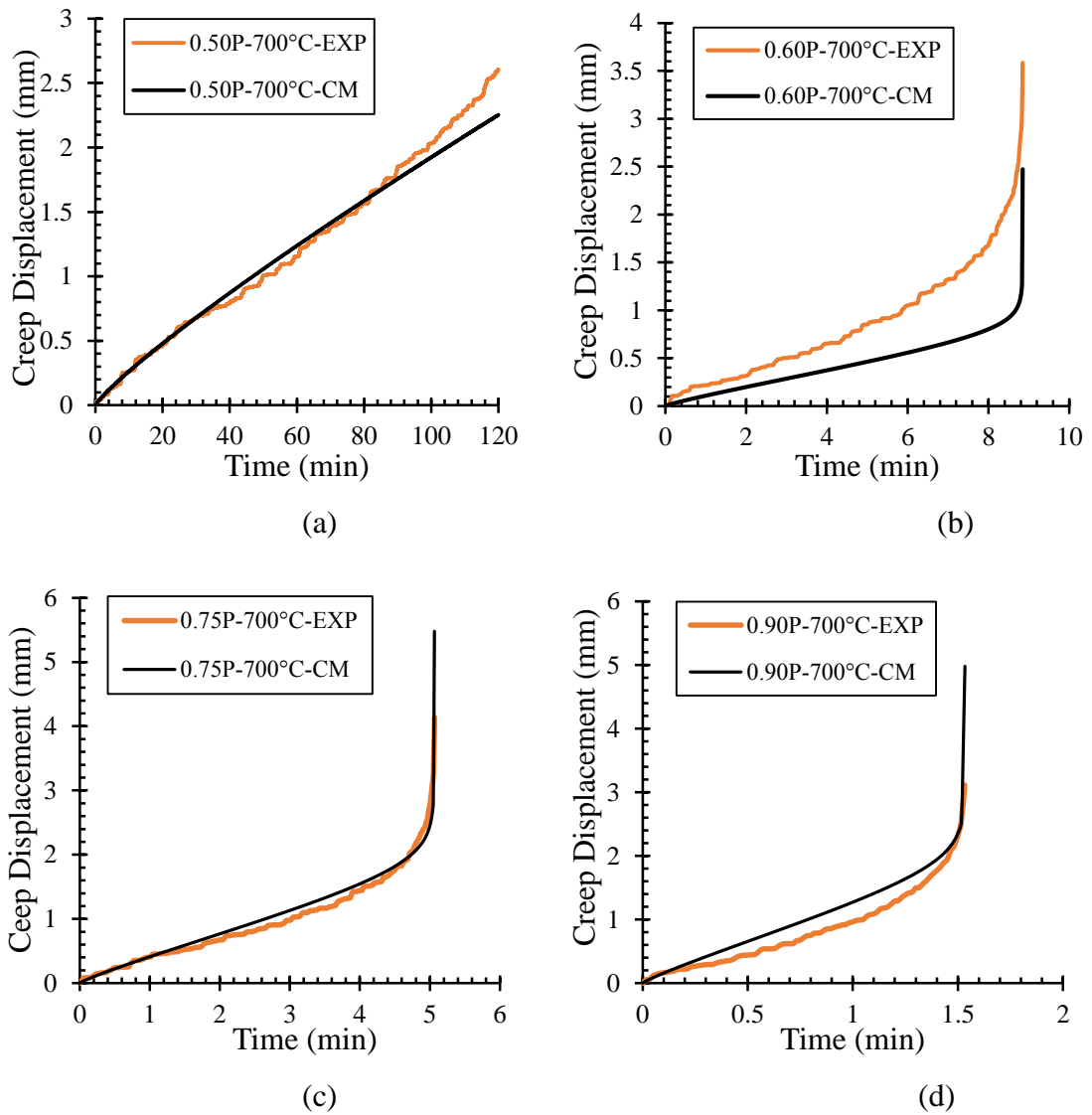


Fig. 29. Creep model versus experimental results at 700°C for: (a) 0.50P, (b) 0.60P, (c) 0.75P, (d) 0.90P

C. FE Modeling

The numerical analysis of the transverse welded lap joints was carried out using ABAQUS [42]. Two series of FE simulations were conducted to reproduce the experimental results of the fast loading tests and creep tests for the transverse welded lap joints. In this section, the FE simulations of the transverse welded lap joints are briefly described.

1. Boundary Conditions

Boundary conditions were applied to the connection elements throughout the analysis. During the loading step, the specimen was connected, from one side, with a spring that represents the *MTS-810* machine stiffness as shown in Fig. 30. In order to evaluate the *MTS-810* machine stiffness, a series of FE simulations with springs of different values were conducted until the FE simulation matched the experimental result at ambient temperature test. Once the spring stiffness was estimated, it was then used for all FE simulations for all elevated temperatures for both analysis (fast and creep tests). The spring stiffness used is equal to 140 kN/mm to represent the machine stiffness. All nodes at both ends were fixed against any translation or rotation except they were free to move in the axial direction.

2. Model Discretization

The connection components were meshed with eight-node brick elements with reduced integration (C3D8-R) as shown in Fig. 30. To improve the accuracy of predictions, a finer mesh was used around the connection region, where failure is likely to occur. Moreover, to account for the stress concentration around the weld region, a mapped meshing technique was used to discretize the fillet welds and their surrounding areas. The surface interactions between the middle plates and the top and bottom plates were modeled using finite sliding, with a friction coefficient of 0.25. Also, tie constraint technique was used to model the contact surfaces between the fillet welds and the structural steel plates as shown in Fig. 30.

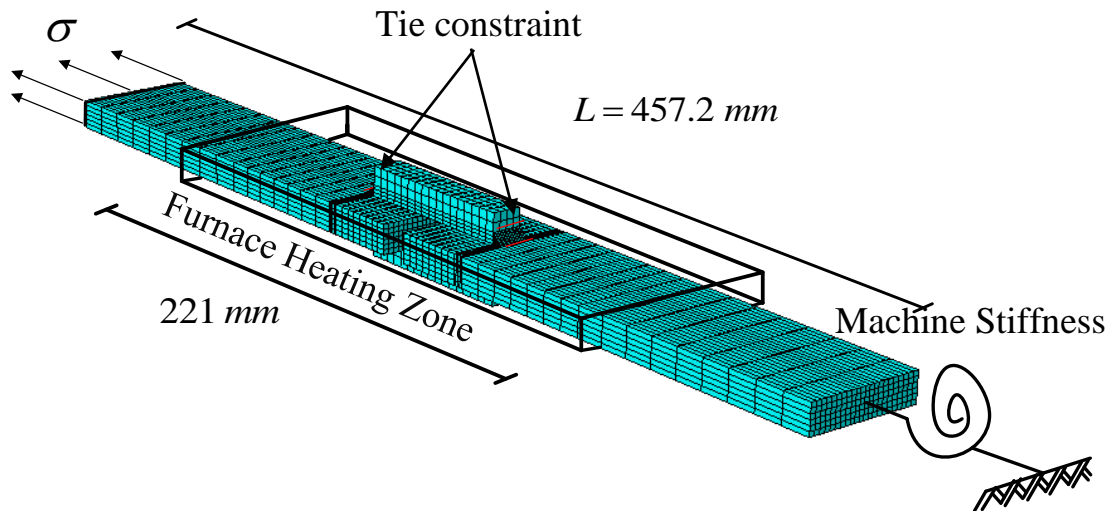


Fig. 30. Transverse welded lap joint model used in ABAQUS [42] simulations

3. Material Properties and Modeling Considerations

An idealized bilinear stress-strain relationship with isotropic hardening was used to model the mechanical behavior of both fillet welds and structural steel. Strength retention factors proposed by Hu et al. [27] with a rate of 0.254 mm/min were used to model the stress-strain characteristics of the structural steel at elevated temperatures. Hu et al. steel base material properties [27] were used since they examined the role of strain rate in coupon tension loading tests for ASTM A992 at elevated temperatures that it is close to ASTM A529 Gr.50. However, for the weld material, the retention factors were calculated from the peak loads predicted in the time-independent fast loading analysis and used in the FE simulations.

4. Creep Modeling

The main purpose of conducting the FE models is to predict the explicit creep behavior of the transverse welded lap joints when subjected to a constant load and a specified temperature. Therefore, two creep material models were proposed and

included in the mechanical properties of the weld and the steel base materials for the welded lap joint. The creep models for the fillet welds and steel base material were included in the FE model within the furnace heating zone only as shown in Fig. 30. This is because creep of steel is highly dependent on temperature especially for temperatures larger than 400°C. However, for the unheated parts of the connection, creep is not significant. In order to model the creep behavior of the weld and steel base materials, an appropriate scaling for the *Norton-Baily* creep equation of the transverse welded lap joint (Eq. 3) was conducted. Similar scaling approach was used by the National Institute of Standard and Technology (NIST) [40] for predicting the creep behavior of steel materials other than ASTM A36 using Fields and Fields creep equation [38]. Therefore, the creep models for both welds and steel base material are as follows:

a. *For the weld material:*

$$(\varepsilon_{cr})_w = A(0.6\sigma)^n t^m \quad (23)$$

Where $(\varepsilon_{cr})_w$ is the creep strain for the weld material, and 0.6 is the scaling factor and it is chosen since the fillet welds failed in shear. Therefore, the temperature-dependent power law creep constants for the weld material are as follows:

$$A_w = A(0.6)^n$$

(24)

$$n_w = n \quad (25)$$

$$m_w = m \quad (26)$$

b. *For the steel base material:*

$$(\varepsilon_{cr})_s = A(R_\sigma \sigma)^n t^m \quad (27)$$

Where $(\varepsilon_{cr})_s$ is the creep strain for the steel base material, and R_σ is the temperature-dependent scale factor and can be calculated at each temperature T ($^{\circ}\text{C}$) as $(\frac{Fy_s}{Fu_w})_T < 1$. Where Fy_s and Fu_w are the steel material yield strength and ultimate weld strength, respectively. Therefore, the power law creep model for the steel base material can be also written as follows:

$$(\varepsilon_{cr})_s = A_s \sigma^{n_s} t^{m_s} \quad (28)$$

Where, A_s , n_s , and m_s are the temperature-dependent constants for the steel base material creep model and can be calculated as :

$$A_s = A(R_\sigma)^n \quad (29)$$

$$n_s = n \quad (30)$$

$$m_s = m \quad (31)$$

These two creep models for welds and steel base material were used in ABAQUS [42] simulations to predict the primary and secondary stages of the creep curves of the transverse welded lap joints at elevated temperatures. However, the tertiary creep stage was neglected in the FE simulations since it is highly dependent of the failure time for each test. Also, additional FE models were conducted where Fields and Fields creep model [38] was used for the structural steel creep material properties only for comparison purposes. It should be noted that Fields and Fields [38] is capable of predicting the primary and secondary stages of creep in the temperature range of 350 $^{\circ}\text{C}$ to 650 $^{\circ}\text{C}$ and for creep strains up to 6-percent.

5. Creep Models Calibration

The creep models for the welds and steel base material were provided based on the *Norton-Baily* power law creep equation for the transverse welded lap joint. These material creep models were calibrated using FE simulations to best fit the experimental creep curves at different load ratios and temperatures. To address this issue, the calibrated creep power law equation for the lap joint is as follows:

$$\varepsilon_{cr} = A' \sigma^{n'} t^{m'} \quad (32)$$

Where A' , n' , and m' are the calibrated creep constants for the creep model of the transverse welded lap joint. These constants were calibrated such that ε_{cr} of the lap joint is a constant value. That means, by equating Eq. 3 to Eq. 32 and changing only n' , the calibrated creep constants will be as follows:

$$A' = \frac{A\sigma^n}{\sigma^{n'}} \quad (33)$$

$$m' = m \quad (34)$$

The stress σ in Eq. 33 can be randomly selected. Although A' is dependent on σ , A' is calibrated as n' is changing only. That means, A' , n' , and m' are temperature-dependent creep constants for the calibrated creep model of the transverse welded lap joint. These calibrated creep constants were then scaled again as discussed in Eqs. 23 to 31. A series of FE simulations was conducted to calibrate the creep models for the weld and steel base materials and these constants are tabulated in Tables 7 and 8 for the welds and steel base material, respectively.

Table 7. Calibrated power law creep constants for the fillet weld material

Temperature (°C)	A_w	n_w	m_w
400	0.087557	2.80	0.094256
450	0.074961	2.73	0.143422
475	0.260808	3.10	0.249102
500	2.046608	3.65	0.188200
600	6.284234	3.65	0.611500
700	221.4650	3.80	0.864753

Table 8. Calibrated power law creep constants for the steel base material

Temperature (°C)	A_s	n_s	m_s	R_σ
400	0.014163	2.80	0.094256	0.313
450	0.020613	2.73	0.143422	0.374
475	0.060206	3.10	0.249102	0.374
500	0.812982	3.65	0.188200	0.466
600	2.059028	3.65	0.611500	0.442
700	94.28665	3.80	0.864753	0.479

6. FE Results

Representative results of FE analysis versus experimental results for fast tests under 0.254 mm/min are shown in Fig. 31. The experimental and FE predictions are in the form of load-displacement curves at ambient and elevated temperatures. Figure 31 shows that the FE simulations can predict with reasonable accuracy the strength, stiffness, and ductility when compared with the experimental results. Note that, fracture modeling was not included in the simulations and the FE models were not capable to

predict the test specimens behavior after the first component failure. Also, both the FE simulations and the experimental results show that all specimens failed by shear fracture at the throat of the fillet welds. Figures 32(a) and 32(b) show a comparison of actual deformed shape and failure modes observed in the experiments of the transverse welded lap joints performed at 500°C and 700°C, respectively, against the corresponding ones from the FE simulations. It can be seen that the FE simulations can predict closely the deformation response of the connection as well as its failure mode which is fracture at the throat of the fillet weld.

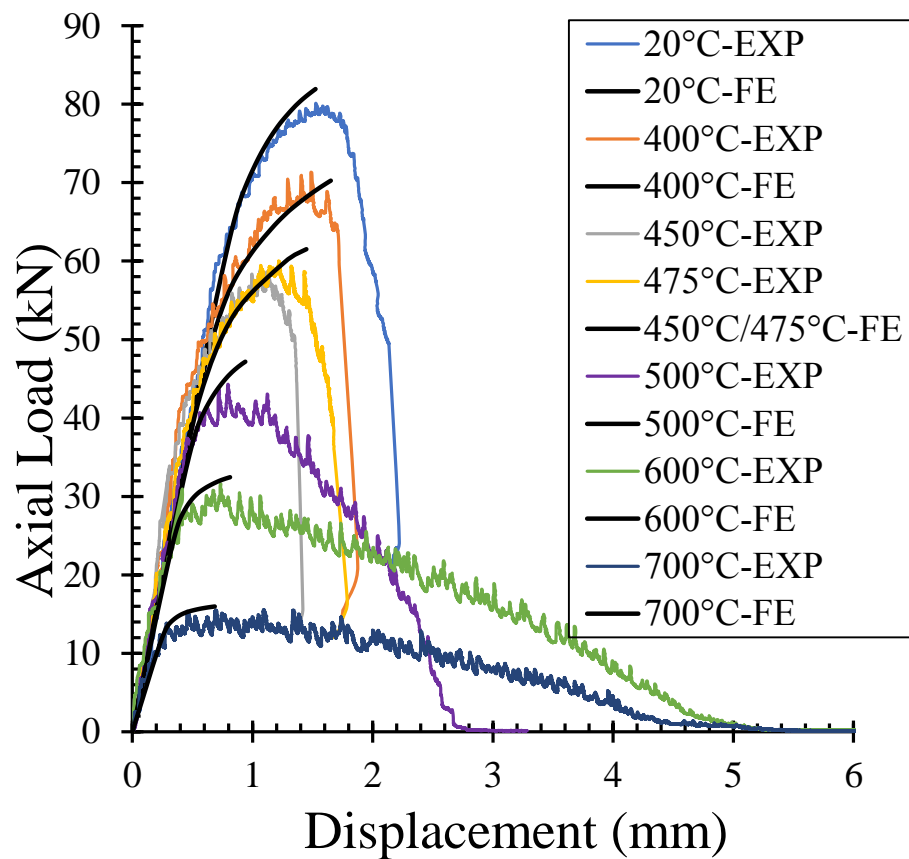


Fig. 31. FE results versus experimental results for the fast tests

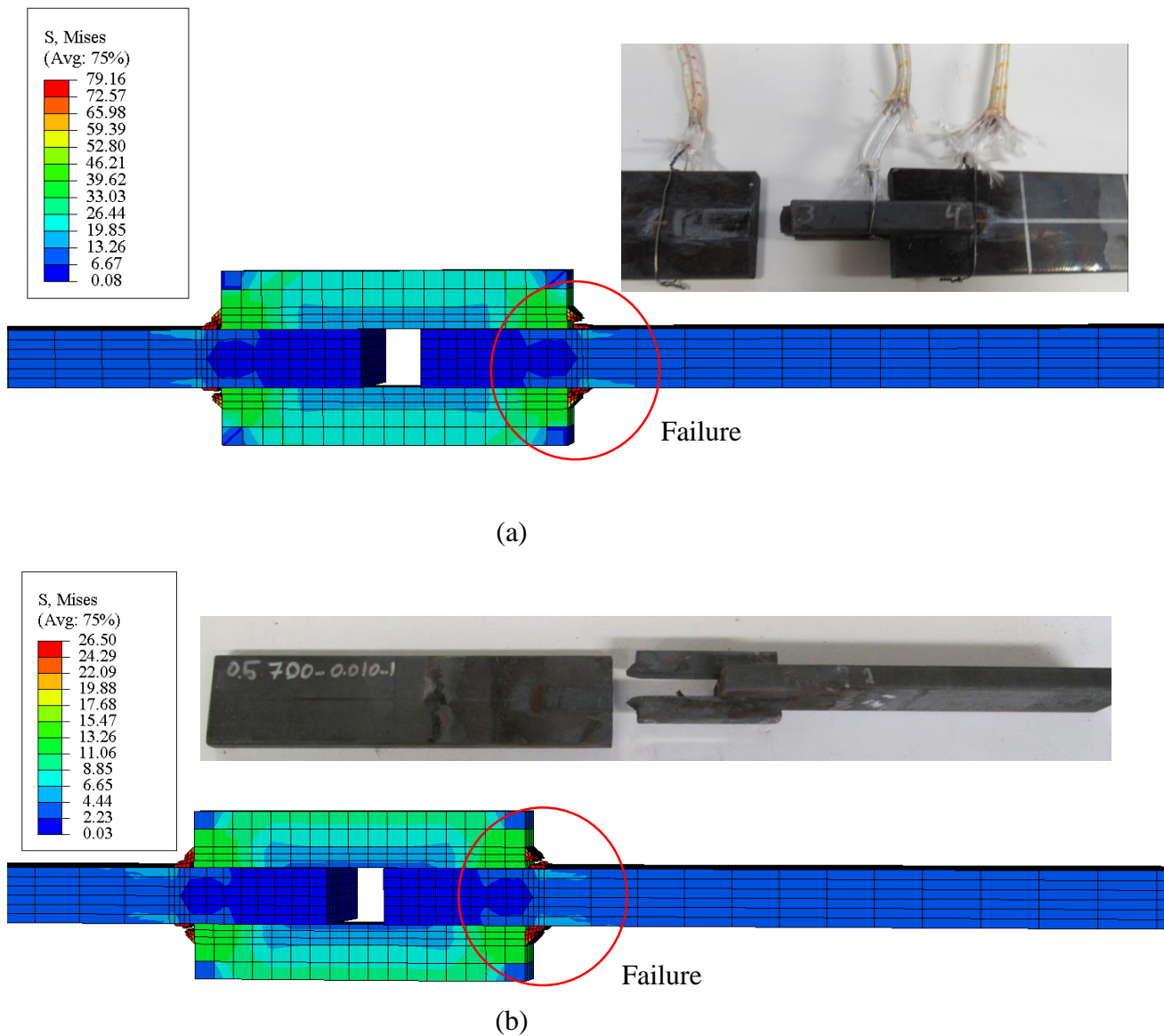
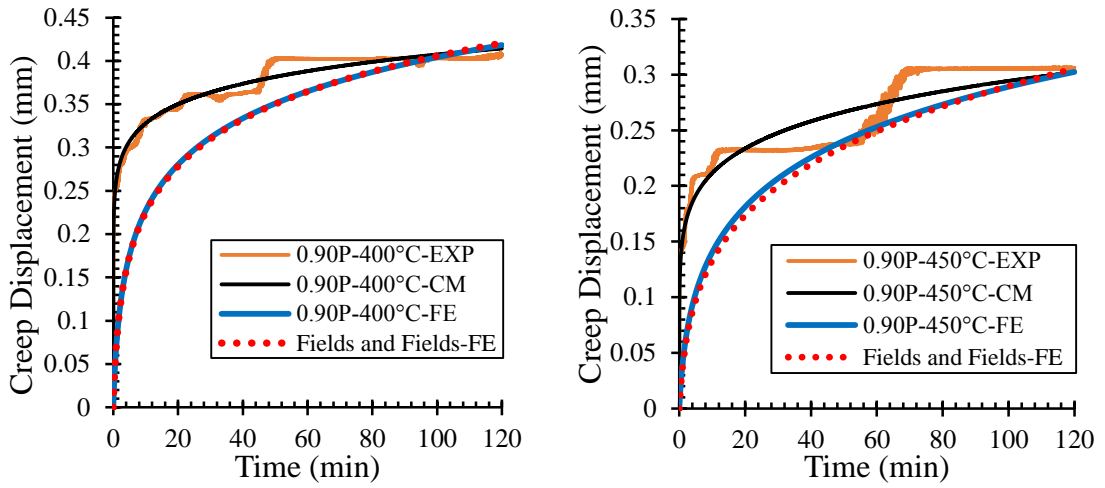


Fig. 32. FE versus experimental failure mode for fast tests analysis at: (a) 500°C (b) 700°C

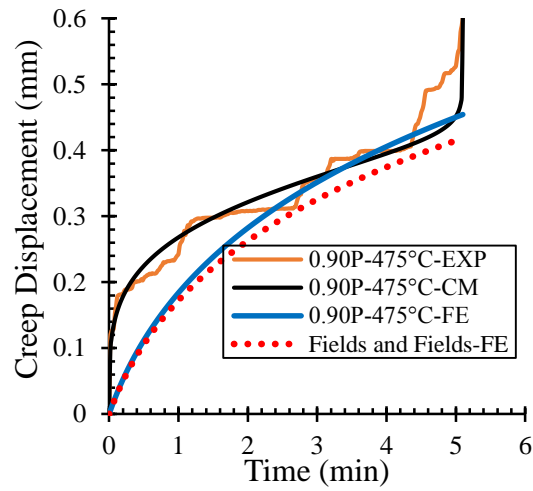
For the time-dependent creep analysis, representative FE results against the experimental ones as well as the transverse welded lap joint creep model are presented in Figs. 33 to 36. It can be seen from these figures that the calibrated creep models used in the FE simulations predict with reasonable accuracy the experimental results. This indicates that the assumptions and scaling factors used in the creep model are practical

to be used for different materials in other steel welded connections. The creep curves predicted using Fields and Fields creep model [38] are also compared with those predicted using the proposed creep model for the steel base material. Recall that, Fields and Fields creep model [38] cannot predict the creep behavior of steel base material at 700°C. Therefore, creep curves based on Fields and Fields [38] is disregarded in Fig. 36. Whereas for Fig. 33, the creep curves predicted by the proposed creep model and Fields and Fields [38] result in approximately same results for temperatures below 500°C. However, for 500°C and 600°C, the proposed creep model for the steel base material results in a more accurate prediction of the experimental creep curves than that of Fields and Fields [38] as shown in Figs. 34 and 35, respectively. Also, Figs. 34 to 35 indicate that Fields and Fields creep model and the proposed one for the steel base material can be used to predict the creep behavior of steel base material in welded connections. More experimental tests on large-scale steel connections are still needed to be conducted to develop a more general and accurate creep models for welds, bolts, and base materials.



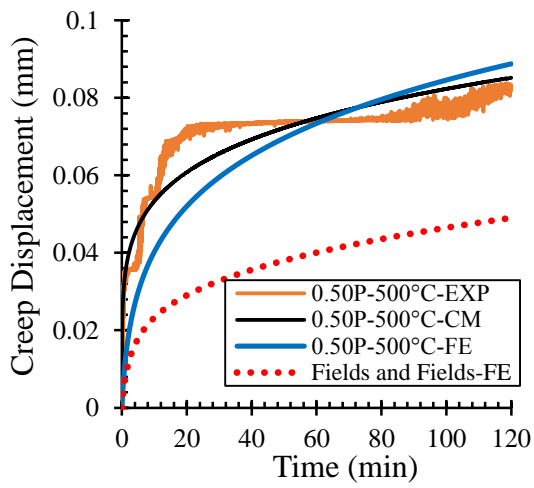
(a)

(b)

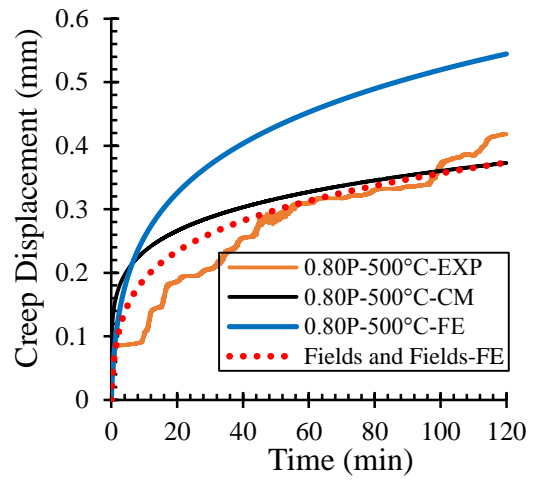


(c)

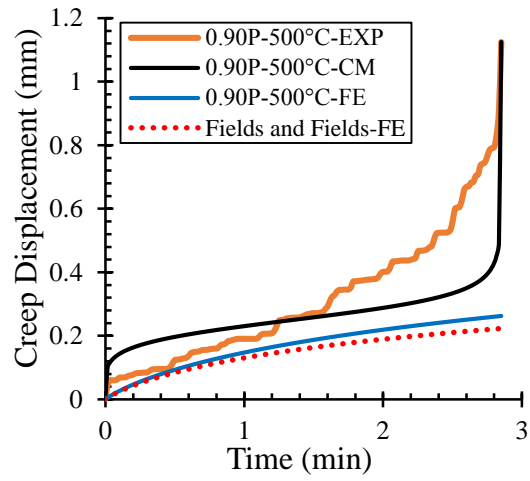
Fig. 33. Time-dependent results for FE and creep models versus experimental results for: (a) 400°C, (b) 450 °C, (c) 475 °C



(a)

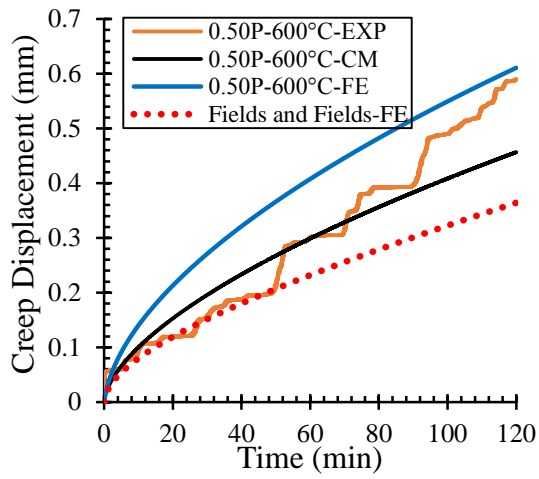


(b)

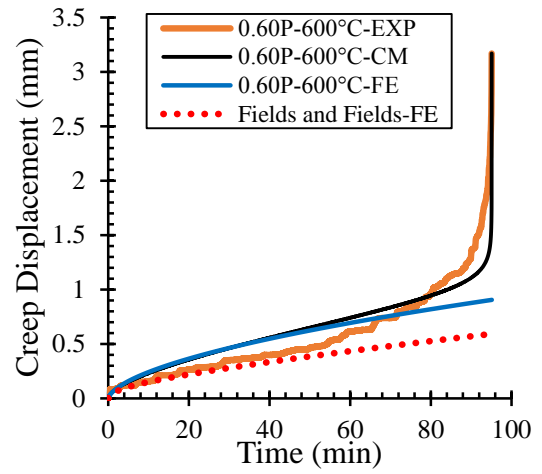


(c)

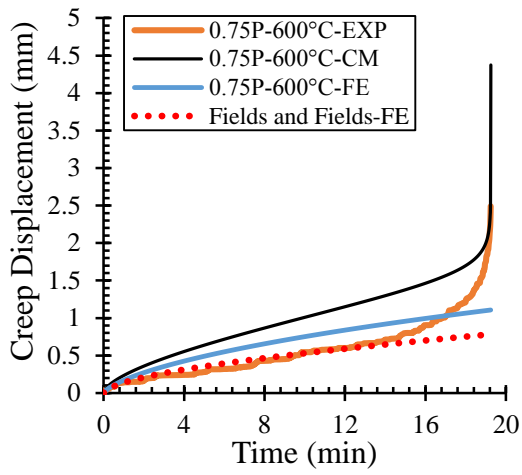
Fig. 34. Time-dependent results for FE and creep models versus experimental results at 500°C for: (a) 0.50P, (b) 0.80P, (c) 0.90P



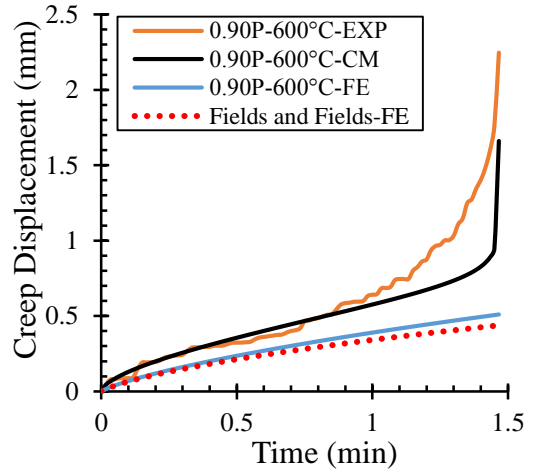
(a)



(b)

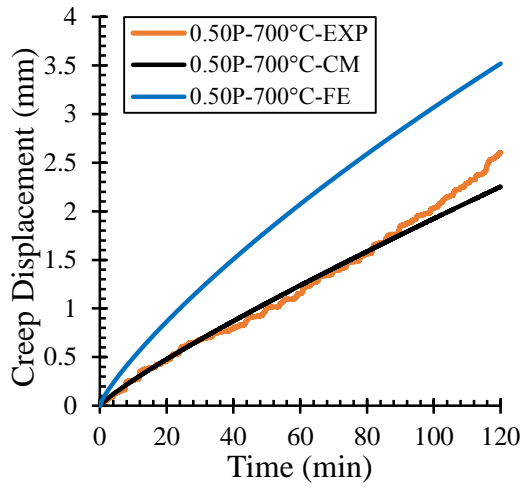


(c)

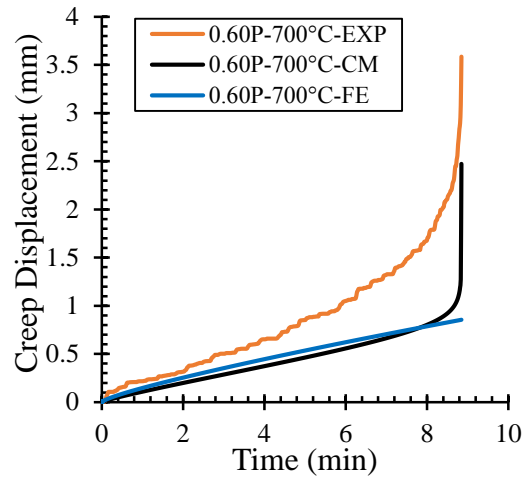


(d)

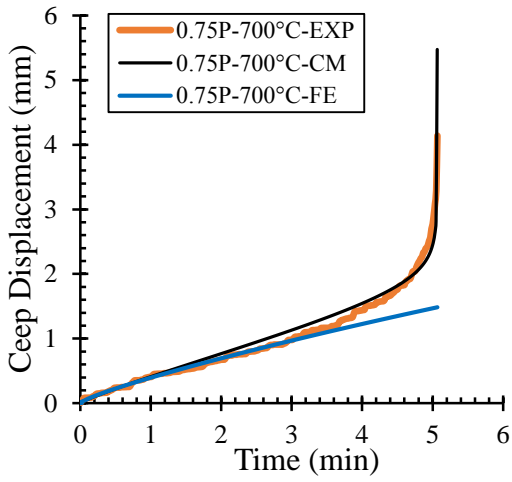
Fig. 35. Time-dependent results for FE and creep models versus experimental results at 600°C for: (a) 0.50P, (b) 0.60P, (c) 0.75P, (d) 0.90P



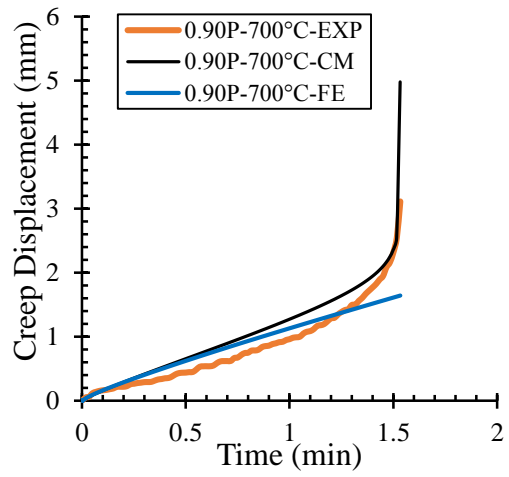
(a)



(b)



(c)



(d)

Fig. 36. Time-dependent results for FE and creep models versus experimental results at 700°C for: (a) 0.50P, (b) 0.60P, (c) 0.75P, (d) 0.90P

CHAPTER V

EXPERIMENTAL INVESTIGATION ON THE EFFECT OF LOAD ANGLES ON WELD BEHAVIOR AT ELEVATED AND POST-ELEVATED TEMPERATURE CONDITIONS

A. Experimental Program

The two other experimental parts that will be discussed in this chapter were performed at Riad Kamal Structural Engineering Laboratory at the American University of Beirut.

1. Test Specimens

An experimental program was performed to examine the rate-dependent behavior of fillet welds for three different welded lap joint configurations under steady-state thermal conditions. The lap joints are classified as longitudinal, inclined, and transverse where the angle between the axis of the fillet weld and the direction of the applied load is 0° , 45° , and 90° , respectively. The details of three welded lap joint configurations are shown in Figs. 37 and 38. The welded specimens were made of two large plates connected with two smaller plates with equal-leg fillet welds size of 8 mm with 50 mm length. The only difference among these welded lap joint configurations is the weld orientation with respect to the line of action of the applied load. The fillet welds were designed such that the failure occurs in the fillet weld at both ambient and elevated temperatures in accordance with ANSI/AISC 360 [46]. The elevated temperature design capacities were computed based on the retention factors proposed by Eurocode 3 [10]. All plate materials were made of S355 (ASTM A572 Gr.50) with measured yield and tensile strengths of 382 MPa and 547 MPa, respectively. The

welding process adopted was shielded metal arc welding (SMAW) using E7018 electrodes [43]. The surfaces of the steel plates were grinded with sanding discs and then cleaned with acetone material to remove rust and impurities before the welding process. After the welding process occurred, the welds were air-cooled (in the furnace) to ambient temperature.

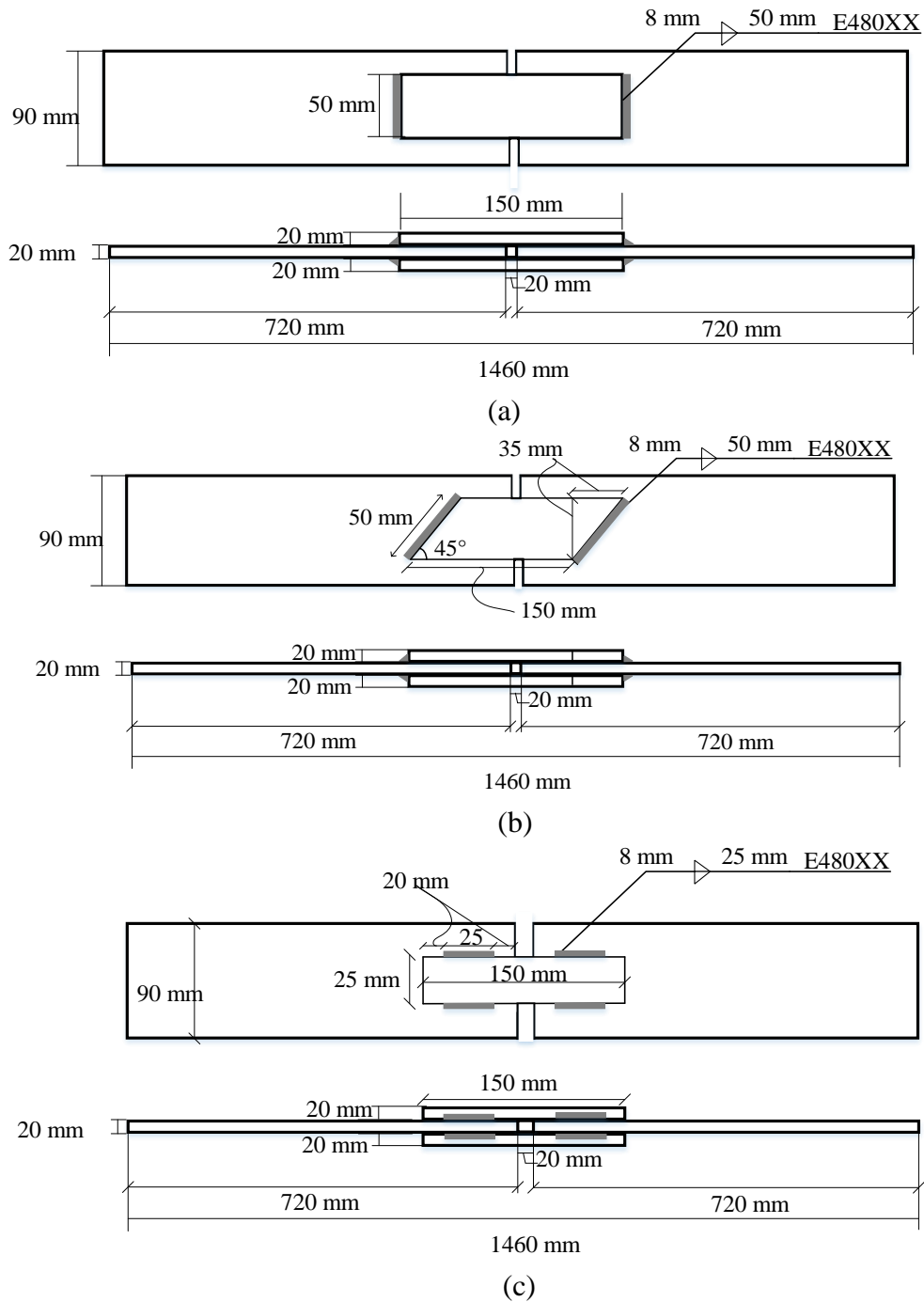


Fig. 37. Welded lap joints configuration: (a) Transverse, (b) Inclined, (c) Longitudinal



Fig. 38. Welded lap joint specimens

2. Setup and Instrumentation

A 200 tons capacity *Tinius-Olsen Universal Testing Machine* was used to perform the direct tension tests for the welded lap joints coupled with a 800 mm x 550 mm x 830 mm electric furnace as shown in Fig. 39. The furnace is made up of three separate heating zones that can be controlled by a temperature controller system. Heating rate for all test specimens were approximately the same since the temperature controller cannot provide different heating rates. To control the uniform temperature distribution around the weld region, thermocouples (*Type K*) were used to measure the surface temperature at different locations throughout the length of the specimen as shown in Figs. 40 and 41 for elevated and post-elevated temperature tests, respectively. Also, the specimens were wrapped by *stainless steel foils (SSF)* to protect the thermocouples from direct exposure to thermal radiation from heating coils of the furnace as shown in Figs. 40 and 41 knowing that the distance between the electric coils and the welded specimen is 20 cm. It is noted that part of the welded specimens (700 mm) was heated and no thermocouples were located at the plates outside the furnace. However, a temperature gun was used to check if there was any increase in temperature of the plates near the machine grips. No high temperature extensometer was used and

crossheads displacement was assumed to be controlled by the heated portion of the welded specimens.

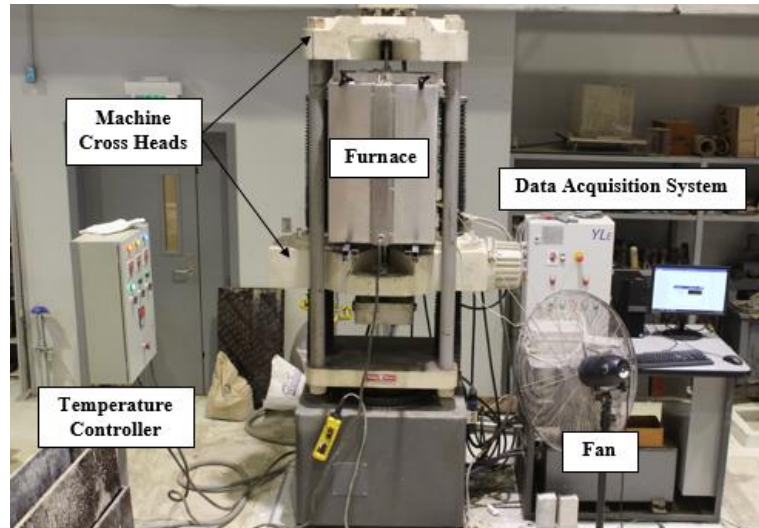


Fig. 39. Tinius-Olsen Universal Testing Machine coupled with the electric furnace

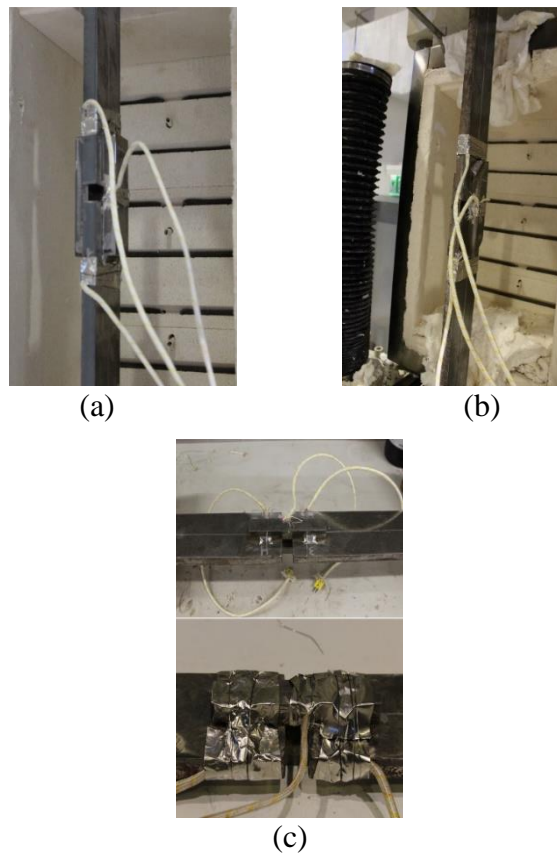


Fig. 40. Thermocouple implementation for elevated temperature tests: (a) Transverse (90°), (b) Inclined (45°), (c) Longitudinal (0°)

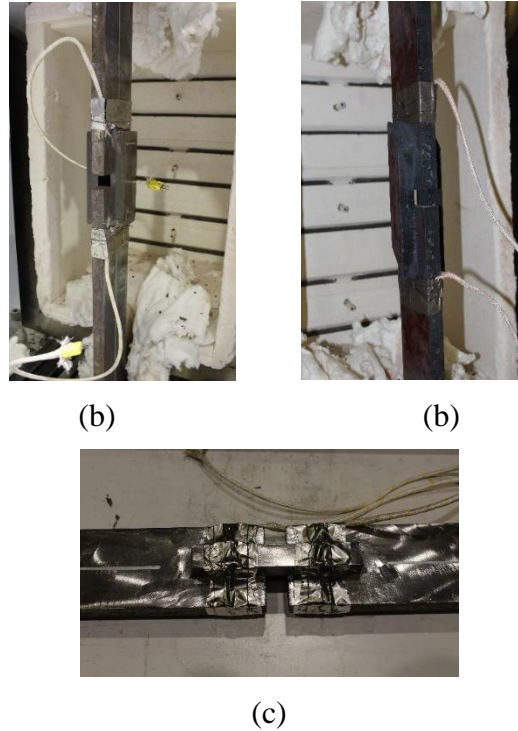


Fig. 41. Thermocouple implementation for post-fire analysis: (a) Transverse (90°), (b) Inclined (45°), (c) Longitudinal (0°)

B. Rate-dependent Thermal Behavior of Fillet Welds Subjected to Various Load Angles

1. Load Protocol

The welded lap joints (Fig. 37) were heated up to a target temperature so that no load was applied to the specimen. Once the temperature reached the target value, the temperature was held constant for 30 min to ensure uniform temperature distribution around the weld regions. After that, the specimens were loaded until failure at constant temperature with two displacement-controlled loading rates 1.5 mm/min (fast) and 0.1 mm/min (slow). These rates were chosen randomly with fifteen times difference to examine the effect of loading rate or the implicit creep on the fillet weld behavior. Also, the fifteen times difference was chosen to guarantee that the predictions of time-dependent thermal behavior of the weld material will cover the fire resistance ratings

(half an hour to four hours) that are recommended by building codes [47]. The test matrix of three welded lap joints at ambient and elevated temperatures under fast and slow loading conditions is tabulated in Table 9.

Table 9. Test matrix of the welded lap joints subjected to different load angles and rates

Test Name	Temperature (°C)	Angle (°)	Loading Rate (mm/min.)	Welded Lap Joint Configuration
20°C-90°-Fast	20	90	1.5	Transverse
400°C-90°-Fast	400	90	1.5	Transverse
500°C-90°-Fast	500	90	1.5	Transverse
600°C-90°-Fast	600	90	1.5	Transverse
700°C-90°-Fast	700	90	1.5	Transverse
20°C-90°-Slow	20	90	0.1	Transverse
400°C-90°-Slow	400	90	0.1	Transverse
500°C-90°-Slow	500	90	0.1	Transverse
600°C-90°-Slow	600	90	0.1	Transverse
700°C-90°-Slow	700	90	0.1	Transverse
20°C-45°-Fast	20	45	1.5	Inclined
400°C-45°-Fast	400	45	1.5	Inclined
500°C-45°-Fast	500	45	1.5	Inclined
600°C-45°-Fast	600	45	1.5	Inclined
700°C-45°-Fast	700	45	1.5	Inclined
20°C-45°-Slow	20	45	0.1	Inclined
400°C-45°-Slow	400	45	0.1	Inclined
500°C-45°-Slow	500	45	0.1	Inclined
600°C-45°-Slow	600	45	0.1	Inclined
700°C-45°-Slow	700	45	0.1	Inclined

20°C-0°-Fast	20	0	1.5	Longitudinal
400°C-0°-Fast	400	0	1.5	Longitudinal
500°C-0°-Fast	500	0	1.5	Longitudinal
600°C-0°-Fast	600	0	1.5	Longitudinal
700°C-0°-Fast	700	0	1.5	Longitudinal
20°C-0°-Slow	20	0	0.1	Longitudinal
400°C-0°-Slow	400	0	0.1	Longitudinal
500°C-0°-Slow	500	0	0.1	Longitudinal
600°C-0°-Slow	600	0	0.1	Longitudinal
700°C-0°-Slow	700	0	0.1	Longitudinal

2. Experimental Test Observation

The welded lap joints failed at the welds region for all tests at ambient and elevated temperatures under different loading rates and angles as shown in Fig. 42. The welded lap joints exhibited a change in surface textures and colors. Figure 43 represents the failure modes for the transverse welded lap joints at ambient and elevated temperatures under fast and slow loading rates. It can be seen that the failure occurred at the throat of the welds for all tests. The effect of loading rate and temperature are not significant on the welds fracture angle for the transverse welded lap joints.



(a)

(b)

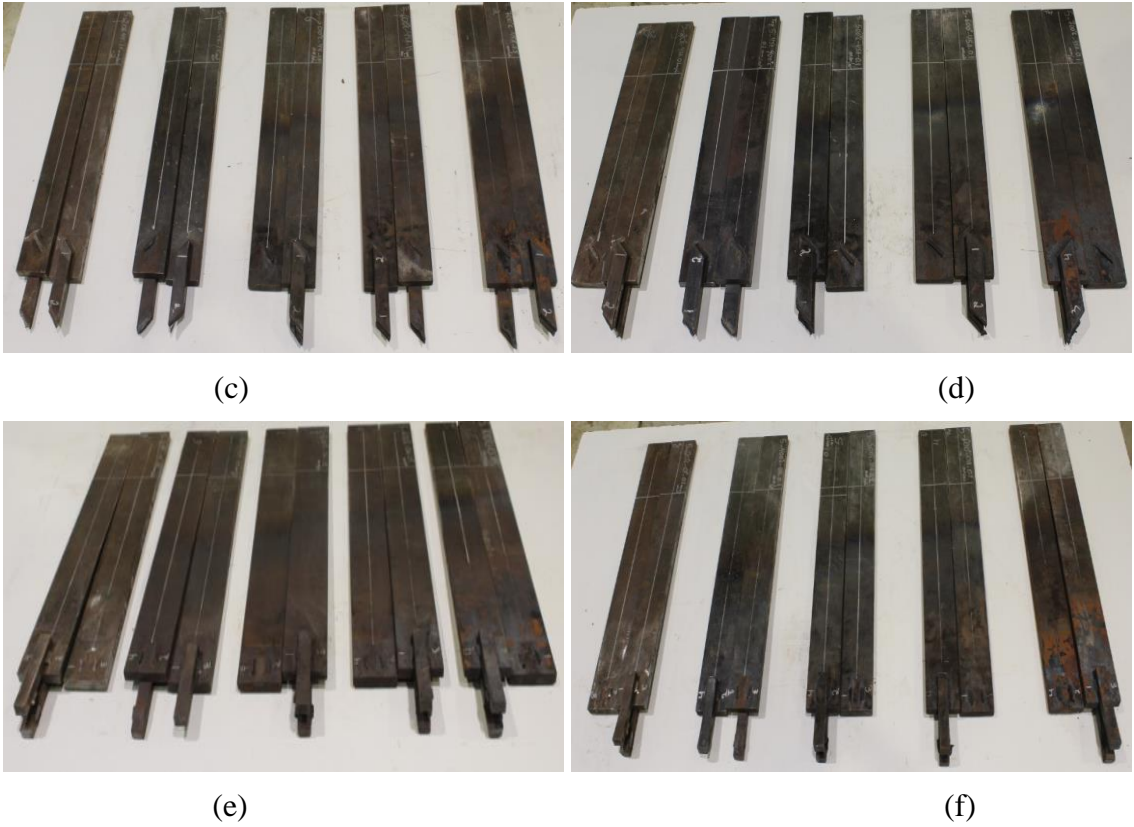


Fig. 42. Failure at the throat of the weld for all test specimens at ambient and elevated temperatures: (a) Transverse-fast tests, (b) Transverse-slow tests, (c) Inclined-fast tests, (d) Inclined-slow tests, (e) Longitudinal-fast tests, (f) Longitudinal-slow tests



(a) Fast-20°C



(b) Slow-20°C



(c) Fast-400°C



(d) Slow-400°C



(e) Fast-500°C



(f) Slow-500°C



(g) Fast-600°C



(h) Slow-600°C



(i) Fast-700°C



(j) Slow-700°C

Fig. 43. Failure modes for the transverse welded lap joints subjected to fast and slow loading rates

Figures 44 and 45 show the failure modes for all tests conducted on inclined welded lap joints. In Fig. 44, the failure occurred at the throat of the weld for tests conducted at fast loading rate under ambient and elevated temperatures. However, for the slow loading rate tests, the failure mode shifted from the weld throat to a fracture surface near the toe of the weld for temperature larger than 500°C. Also, Fig. 44 shows that the welds failed with a regular fracture plane surfaces with a change in texture and colors from one side of the connected plates. However, the another side of the connected plates showed that the weld fracture has an irregular shape for all tests as shown in Fig. 45. More specifically, for temperatures equal or larger than 400°C, the

fracture of the weld started at weld throat at the tip of the inclined plate and then propagated till it reached the toe of the weld at the end of the plate or verse versa. This can be due to the fact that the inclined welded lap joint is subjected to combined shear and tension loads that resulted in an irregular shape of the fracture surfaces.

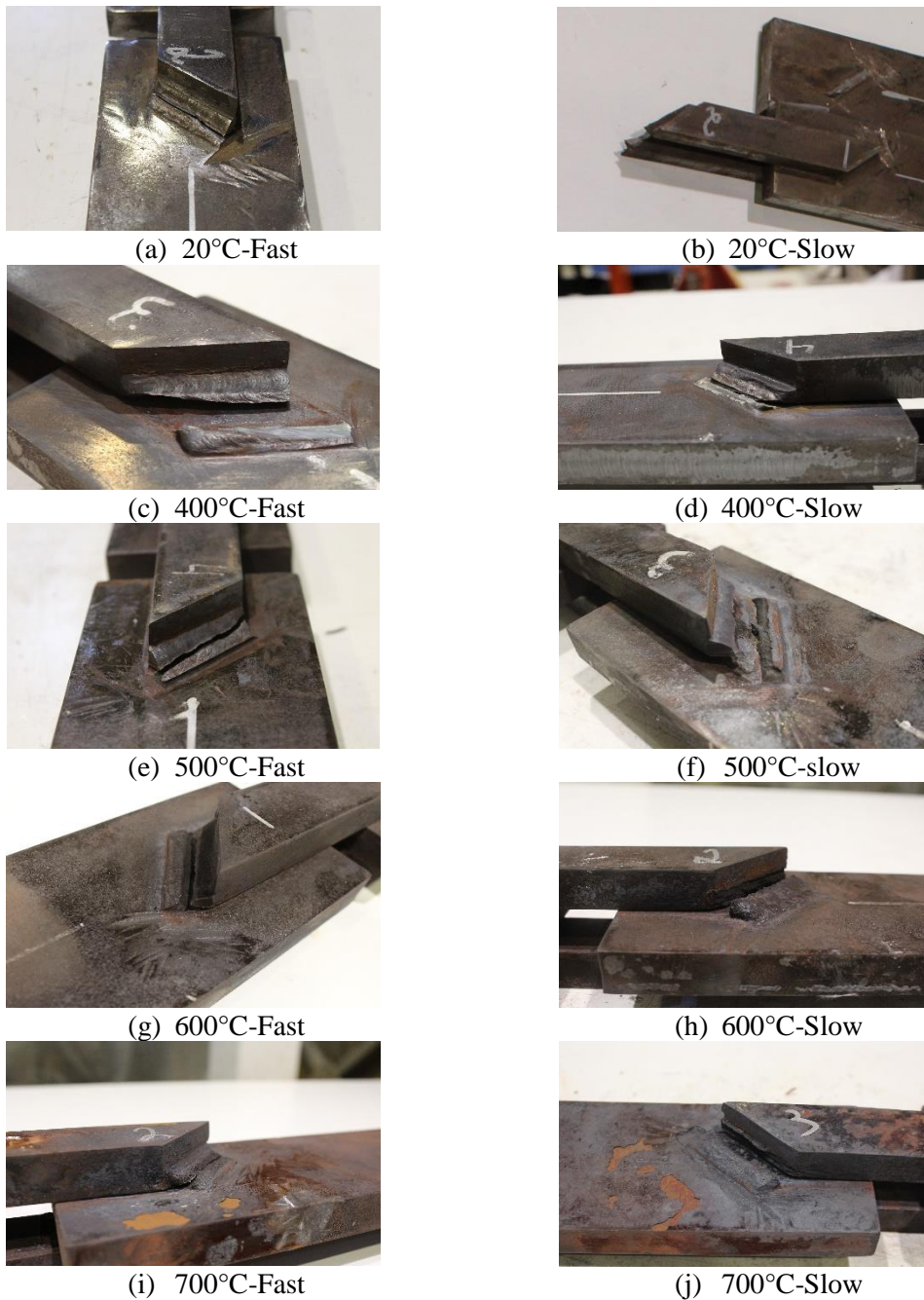
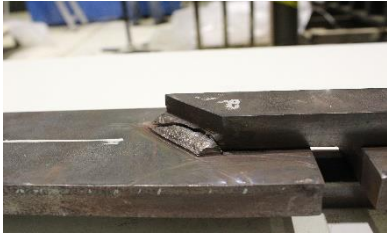


Fig. 44. Failure modes for the inclined welded lap joints subjected to fast and slow loading rates



(a) 20°C-Fast



(b) 400°C-Fast



(c) 400°C-slow



(d) 500°C-Fast



(e) 500°C-Slow



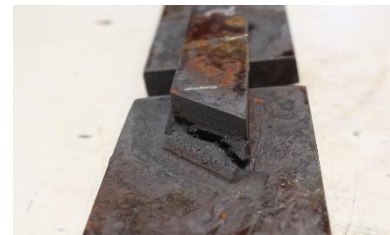
(f) 600°C-Fast



(g) 600°C-Slow



(h) 700 °C -Fast



(i) 700°C -Slow

Fig. 45. Irregular fracture mode for the inclined welded lap joints subjected to fast and slow loading rates

Further, Fig. 46 shows the failure modes of the longitudinal welded lap joints at ambient and elevated temperatures under different loading rates. All tests indicated that the failure occurred at the throat of the weld and the effect of loading rate and temperature on the weld fracture angle is not significant. Figure 47 shows that the longitudinal welds, unlike the transverse and inclined welds, experienced extensive deformation for the unfailed welds especially for high temperatures (700°C). This is due to the combined effect of load and temperature on the elongation of the weld material in the longitudinal direction (parallel to the load application).



(a) 20°C-Fast



(b) 20°C -slow



(c) 400°C -Fast



(d) 400°C -Slow



(e) 500°C -Fast



(f) 500°C -Fast



(g) 600°C -Fast



(h) 600°C -Fast

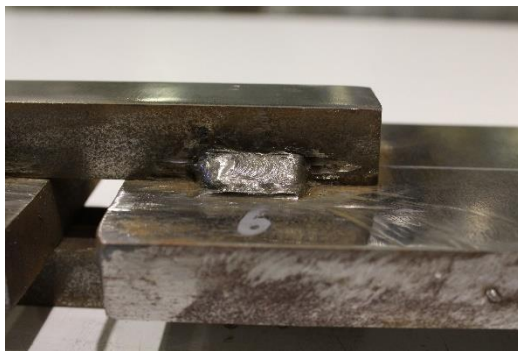


(i) 700-Fast



(j) 700-Fast

Fig. 46. Failure modes for the longitudinal welded lap joints subjected to fast and slow loading rates

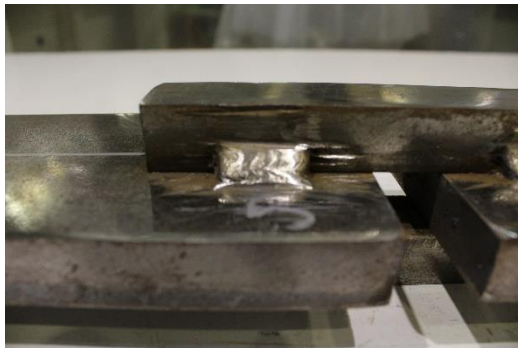


Before



After

(a)



Before



After

(b)

Fig. 47. Excessive deformation for the longitudinal welded lap joints at 700°C: (a) Fast loading rate, (b) Slow loading rate

The effect of temperatures and loading rates on the weld fracture surfaces for all welded specimens is shown in Fig. 48. It can be seen that the loading rates and angles have no significant effect on the weld fracture surfaces. However, when the welded lap joint is exposed to different elevated temperatures, the weld fracture surfaces exhibited

changes in color and texture. More specifically, all welded lap joints exhibited a blue color at 400°C with smooth fracture surfaces as shown in Fig. 48(b). As temperature increases (equal or larger than 500°C), the welded lap joints exhibited a brown to dark brown color and a rough fracture surface appearance as shown in Figs. 48 (c), 48(d), and 48(e). These visual observations indicate that welds exhibit an increase in ductility as temperature increases (equal or larger than 500°C).



(a) 20°C



(b) 400°C



(c) 500°C



(d) 600°C



(e) 700°C

Fig. 48. Fracture surfaces: Texture and color for the welded configuration at ambient and elevated temperatures

3. Effect of Temperatures on the Fillet Weld Behavior

In order to investigate the influence of temperature on the axial load-displacement performance of fillet welds when subjected to different loading rates and angles, representative curves are shown in Fig. 49. It can be seen that as temperature increases the strength capacity decreases and the displacement increases. Also, higher strength capacities are obtained for higher loading rate especially for temperatures equal or larger than 500°C. Reloading kinks are observed for all tests due to progressive failure of fillet welds and this progression continues until failure of the specimen. Also, large gaps are shown between strength capacities resulted from tests conducted at 500°C and 600°C and between those conducted at 600°C and 700°C for both fast and slow tests. However, for tests subjected to slow loading rate, the difference between the slow tests conducted at 400°C and 500°C is also noticeable. This indicates that the temperature has a great influence on the behavior of weld material and welded connections in case of fire and experimental data are necessary to be provided to support the development of fire design procedure for welded connections.

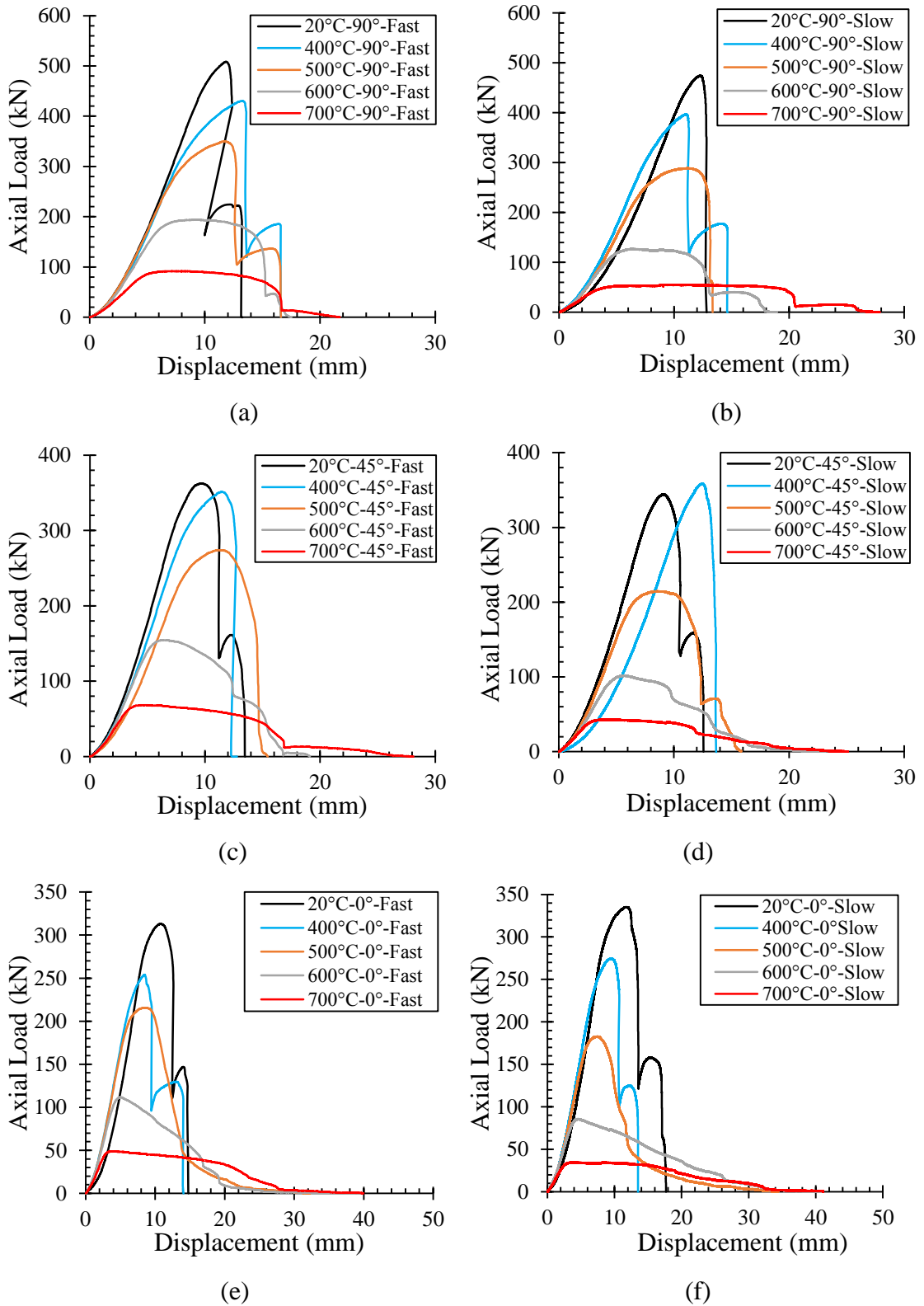


Fig. 49. Axial load-displacement characteristics of the welded lap joints at ambient and elevated temperatures: (a) Transverse-fast tests, (b) Transverse-slow tests, (c) Inclined-fast tests, (d) Inclined-slow tests, (e) Longitudinal-fast tests, (f) Longitudinal-slow tests

4. Effect of Loading Rate and Load Angle on the Fillet Weld Behavior

Figure 50 illustrates a comparison between the axial load-displacement behavior of fillet welds when subjected to combined effect of loading rate and angle at ambient and elevated temperatures. It can be seen that at 20°C (Fig. 50(a)) and 400°C (Fig. 50(b)) the effect of loading rate on the strength capacities of the three welded lap joints is not significant. Previous studies showed that at low temperatures, fast loading rate can result in slightly higher strength capacity of the steel material [28]. However, in Fig. 50 (a) and 50 (b), the slower loading rate resulted in slightly higher strength capacities for longitudinal welded lap joints at 20°C and 400°C, respectively. Also, same observation is shown in Fig. 50 (b) for the inclined welded lap joint at 400°C. This indicates that at low temperatures (less than or equal 400°C), the effect of implicit creep on weld material properties is not significant. When temperature is larger than 400°C, the effect of loading rate becomes significant at temperatures equal to 500°C, 600°C and 700°C as shown in Figs. 50 (c), 50 (d) and 50(e), respectively. Table 10 illustrates the percentage decrease in strength capacity of the welded lap joints as loading rate is changing from 1.5 mm/min to 0.1 mm/min. At 20°C and 400°C, the effect of loading rate on all lap joints is not significant with maximum of 6.70% and 7.70% decrease for the transverse welded lap joint, respectively. This change in strength capacities of fillet welds is due to the variation of material and geometric properties. For 500°C, the effect of slow loading rate becomes more significant with 17.40%, 21.60%, and 15.10% decrease in strength capacities for transverse, inclined, and longitudinal welded lap joints, respectively. This indicates that the effect of loading rate becomes significant for temperatures larger than 400°C. This is due to the effect of implicit creep. The effect of slow loading rate becomes more prominent at 700°C with a percentage decrease in the

fillet weld strength capacity of 40.30%, 37.40%, and 29.10% for transverse, inclined, and longitudinal welded lap joints, respectively. It can be seen that the effect of loading rate is more significant on the strength capacities of the transverse and inclined welded lap joints more than on the longitudinal ones. This indicates that the creep behavior of weld is not only dependent on material properties, stress, time, and temperature but also dependent on the applied load direction.

The effect of load angle on the fillet weld behavior is also shown in Fig. 50. The transverse welded lap joints (90°) have larger strength capacities than that of the inclined (45°) and the longitudinal (0°) lap joints for all temperatures and loading rates. However, by decreasing the load angle from 90° to 0° , the welded specimens undergo higher displacement and ductility. Therefore, all these observations indicate that as the load angle increases, the fillet weld strength increases and ductility decreases for all ambient and elevated temperatures and loading rates.

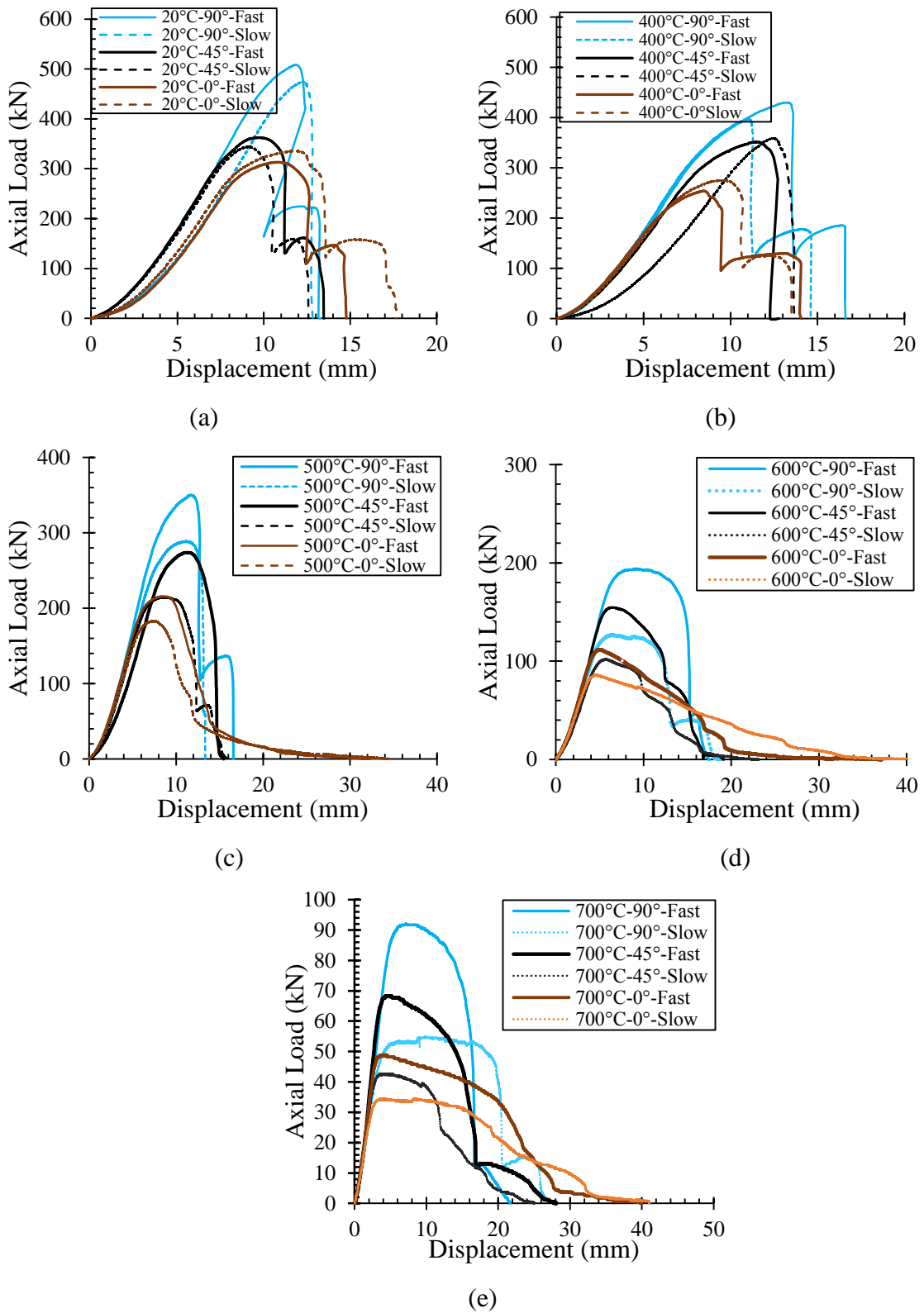


Fig. 50. Effect of loading rate on the behavior of the welded lap joints at: (a) 20°C, (b) 400°C, (c) 500°C, (d) 600°C, (e) 700°C

Table 10. Retention factors for the strength of fillet welds exposed to elevated temperatures and their percentage decrease in capacities due effect of loading rate.

Fast test name	Maximum axial load (kN)	Retention factor	Slow test name	Maximum axial load (kN)	Retention factor	Decrease in capacity (%)
20°C-90°-Fast	508.17	1.00	20°C-90°-Slow	474.07	1.00	6.71
400°C-90°-Fast	429.88	0.85	400°C-90°-Slow	369.85	0.84	7.68
500°C-90°-Fast	349.95	0.69	500°C-90°-Slow	289.03	0.61	17.41
600°C-90°-Fast	194.17	0.38	600°C-90°-Slow	126.87	0.27	34.66
700°C-90°-Fast	92.19	0.18	700°C-90°-Slow	55.06	0.12	40.28
20°C-45°-Fast	362.46	1.00	20°C-45°-Slow	344.39	1.00	4.99
400°C-45°-Fast	351.32	0.97	400°C-45°-Slow	358.83	1.04	-2.14
500°C-45°-Fast	273.70	0.76	500°C-45°-Slow	214.71	0.62	21.55
600°C-45°-Fast	154.49	0.43	600°C-45°-Slow	101.89	0.30	34.05
700°C-45°-Fast	68.28	0.19	700°C-45°-Slow	42.75	0.12	37.39
20°C-0°-Fast	313.02	1.00	20°C-0°-Slow	335.15	1.00	-7.07
400°C-0°-Fast	254.05	0.81	400°C-0°-Slow	247.97	0.74	2.39
500°C-0°-Fast	215.56	0.69	500°C-0°-Slow	183.01	0.55	15.10
600°C-0°-Fast	111.46	0.36	600°C-0°-Slow	85.69	0.26	23.12
700°C-0°-Fast	48.91	0.16	700°C-0°-Slow	34.68	0.10	29.09

5. Effect of Loading Rate on the Fillet Weld Orientation

At ambient temperature, the strength of transverse and longitudinal welds represent the upper and the lower bounds of weld strength capacities, respectively. That is, the strength of transverse welds equals to 1.5 times of that of the longitudinal welds, and for all other weld orientations, the weld strength is set between these two weld strength capacities as per ANSI/AISC 360 [13, 48]. To investigate the effect of rate and temperature on the fillet weld strength when subjected to different load angles, an illustrative plot is shown in Fig. 51. Figure 51 represents the load angle effectiveness ratio with the increase of temperature as two different loading rates (fast and slow) are considered. The load angle effectiveness ratio can be calculated by dividing the strength capacities of the transverse and inclined welded lap joints to that of the longitudinal welds at ambient and elevated temperatures for both fast and slow tests. To examine the effect of temperature solely on the load angle effectiveness ratio, fast and slow tests are considered separately. As shown in Fig. 51, when the welds are subjected to high temperatures, both transverse and inclined welds result in a higher load angle effectiveness ratio than that of the ambient test. The load angle effectiveness ratio is compared with the one provided in ANSI/AISC 360 [13] for both transverse and inclined welded lap joint. The angle effectiveness ratio proposed by the ANSI/AISC 360 [13] is $1.0 + 0.5 \sin^{1.5} \theta$. It can be seen that the load angle effectiveness ratio proposed by the ANSI/AISC 360 [13] is conservative for fast tests at elevated temperatures. However, for the slow loading rate, the ANSI/AISC 360 [13] angle effectiveness ratio can lead to unsafe predictions of the weld strength at high temperatures especially for the inclined welded lap joints. This indicates that the

combined effect of temperature and loading rate affects the behavior of fillet welds as the applied load angle changes.

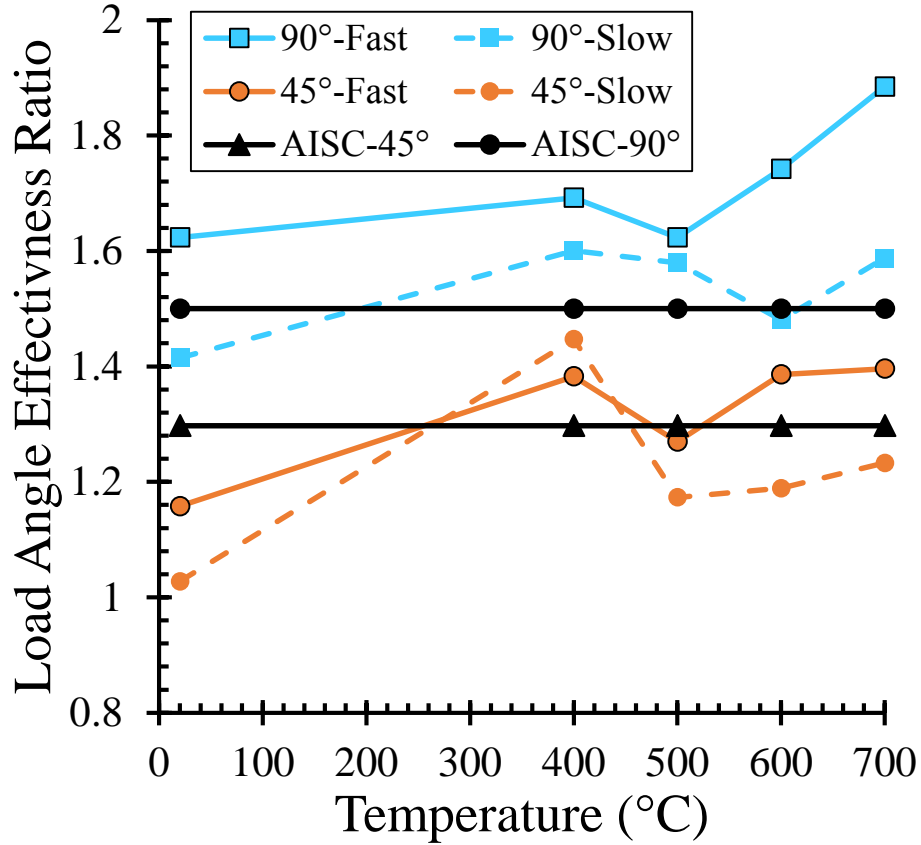


Fig. 51. Effect of loading rate on fillet weld orientation

6. Effect of Loading Rate, Angles, and Temperature on the Ductility of Welded Lap

Joints

At ambient temperature, the ductility of welds is highly dependent on the angle between the axis of the weld and the line of action of the applied load. That is, the larger load angle results in less ductility for the welded lap joints. However, at elevated temperatures, the behavior of welds becomes more complex and the effect of temperature and time can affect the ductility of the welded lap joint in fire. Since the inelastic creep displacements are implicitly added to the axial load-displacement curves

due to the effect of different loading rates, the ductility of the welded lap joint is normalized and can be computed as follows:

$$\phi = \frac{A}{PL} \quad (35)$$

Where ϕ is the normalized ductility, A is the area under axial-load displacements curve, P is the peak load predicted for each test, and L is total length of the specimen (1460 mm). Figure 52 illustrates the variation of the normalized ductility for the welded lap joints subjected to fast and slow loading rates at ambient and elevated temperatures. At ambient temperature, the ductility of the welded lap joints increases when the angle between the axis of the weld and the line of action of the applied load decreases. However, at elevated temperatures the ductile behavior of welds changes with temperatures. Figure 52 shows that when temperature increases beyond 400°C, the ductility of the weld material increases with the increase of temperature especially for temperatures larger than 500°C. This conforms with the experimental observations presented in Figs. 44, 45 and 46 where rough fracture surfaces of the welds were shown for tests conducted at temperature equal or larger than 500°C.

In order to study the combined effect of temperature and applied load angle on the ductility of the weld material, all tests at the same loading rate, either fast or slow, are considered solely. It can be seen from Figure 52 that as temperature increases up to 400°C, only tests conducted on transverse welded lap joints show an increase in ductility under both fast and slow loading rate scenarios. As temperature increases beyond 400°C, the longitudinal welded lap joints gain more ductility than that of transverse and inclined welded lap joints for both loading rates. Also, the transverse welded lap joints gain slightly more ductility when compared to the inclined welded lap joints for fast loading tests. However, under slow loading rate scenario (dashed plots in

Fig. 52), the transverse welded lap joints become significantly more ductile than the inclined ones especially for temperatures larger than 500°C.

In order to study the effect of loading rate on the normalized ductility of the fillet weld material subjected to different load angles, results from fast and slow tests need to be considered together for each lap joint. The effect of loading rate on the ductility of fillet welds becomes significant for longitudinal and transverse welded lap joints for temperatures larger than 500°C and 600°C, respectively. However, for the inclined welded lap joints the effect of loading rate on the ductility of the fillet weld material is not significant.

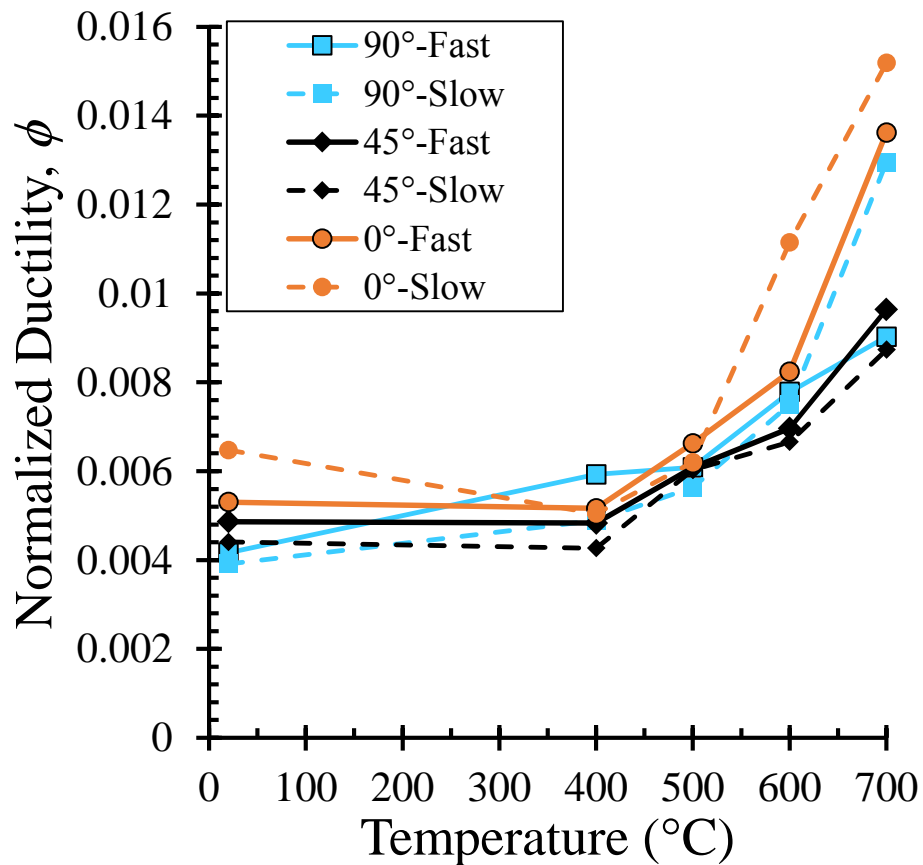


Fig. 52. Effect of temperature on the normalized ductility of weld materials under fast and slow loading rates

7. Retention Factors

The experimental results shown in Fig. 49 were used to compute the rate- and temperature- dependent retention factors for the transverse, inclined, and longitudinal welded lap joints. The rate- and temperature-dependent retention factors can be calculated by dividing the maximum capacities (Table 10) of each type of the welded lap joint at each temperature to that obtained at ambient for both fast and slow loading rates. These retention factors are illustrated in Fig. 53 and tabulated in Table 10. It can be seen that for all welded lap joint configurations, the effect of loading rate on the retention factors of welded lap joints is significant for temperature larger than 400°C. Also, the maximum retention factors are obtained from tests conducted on the inclined welded lap joints at both fast and slow loading rates. Whereas the least ones are obtained from the longitudinal welded lap joints. However, the retention factors computed for the transverse welded lap joints are set between those estimated for the inclined and longitudinal welded lap joints.

In addition, Fig. 53 shows a comparison between retention factors proposed in this study with those provided in Eurocode 3 [10] and those proposed by Conlon [22]. It should be noted that the retention factors specified in Eurocode 3 [10] are for cruciform fillet welded connections that are computed based on the work done by Latham and Kirby [11]. Recall, the steady-state thermal tensile tests were carried out at a rate of 0.02/min up to 5% plastic strain and then the rate altered to a nominal strain rate of 0.1/min [11]. This loading protocol is different from the conventional one where higher strain rates are used [11]. However, the retention factors proposed by Conlon [22] were based on an experimental program on transverse fillet welds (38 mm leg size) under steady-state temperature conditions with 0.1 in./min (2.54 mm/min). It can be seen that

the retention factors proposed by Conlon [22] is higher than those obtained from the tests conducted on transverse welded lap joints at both fast and slow loading rates. This is due to the fact that the loading rate used by Conlon [22] is higher with 1.7 and 25.4 times than those used for fast and slow tests, respectively. However, the retention factors proposed by the Eurocode 3 [10] is set to be in between the retention factors proposed by this study for transverse welded lap joint under fast and slow loading rates. This is because Eurocode 3 [10] accounted for the implicit creep in the stress-strain curves of the weld materials. Also, Fig. 53 shows that Eurocode 3 retention factors [10] are only conservative for the weld material subjected to different load angles for fast tests especially for temperature larger than 450°C. This indicates that ignoring the effect of loading rate and load angle in fire design of welds and welded connection can potentially lead to unsafe predictions.

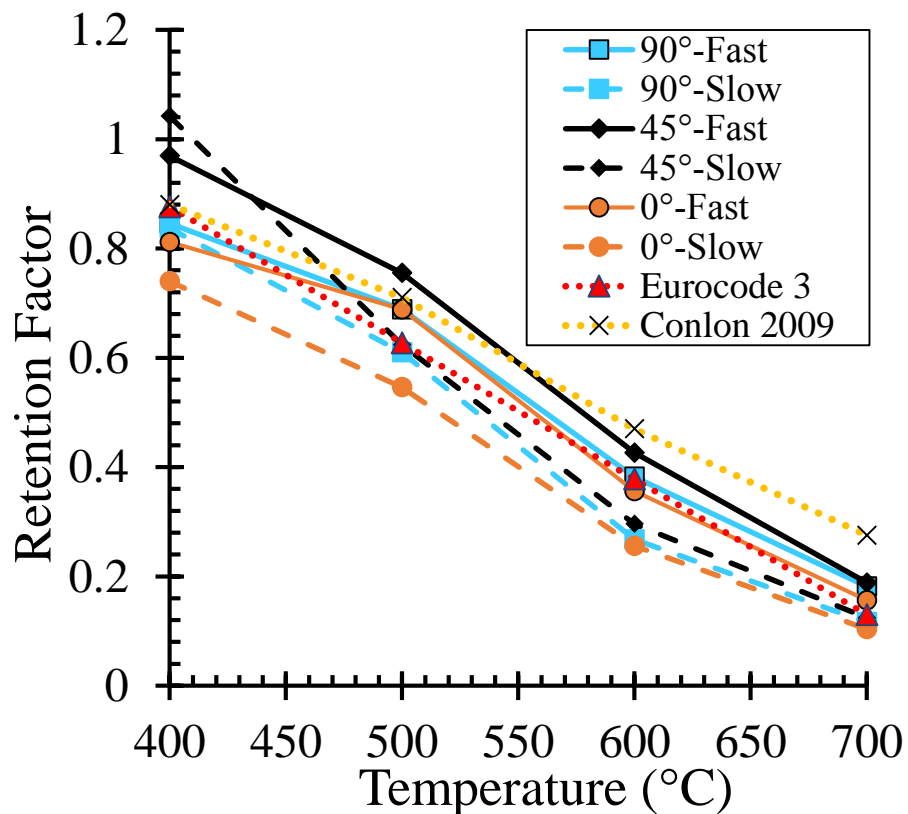


Fig. 53. Retention factors for the three different welded lap joint configurations

8. Fire Design Equation for Weld Material

The ANSI/AISC 360 [13] provides an equation (J2-4) for designing a linear weld group with a uniform leg size and loaded through its center of gravity at ambient temperature. However, in case of fire, this equation cannot be applied due to the combined effect of loading rate, load angle, and temperature. To address this issue, equation J2-4 [13] can be modified to account for the rate and temperature effects as follows:

$$(R_{nw})_T = K_L \alpha 0.60 F_{EXX} A_{we} (1.0 + 0.5 \sin^{1.5} \theta) \quad (36)$$

Where $(R_{nw})_T$ is the nominal weld strength at a specified temperature (T), F_{EXX} is the filler metal strength, A_{we} is the effective area of the weld, $(1.0 + 0.5 \sin^{1.5} \theta)$ represents the effect of load angle (θ) on the strength capacity of the fillet weld material, K_L is the retention factors proposed for the longitudinal welded lap joints performed under fast tests (Table 10), and α represents the ratio of the slow to fast loading rate strength capacity and can be computed by dividing the maximum load obtained from the slow tests to that of the fast ones for each load angle and temperature. Alternatively, α can be also computed by dividing the slow retention factor to the fast one for each lap joint configuration. Note that α is taken as the lower bound for the slow to fast loading rate strength capacity ratios computed for each load angle and temperature (T) ranging from 400°C to 700°C as shown in Fig. 54 and can be calculated as follows:

$$\alpha = 42.778T^{-0.642} \quad (37)$$

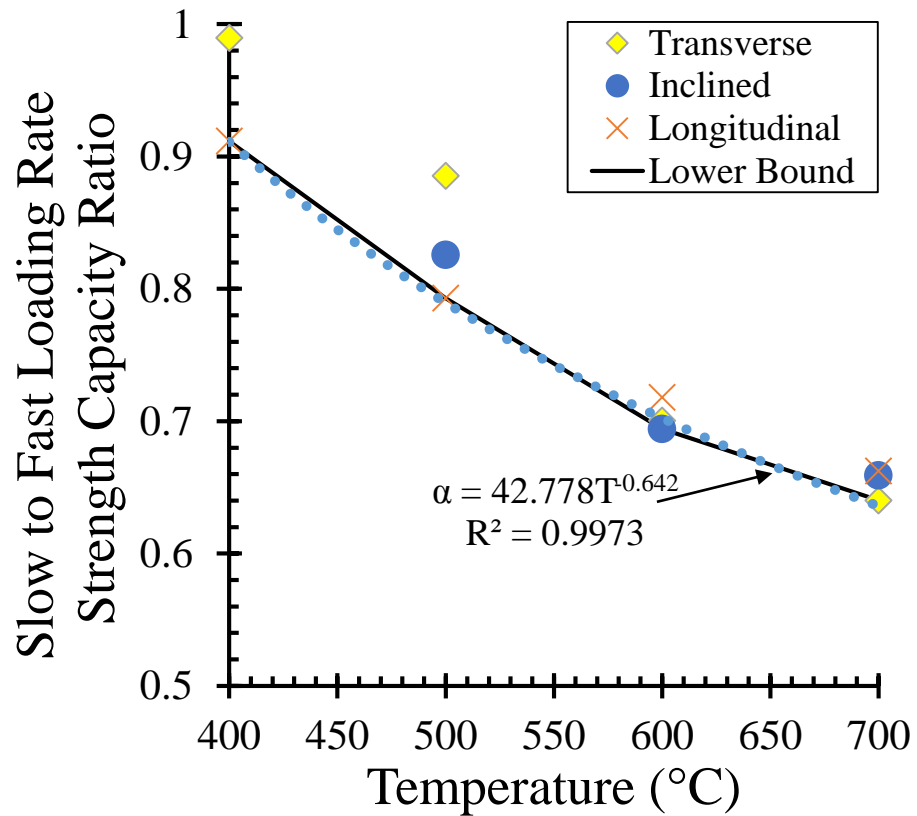


Fig. 54. Slow to fast loading rate capacity ratio versus temperature

Figure 55 represents the strength capacities of the welded lap joints obtained from the experimental tests at slow rate against the proposed elevated temperatures welded strength model (Eq. 36). It can be seen that the proposed model resulted in a conservative strength capacities and can be used to ensure a safe design.

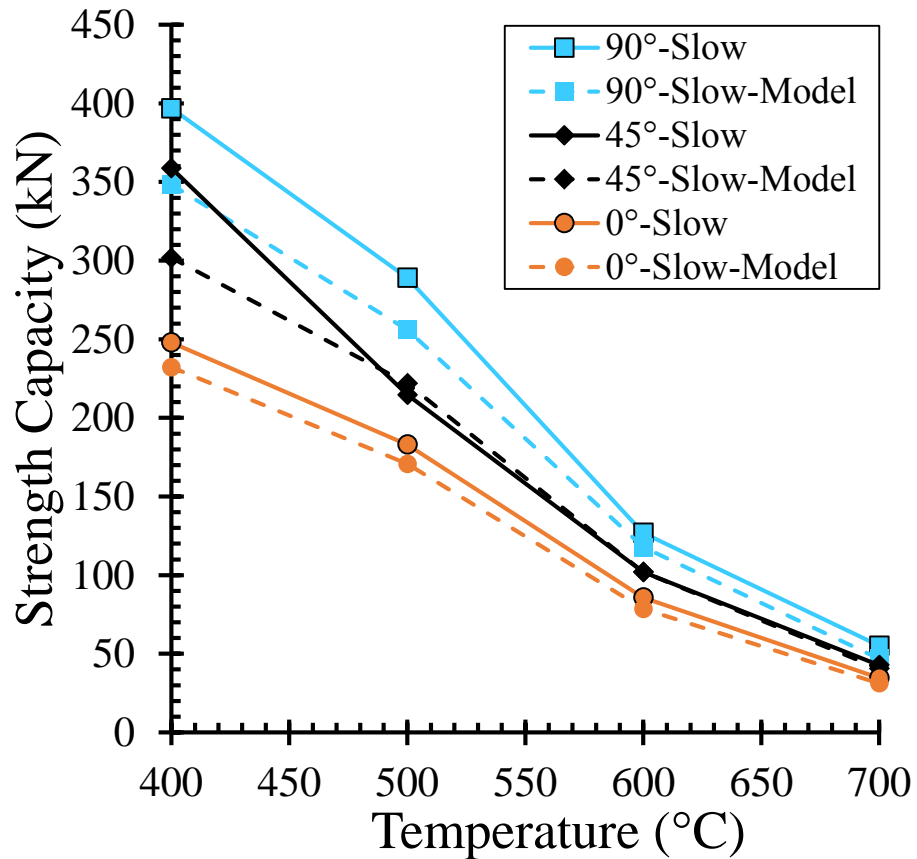


Fig. 55. Strength capacity model calculation versus temperature

C. Post-Elevated Temperature Tests

1. Load Protocol

In the post-elevated temperature analysis, the three welded lap joints shown in Figs. 37 and 38 were heated up to a target temperature and then kept constant without applying any load for 60 min. Then the furnace was turned off, so the specimens were cooled back to ambient. Note that, one of the furnace compartment was taken out when the surface temperatures reached around 60°C as shown in Fig. 56. Also, in some cases when the specimen temperature reached around 40°C, the fan was turned on to accelerate the cooling phase. After the surface temperatures cooled back to 20°C, the welded specimens were loaded with 1.5 mm/min until failure. Figure 57 shows a

sample of temperature profiles applied to 45° inclined welded lap joint for the post-fire analysis. It can be seen in Fig. 57 that all tests were heated approximately with same heating rate till they reached a target temperatures and then held constant for 60 min. After that the specimens were cooled down to ambient temperature. As it can be seen in Fig. 57 that the time needed for the specimen to cool down to ambient temperature ranges from 16 hrs to 25 hrs depending on the target temperature of the post-fire test analysis. Also, rapid decrease is shown in the last stage of the cooling phases (Fig.57) and this is due to the use of the fan. Test matrix of post-elevated temperatures behavior of the three welded lap joints is illustrated in Table 11.

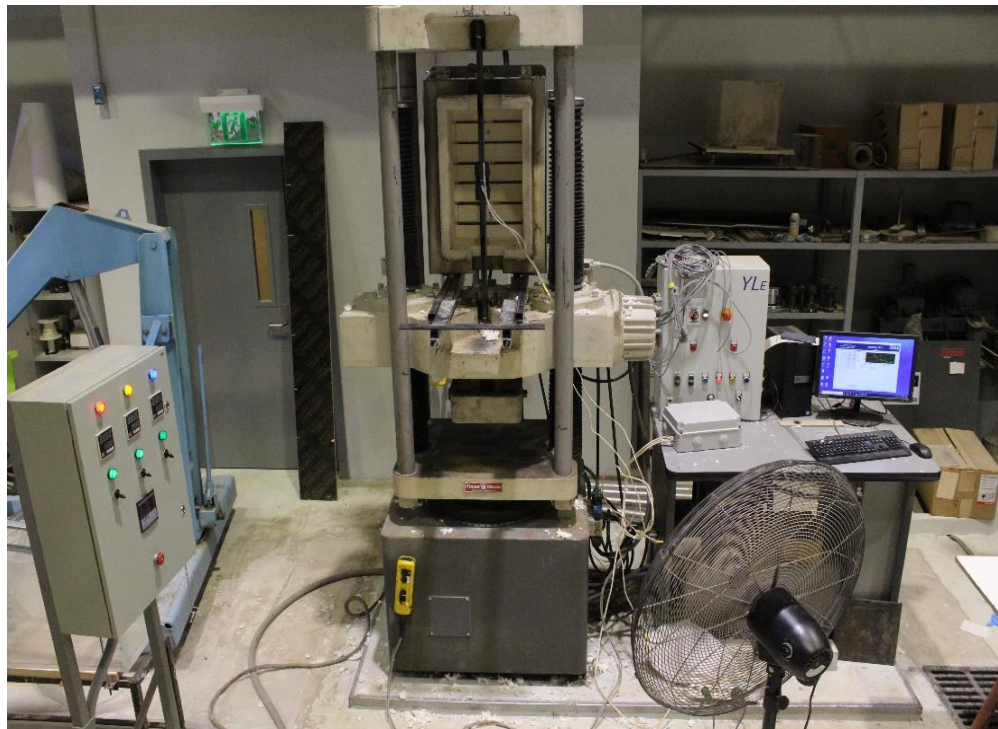


Fig. 56. Tinius-Olsen Universal Testing Machine coupled with the electric furnace: The cooling phase

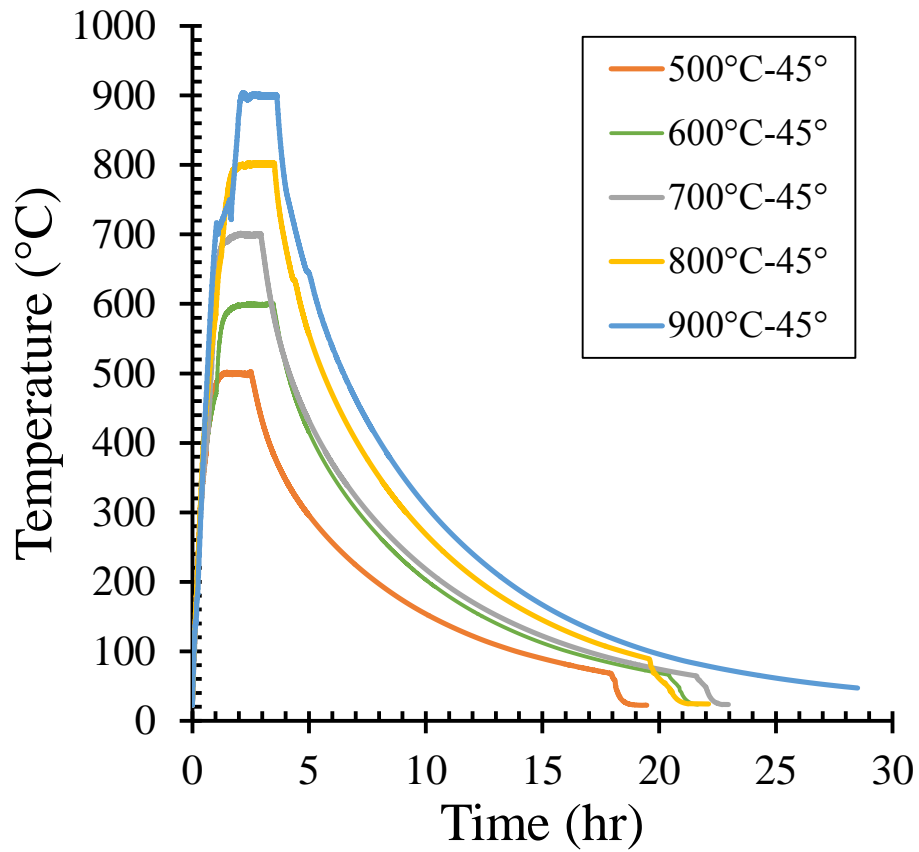


Fig. 57. Temperature profile for post-fire temperature profile

Table 11. Test matrix of the welded lap joints after exposed to fire temperatures

Test Name	Temperature (°C)	Angle (°)	Loading Rate (mm/min.)	Welded Lap Joint configuration
20°C-R-90°	20	90	1.5	Transverse
500°C-R-90°	900	90	1.5	Transverse
600°C-R-90°	800	90	1.5	Transverse
700°C-R-90°	700	90	1.5	Transverse
800°C-R-90°	600	90	1.5	Transverse
900°C-R-90°	500	90	1.5	Transverse
20°C-45°	20	45	1.5	Inclined
500°C-R-45°	900	45	1.5	Inclined

600°C-R-45°	800	45	1.5	Inclined
700°C-R-45°	700	45	1.5	Inclined
800°C-R-45°	600	45	1.5	Inclined
900°C-R-45	500	45	1.5	Inclined
20°C-R-0°	20	0	1.5	Longitudinal
900°C-R-0°	900	0	1.5	Longitudinal
800°C-R-0°	800	0	1.5	Longitudinal
700°C-R-0°	700	0	1.5	Longitudinal
600°C-R-0°	600	0	1.5	Longitudinal
500°C-R-0°	500	0	1.5	Longitudinal

2. Experimental Test Observations

Figure 58 shows the failure modes of the three welded lap joints at ambient temperature and after exposed elevated temperatures. It can be seen that all specimens failed in the weld region at ambient and post-elevated temperatures. Also, the welded lap joints exhibited a change in surface textures and colors. More specifically, Figs. 59, 60 and 61 represent close photographs of the fracture modes at the throat of the weld for the transverse, inclined, and longitudinal welded lap joints, respectively. It can be seen from these figures, that the exposed surfaces of the specimen exhibited a change in color. That is, at 500°C the exposed surfaces exhibited a brown color that altered to dark brown as temperature reaches 600°C. For higher temperatures like 700°C and 800°C, the specimen surfaces showed a reddish brown and reddish gray colors, respectively. Whereas, for 900°C the steel plates exhibited a gray color. However, the color and texture of the weld fracture surfaces did not change noticeably with the increase of temperature. That is, as temperature increases up to 900°C, the fracture

surface of the weld material showed a slightly darker silver color and a slightly more rough texture than that of the ambient temperature tests.



(a)



(b)



(c)

Fig. 58. Failure at the throat of the weld for all test specimens at ambient and post-elevated temperatures: (a) Transverse (b) Inclined, (c) Longitudinal

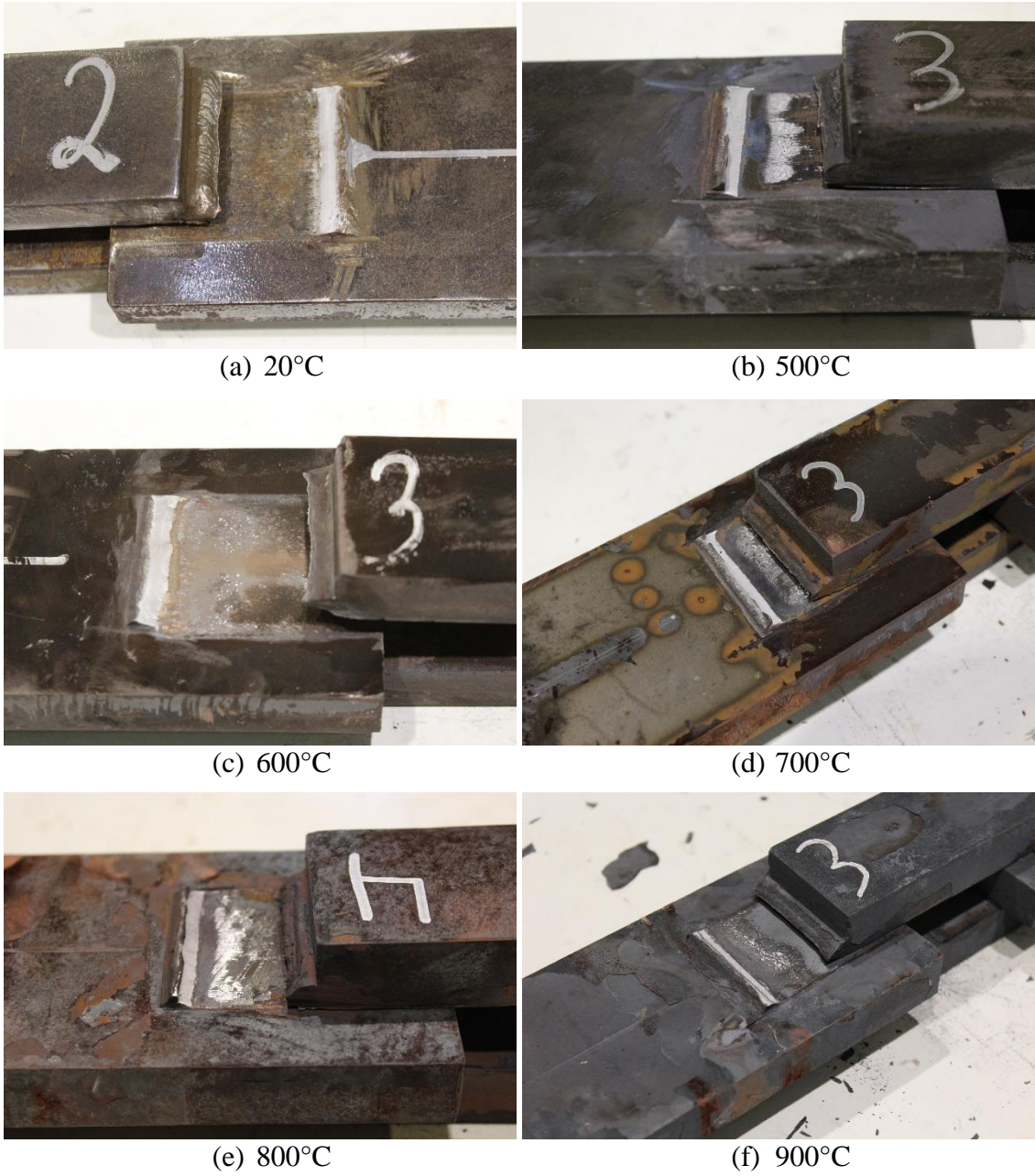


Fig. 59. Failure modes for the transverse welded lap joints after exposed to elevated temperatures

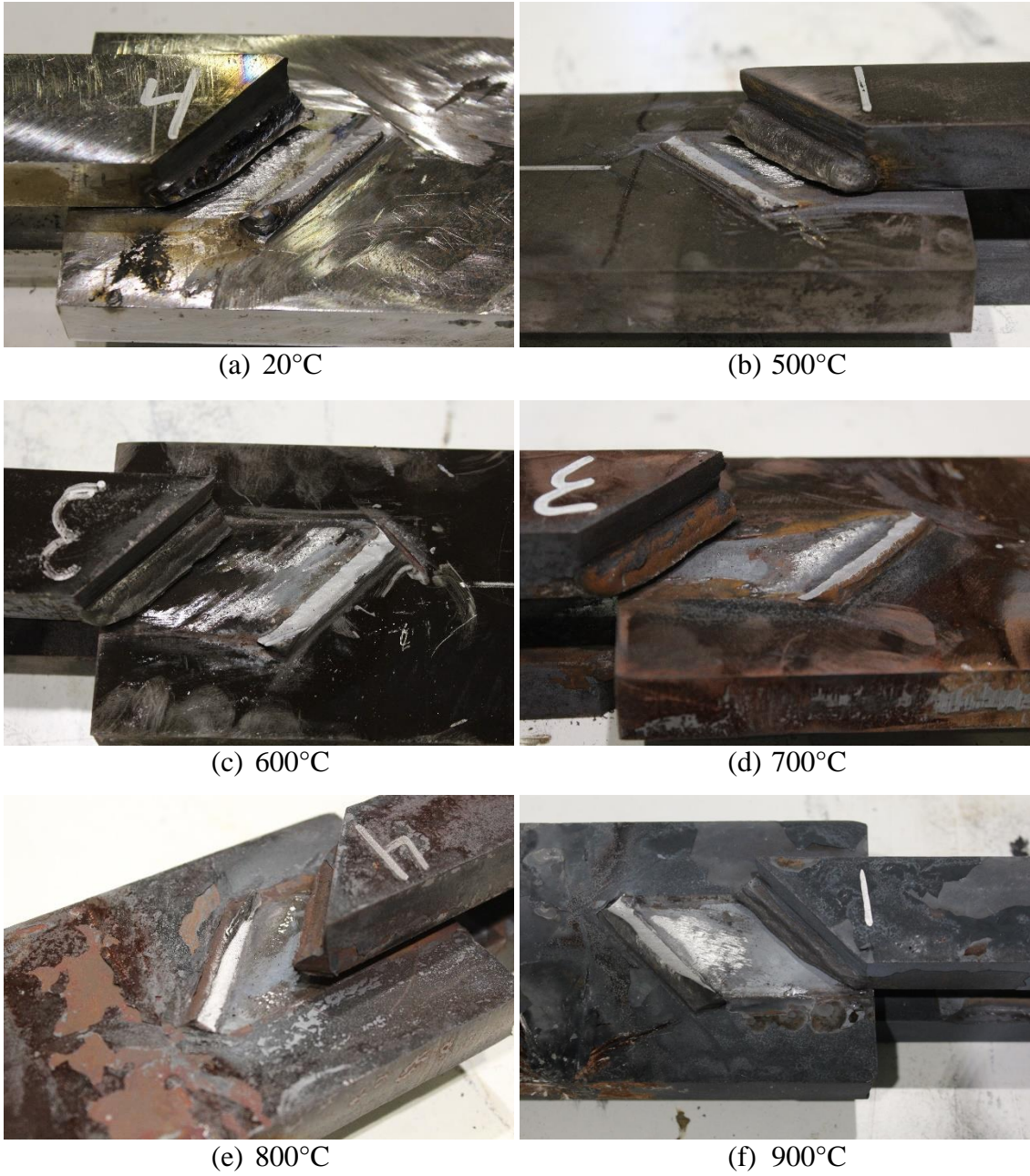


Fig. 60. Failure modes for the inclined welded lap joints after exposed to elevated temperatures

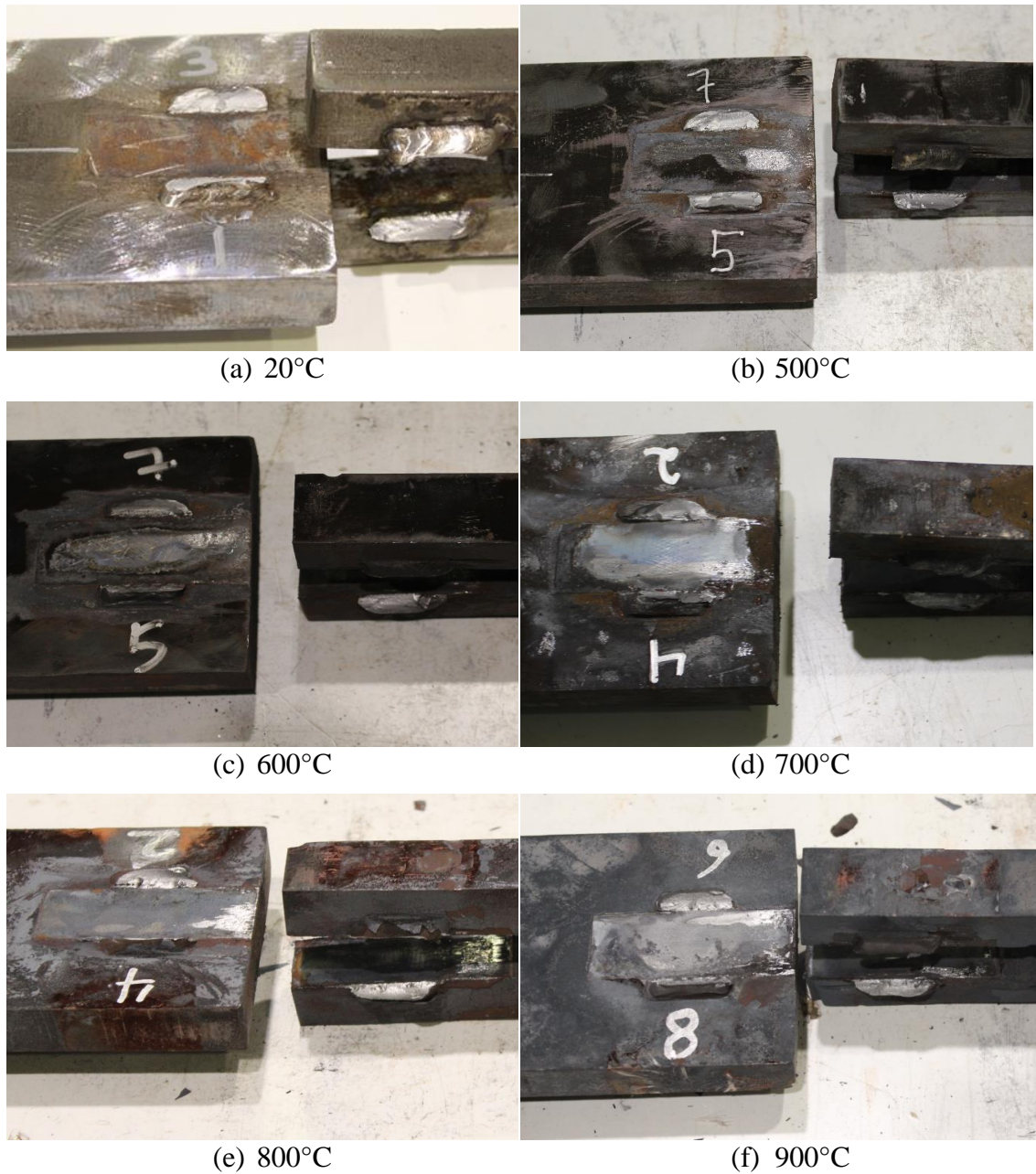


Fig. 61. Failure modes for the longitudinal welded lap joints after exposed to elevated temperatures

3. Residual Load-Displacement Response

Figure 62 represents the residual load-displacement responses of the three welded lap joints after heating and cooling phases. It can be seen from Fig. 62 that the residual peak load decreases as the targeted temperature in post-fire analysis increases. Also, it can be seen that the effect of temperature on residual response is significant for

temperatures larger than 600°C for transverse and longitudinal welded lap joints. However, for the inclined welded lap joints the effect of temperature starts to be noticeable on the residual response of the fillet weld material larger than 500°C. Also, yielding points can be seen for tests conducted at post-fire temperatures equal and above 600°C especially for inclined and longitudinal welded lap joints. Also, the results show that displacement increases as temperature of the heating-cooling cycle increases. Reloading kinks are observed for some tests and this is due to the progressive failure of fillet welds.

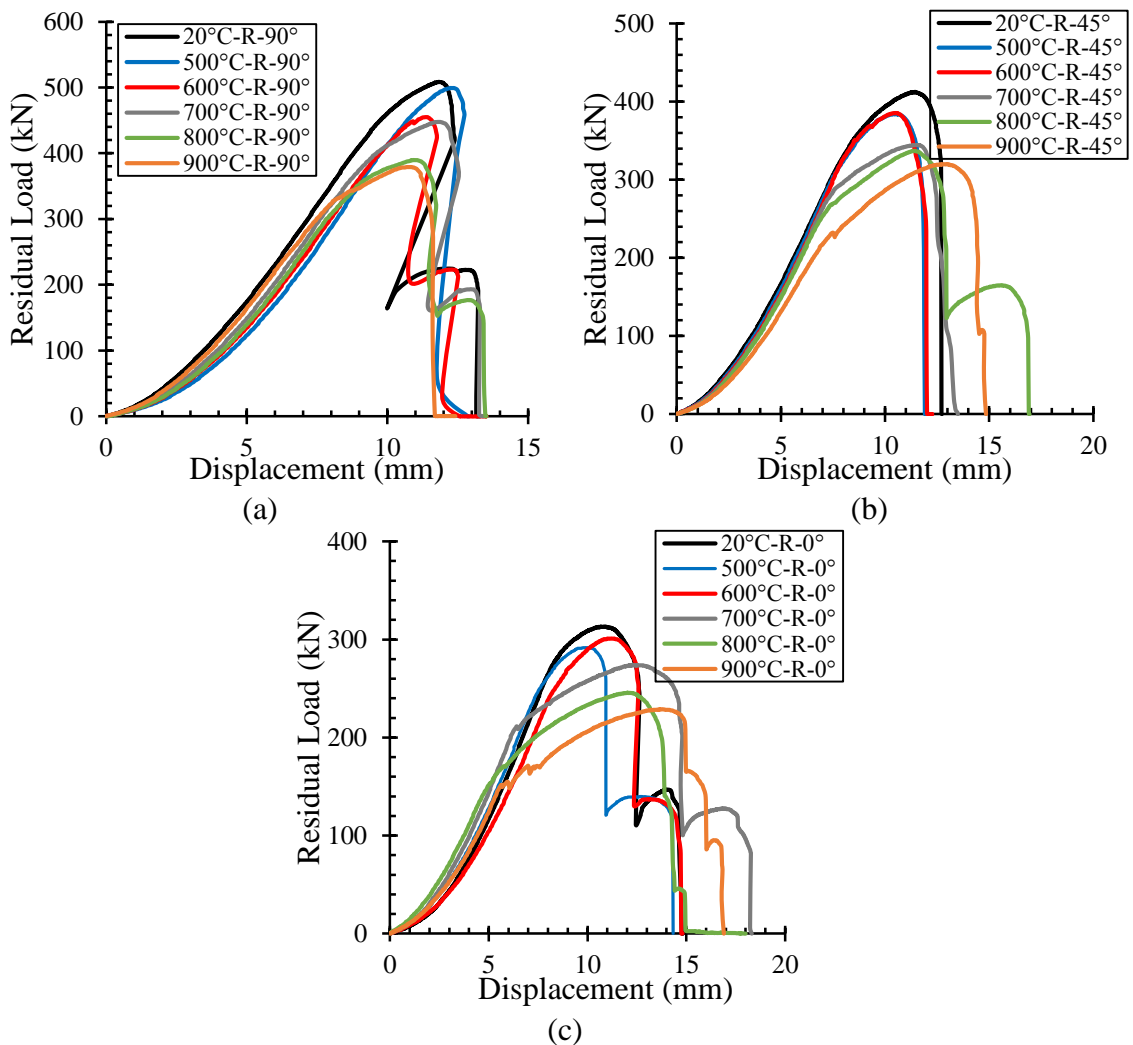


Fig. 62. Residual load-displacement response of welded lap joint: (a) Transverse, (b) inclined, (c) Longitudinal

Figure 63 represents the variation of the percentage decrease or reduction in the ultimate strength of the fillet weld materials post fire analysis while considering the three different load angles. It can be seen that the strength of the fillet weld for all load angles decreases when the targeted temperature of the post-fire test increases. Table 12 illustrates the maximum peak loads for the three welded lap joints as well as the percentage decrease in the weld material strength obtained from the post-fire analysis. It can be seen from Fig. 63 and Table 12 that the reduction in fillet welds strength reaches around 25%, 22%, and 27% of the initial strength as subjected to 0°, 45°, and 90° load angles, respectively, after they were exposed to 900°C post-fire analysis. These percentages are significant and should be considered in fire design application of steel structures. That is, welds and welded connections in steel structures that were exposed to fire should be redesigned to resist gravity loads that are less than 70% of their initial capacities.

Figure 63 shows that the effect of load angles on the strength reduction of fillet weld is not that significant. However, for temperatures beyond 750°C, the longitudinal and transverse welded lap joints undergo a larger reduction in strength when compared with the inclined ones. In order to consider the residual strength capacity in post-fire design application of welds and welded connections, an envelope that represents the maximum reduction in strength (%) among the three welded lap joints is generated as shown in Fig. 63. This envelope can be represented by a linear variation between the reduction in weld strength (%*r*) and temperature *T*(°C) as follows where *T* is ranging from 500°C to 900°C:

$$\%r = 0.053T - 20 \quad (38)$$

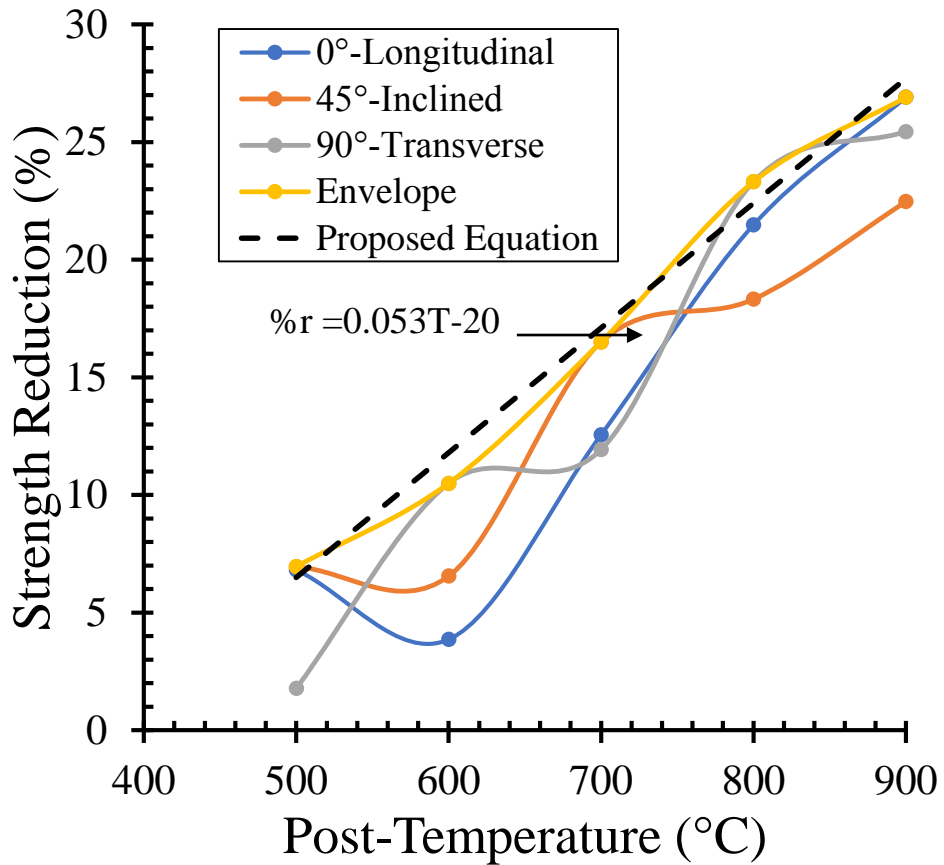


Fig. 63. Percentage decrease for the three welded lap joints after exposed to elevated temperatures

Table 12. Weld strength reduction after exposed to elevated temperatures

Test Name	Temperature (°C)	Angle (°)	Peak Load (kN)	Strength Reduction (%)
20°C-R-90°	20	90	508.26	-
500°C-R-90°	500	90	499.24	1.77
600°C-R-90°	600	90	454.93	10.49
700°C-R-90°	700	90	447.62	11.93
800°C-R-90°	800	90	389.77	23.31
900°C-R-90°	900	90	378.94	25.44
20°C-R-45°	20	45	412.8	-

500°C-R-45°	500	45	384.11	6.95
600°C-R-45°	600	45	385.75	6.55
700°C-R-45°	700	45	344.66	16.51
800°C-R-45°	800	45	337.16	18.32
900°C-R-45	900	45	320.05	22.47
20°C-R-0°	20	0	313.1	-
500°C-R-0°	500	0	291.77	6.81
600°C-R-0°	600	0	301.02	3.86
700°C-R-0°	700	0	273.78	12.56
800°C-R-0°	800	0	245.84	21.48
900°C-R-0°	900	0	228.86	26.91

4. Effect of Load Angle on the Residual Behavior of Fillet Welds

At ambient temperature, the weld material is highly dependent on the angle between the weld axis and the line of action of the applied load. That means, the weld strength is greater when subjected to higher load angle until it reaches its maximum weld strength at a load angle of 90° [13, 48]. However, for non-destructive steel structures, weld material properties can change after heating-cooling cycle exposure. This due to the fact that the chemical composition transformation and metal structure of the base material and weld materials are influenced by the exposed targeted temperature during and after fire event. To address the effect of load angle on the residual response of fillet weld materials, residual load-displacement characteristics for the three welded lap joint configurations at each post-temperature are presented in Fig. 64. It can be seen that, the residual ultimate strength of the weld material decreases as temperature

increases. Also, higher load angle results in a higher residual strength for all post-fire analysis.

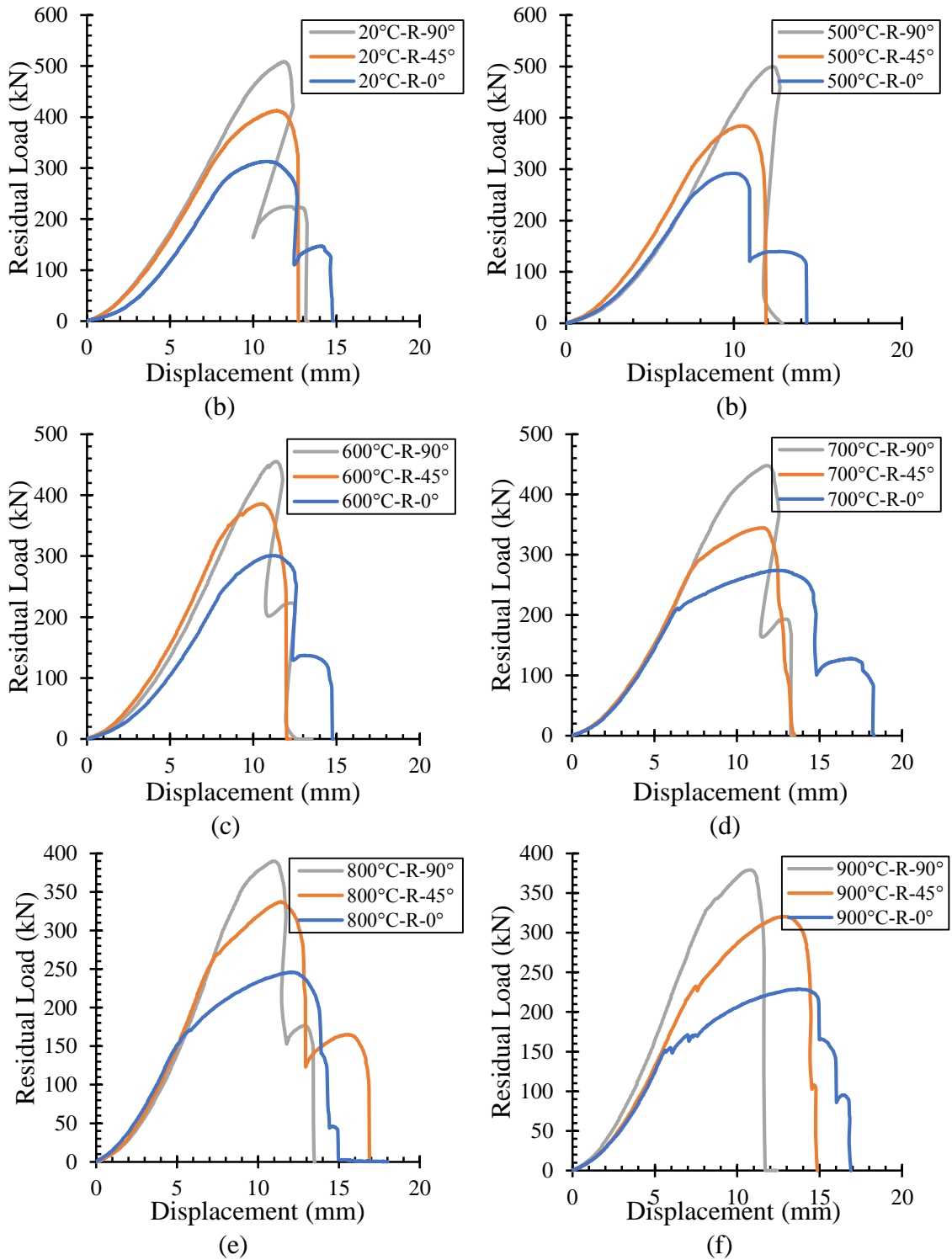


Fig. 64. Residual load-displacement response of the three welded lap joint after exposed to elevated temperatures

To investigate the effect of load angle on the residual ultimate strength of the fillet weld, a load angle effectiveness ratio was calculated. The load angle effectiveness ratio can be calculated by dividing the ultimate residual capacity of the transverse and inclined welded lap joints to that of the longitudinal after exposing to the same post-fire temperature. This is because the load angle effectiveness ratio provide in the ANSI/AISC 360 [13] $(1.0 + 0.5 \sin^{1.5} \theta)$ is 1, 1.5 and 1.29 for longitudinal, transverse and inclined-45°, respectively. Figure 65 represents the variation of load angle effectiveness ratio for transverse and inclined welded lap joints versus post-fire temperature against those provided by ANSI/AISC 360 [13]. It can be seen that for transverse weld lap joints, the ANSI/AISC 360 [13] results are considered conservative for all post-fire temperatures. However, for the inclined ones, the ANSI/AISC 360 [13] is slightly less conservative at 700°C and 800°C. That means, the load angle effectiveness ratio provided at ambient temperature as per ANSI/AISC 360 [13] is still applicable while considering the %*r* factor in calculating the residual capacity of welds as follows:

$$(R_{nw})_{PT} = (1 - \%r) 0.60 F_{EXX} A_{we} (1.0 + 0.5 \sin^{1.5} \theta) \quad (39)$$

Where $(R_{nw})_{PT}$ is the nominal weld strength after post-temperature (*PT*) analysis, F_{EXX} is the filler metal strength, A_{we} is the effective area of the weld, $(1.0 + 0.5 \sin^{1.5} \theta)$ represents the effect of load angle (θ) on the strength capacity of fillet weld material, and %*r* is the percentage decrease as defined in Eq. 38.

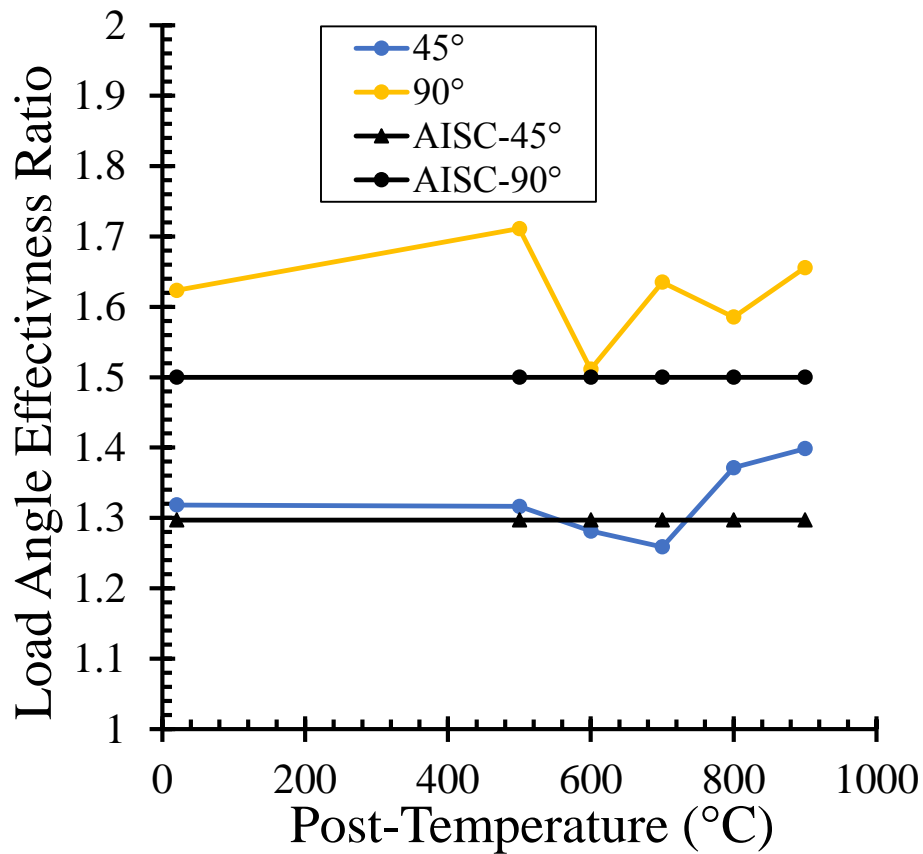


Fig. 65. Load angle effectiveness ratio versus post-temperature

5. Residual Ductility of the Welded Lap Joints

At ambient temperature, the ductility of welds is highly dependent on the angle between the axis of the weld and the line of action of the applied load. That is, larger load angle results in less ductility for the welded lap joints. However, during and after fire temperatures exposure, the behavior of welds becomes more complex and the effect of heating and cooling phases can affect the ductility of the welded lap joints after fire. In order to compare the ductility of the welded lap joints while considering different load angles, normalized ductility can be computed as follows:

$$\phi = \frac{A}{PL} \tag{40}$$

Where ϕ is the normalized ductility, A is the area under residual load displacements curve, P is the residual peak load predicted for each test, and L is total length of the specimen (1460 mm). Figure 66 represents the variation of the normalized ductility for the welded lap joints after subjected to post-fire analysis. It can be seen that the normalized ductility of longitudinal welded lap joints is larger than that of the inclined and transverse welded lap joints at ambient and post-fire temperatures. Also, the inclined welded lap joint gains more ductility than that of the transverse welded lap joint for all tests. In addition, it can be seen that as the welded lap joint is exposed to temperatures larger than 600 °C and then cooled back to ambient, the fillet weld material gains more ductility than that at ambient for all load angles. The relation between the weld strength and weld ductility as the applied load angle is changing can be studied through Fig. 67. It can be seen that as the load angle between the weld axis and the applied load is decreasing from 90° to 0°, the strength decreases and ductility increases.

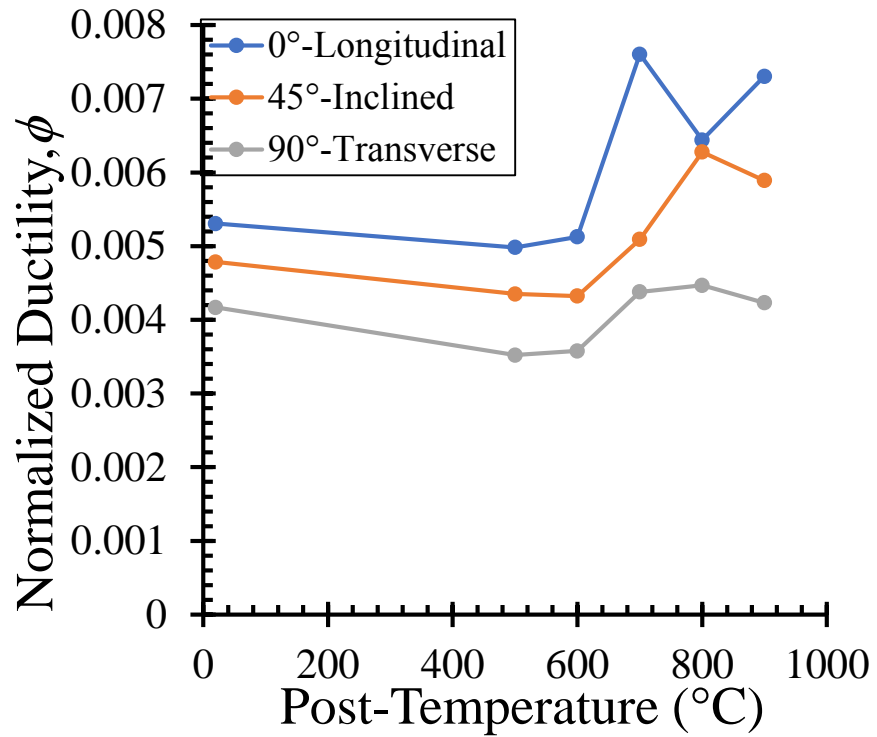


Fig. 66. Post-fire normalized ductility of fillet weld after subjected to different load angles

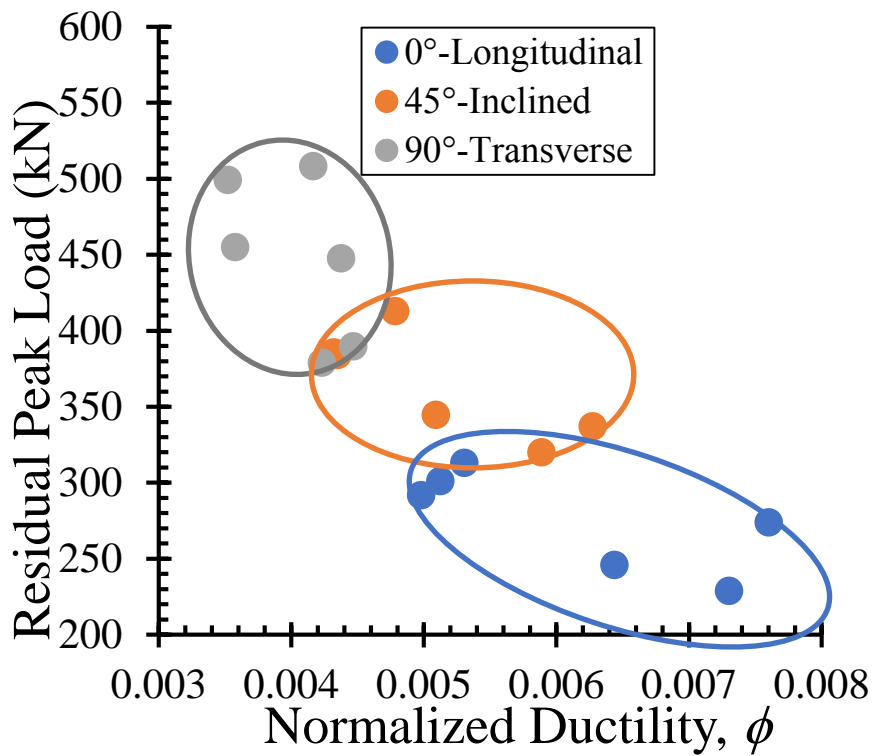
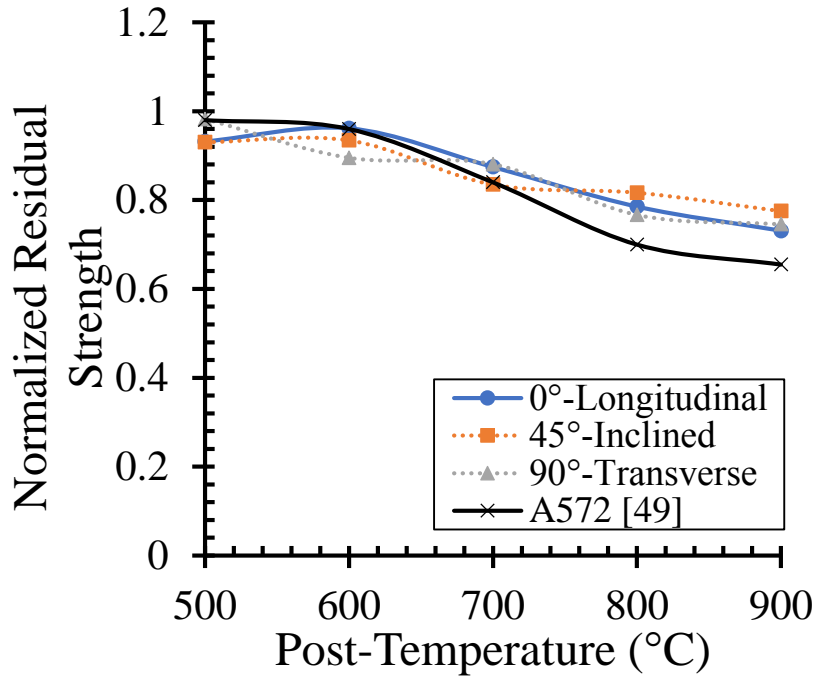


Fig. 67. Residual peak load against post-fire normalized ductility

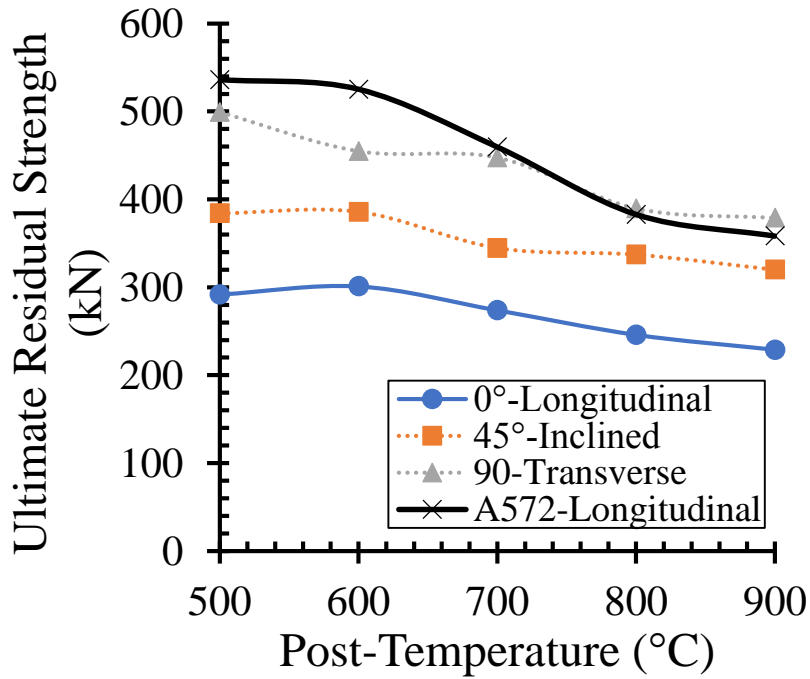
6. Residual Response of the Weld Material versus the Steel Base Material

The three welded lap joint configurations were designed to fail in the weld region. When the welded specimens are subjected to heating-cooling cycle, the material properties and metal structure for both materials change. For a welded steel connection either weld or the steel base material can govern the post-fire failure modes of the connection after fire exposure. To address this issue, the normalized residual strength for the steel base material used in this study (S355 or ASTM A572) obtained from experimental program conducted by Aziz and Kodur [49] were compared with those predicted for the fillet weld material as shown in Fig. 68 (a). The normalized residual strength can be computed by dividing the residual ultimate strength at different post-elevated temperatures to that at ambient temperature. It can be seen in Fig. 68 (a), the residual normalized strength of the S355 (ASTM A572) is less than that of those obtained for the longitudinal, transverse, and inclined fillet welds for temperatures beyond 600°C, 670°C, 700°C, respectively. This indicates that, after fire exposure, the steel base material experiences greater strength degradation than that of welds especially for temperatures larger than 600°C. However, the failure mode was governed by the weld material rather than by the steel base material. In order to investigate the governed failure mode of the lap joints, the residual ultimate strength capacities of the steel base material of the longitudinal lap joints were calculated and compared to those obtained from the experimental tests as shown in Fig. 68(b). The longitudinal lap joint steel base material ultimate capacities were calculated rather than the inclined and transverse, since the upper and bottom plates of the longitudinal lap joint have the smallest cross-section area among the plates in the other lap joints. Figure 68 shows that although the normalized residual strength of the steel base material is less than those of

the welds (Fig. 68(a)), the residual ultimate strength of the steel base metal is larger than that of the weld materials. This proves that the failure mode remains in the weld throat.



(a)



(b)

Fig. 68. Residual behavior of fillet material versus steel base material: (a) Normalized residual strength, (b) Ultimate residual strength

CHAPTER VI

SUMMARY AND CONCLUSIONS

Key results of an extensive experimental study on the time-dependent and post-fire behavior of fillet welds when subjected to elevated temperatures due to fire were presented. Steady-state temperature tests were performed at different loading rates to implicitly examine the time-dependent behavior of weld material in transverse welded lap joints. However for the explicit creep tests, critical times, loads, and temperatures at which welds can fail due to creep effect were investigated and determined. Based on the experimental creep curves resulted as part of this research work, two creep models for fillet welds and steel base material were proposed to predict the thermal creep behavior of transverse welded lap joints in fire. Another experimental program was conducted to further investigate the rate-dependent and post-fire behavior of equal-leg fillet welds as subjected to different load angles.

For the “*implicit creep tests*”, the experimental results showed that all transverse welded lap joints failed due to fracture through the weld. Also, it was observed that when welded specimens were subjected to temperatures greater than approximately 500°C, the weld load-deformation behavior showed greater ductility than at lower temperatures.

The experimental results also showed that the loading rate had a significant effect on the strength of the weld test specimens for temperatures higher than about 450°C and becomes more pronounced for higher temperatures. More specifically, the slow loading rate specimens showed peak strengths that were 11% to 29% less than the strength obtained from the fast tests as temperature increases from 475°C to 700°C.

This indicates that, the failure of welded connections due to fire temperatures does not only depend on the applied loads and temperatures, but also on the rate at which the load is applied.

Retention factors for the transverse welded specimens subjected to fast and slow test scenarios at ambient and elevated temperatures were computed and compared with Eurocode 3 [10] and another weld study [22] available in the literature. The results indicated that higher retention factors are obtained from faster applied loads.

For the “*explicit creep tests*”, the experimental results showed that the creep of weld material has a large impact on the welded connections for temperatures greater than 450°C and becomes more prominent for larger elevated temperatures. More specifically, for temperatures larger than 450°C, the transverse welded lap joint starts to undergo excessive deformation due to creep and failed at earlier stages as load and temperature increase.

The results showed that the welded specimen can sustain a load up to 80% of the peak load predicted in the fast temperature test at 500 °C for 120 min time duration. However for 90% of the peak load, failure in welds occurs after *2 min and 51 sec* from the beginning of the creep test. Nevertheless, for higher temperatures (600°C and 700°C) the transverse welded lap joint cannot resist a load more than 50% of the corresponding temperature peak load for 120 min time duration. Also, the results showed that as the load ratio increases, failure occurs in the welds more rapidly.

The isochronous curves showed that for temperatures where the creep effect is not that significant, the stress level can dominate the time-dependent response of transverse welded lap joint. However, for larger temperatures, the effect of temperature

dominates the creep response of the welds or the steel base material due to higher activation of atoms mobility.

The creep curves of a welded connection were compared with the classical one of a steel base material. The results showed that, for temperatures or loads where creep is unlikely to occur, each connection component tends to creep separately. However, for conditions where creep is significant, the connection components act as one unit and having explicitly three stages of a classical creep curve.

A “*creep model*” based on time-hardening *Norton-Bailey* creep power law equation is proposed to predict the three stages of creep behavior of the transverse welded lap joints. The results showed that the proposed creep model for the lap joint matches with reasonable accuracy the experimental creep curves. Also, the creep model is very sensitive where the creep constants are temperature-dependent only. Tertiary stage of the creep curve was also predicted and it is highly dependent on the failure time. More data are still needed to develop a more general creep model capable of predicting the tertiary part of the creep curves under different load ratios and temperatures.

FE simulations predict with reasonable accuracy the load-connection displacement response and creep behavior of the transverse welded lap joints as subjected to elevated temperatures. For the time-independent tests, the FE simulations and experimental results showed that shear fracture occurred at the throat of the weld for all test specimens. For the time-dependent FE analysis, the results showed that the proposed creep models used for the welds and steel base material in the welded lap joint model predict with reasonable accuracy the experimental creep curves. Fields and Fields creep model [38] was also incorporated in the analysis to be compared with the

proposed steel base material creep model. The results showed that the proposed creep model for the base material can predict more accurately the creep behavior of the transverse weld lap joint than using Fields and Fields model. Fracture modeling was not included in the simulations and the FE models were not capable to predict the tertiary part of the creep curve.

The creep models for the welds and steel base material were based on the experimental tests conducted previously as part of this research. Although the creep models for the welds and steel base material provided in this research work predict the creep behavior of the welded connection, they are still limited. More creep tests should be tested and repeated at least three times to have more accurate creep models. Also, more tests under a wider range of temperatures and stress levels should be tested to develop a more general creep model.

For the “*rate-dependent behavior of fillet welds as subjected to various load angles*”, the experimental results showed that all welded specimens failed in the weld material at ambient and elevated temperatures. More specifically, the transverse and longitudinal welded lap joints failed at the throat of the weld at ambient and elevated temperatures under both fast and slow loading rates. However, for the inclined welded connection, the failure occurred at the throat of the weld for all tests conducted at fast loading rate. Whereas for slow loading rate tests, the failure mode shifted from the weld throat to a fracture surface near the toe of the weld for temperatures larger than 500°C.

The experimental results showed that the behavior of fillet weld is highly dependent on load angle, loading rate, and temperature. That is, as the load angle increases, the fillet weld strength increases for all temperatures and loading rates. Also, the effect of loading rate is significant for temperatures larger than 400°C and becomes

severely significant at higher temperatures. At temperature of 700°C and for slow loading rate (0.1 mm/min), the effect of loading rate drops around 40 %, 37%, and 29% in strength capacities for transverse, inclined, and longitudinal welded lap joints, respectively. This indicated that the creep behavior of welds is not only dependent on material properties, time, stress, and temperature, but also on the angle at which the load is applied.

The experimental results also showed that the loading rate and load angle affect the ductility of welds in welded lap joints when subject to high temperatures. The results showed that the ductility of the weld material increases with the increase of temperature especially for temperatures larger than 500°C. Also, the effect of loading rate on the ductility of welds is significant for longitudinal and transverse welded lap joints for temperatures larger than 500°C and 600°C, respectively. However, for the inclined lap joint there is no effect of loading rate on ductility of the weld material.

Retention factors for the fillet weld material subjected to different loading rates and angles at elevated temperatures were computed and compared to the ones available in Eurocode 3 [10] and Conlon [22]. The results showed that the higher retention factors were obtained from tests conducted with faster loading rate. Also, the maximum retention factors were obtained for the inclined welded lap joints at both fast and slow loading rates, whereas the least ones were obtained for longitudinal welded lap joints.

For the “*post-fire analysis*”, the experimental results showed that all welded specimens failed at the throat of the weld material at ambient and post-elevated temperatures. The exposed surfaces of the welded lap joints exhibited a change in surface textures and colors from brown color at 500°C to gray color at 900°C. This change in color can play an important in detecting and investigating the steel

temperatures in a non-destructive steel structures for repair purposes. However, the color and texture of the weld fracture surfaces slightly changes as the targeted temperature increases.

The results showed that the residual peak loads for the three welded lap joints decreases as the targeted temperature of the post-fire analysis increases. More specifically, the reduction in fillet welds strength reaches around 25%, 22%, and 27% of the initial strength as subjected to 0° , 45° , and 90° load angles and after exposed to 900°C post-fire analysis. This reduction in strength should be considered in designing steel structures that are highly exposed to fire such as industrial buildings and offshore structures.

The results showed that the effect of load angles on the strength reduction of fillet weld is not significant. Also, the load angle effectiveness ratio provided by the ANSI/AISC 360 [13] is considered to be conservative for all post-fire analysis.

The results also showed that the normalized ductility of longitudinal welded lap joints is larger than that of the inclined and transverse welded lap joint at ambient and post-fire temperatures. Whereas the inclined welded lap joint gains more ductility than that of the transverse welded lap joint for all tests. In addition, fillet weld material gains more ductility than that at ambient for all load angles for post-temperatures larger than 600°C .

The relation between the weld strength and weld ductility while considering different load angles was also studied. The results showed that as the load angle between the weld axis and the applied load is decreasing from 90° to 0° , the strength decreases and ductility increases.

CHAPTER VII

SIGNIFICANCE, LIMITATIONS, AND FUTURE WORK

A. Significance

Unlike the Eurocode 3 [10], the ANSI/AISC 360 [13] Appendix 4 did not include till now the retention factors for welds due to the lack of experimental data on elevated temperature properties of welds that made using typical U.S. welding process and procedures. To address this knowledge gap, an extensive experimental program was performed on the welded lap joints to investigate their performance when exposed to fire temperatures including time rate effects. As a result, retention factors for welds under different loading rates, load angles and temperatures were proposed. These retention factors can be used to develop design guidelines of welded connections for structural-fire engineering application. Furthermore, time effect due to creep can dominate the weld performance as exposed to fire. Therefore, this proposed research study provides time-dependent mechanical properties of weld materials and a creep model for predicting the real performance of welded steel connections in fire. Finally, steel in general loses its strength after a heating-cooling cycle of a real fire and, in many cases, steel structures can be reused after fire events. Therefore, a deep understanding of the post-fire residual capacities of welded connections was provided to ensure safe design of welded connections during and after fire exposure. Design equations for weld material strength capacities as subjected to different load angles were provided for time-dependent thermal conditions and post-fire analysis.

B. Limitations

This study is considered to be a preliminary step towards the goal of a more complete understanding the time-dependent and post-fire behavior of fillet welds in welded connections subjected to fire temperatures. Although a significant number of specimens were tested in this study, the specimens had small and short fillet welds. Larger and longer fillet weld joints used in actual structures or large connections are needed to be tested in future research. Also, limited loading rates were chosen arbitrary to examine the effect of loading rates on the weld behavior when exposed to elevated temperatures. This assumption is based on the fact that in real fire, unexpected induced forces can be developed in welded connections due to different fire-time exposures. This study provides an overview of the effect of implicit creep on the strength capacity of welded lap joints when exposed to different fire loadings. The retention factors proposed in this study for slow tests showed to be more conservative than those provided by the Eurocode [10] and Conlon [22]. Also, using these retention factors in designing welded connections exposed to elevated temperatures can result in a safe design more than those available in the literature. However, more loading rates are still needed to be tested to develop a general fire-design procedure for welded connections while considering the effect of time or rates. Regarding the creep tests, more tests are needed to be conducted while considering different material types, loading angles, welding electrodes, welding processes. Also, more general creep models for fillet welds and steel base materials taking into account different geometric and material properties are still needed. For the post-fire analysis, this research work was limited to one cooling regime where the specimen is cooled back to ambient in the furnace without any direct exposure to air or water. Therefore, future work is needed to study the residual

responses of large-scale welded connections having different weld geometry, weld type, welding electrodes, weld processes, and steel base materials under a larger spectrum of targeted temperatures and cooling regimes. Generally, future tests should be repeated at least three times to accurately understand more the time-dependent and post-fire behavior of fillet welds and welded connections in fire.

C. Future Work

For a more complete understanding of the time-dependent and post-fire behavior of steel welded connections subjected to fire temperatures, future work should cover the following topics:

- 1- Time-dependent behavior of all welded material specimens subjected to elevated temperatures:
 - a. An experimental program can be conducted to examine the implicit and explicit creep behavior of all welded material specimens as exposed to elevated temperatures.
 - b. The all welded material specimens are composed of only weld material (E7018) and can be machined like coupon test specimens.
 - c. In order to investigate implicitly the creep behavior of the weld material at elevated temperatures, three different loading rates (fast, moderate, and slow) can be used. Time-dependent stress strain curves, peak loads “ P ”, and time-dependent retention factors for the weld material under different loading rates can be presented. These results can be used to develop an implicit time-dependent fracture model.

- d. For explicit creep tests, the all welded material specimens will be subjected to a constant load at a specific temperature for 120 min or until fracture. More specifically, creep tests will be conducted under wide range of temperatures ranging from 400°C to 900°C with 50°C under different constant peak loads (predicted from the fast tests) ranging from 0.5P to 0.9P with 0.1P increment. In this analysis, critical times, loads, temperatures at which welds can fail due to creep will presented and specified.
- e. The results obtained from the creep tests can be used to develop a creep model for the E7018 weld material. This creep model will be capable of predicting the three stages of the creep curves.

2- Investigation on some major parameters on time-dependent and post-fire behavior of fillet welds exposed to fire:

Same analysis that were discussed throughout this research work can be applied to investigate some major parameters that influence the time-dependent and post-fire behavior of welds when exposed to fire. Such parameters are as follows:

- a. Weld geometry: different fillet weld size and length.
- b. Weld type: Butt welds, slot welds, and plug welds.
- c. Welding electrodes: E60XX, E80XX, E100XX, or E110XX.
- d. Weld processes: Gas metal arc welding (GMAW), submerged arc welding (SAW), and flux cored arc welding (FCAW).
- e. Steel base materials: steel materials other than ASTM A529 or S355.

- f. All these aforementioned parameters can be tested under a large spectrum of temperatures, loading rates, and cooling regimes.
- 3- Time-dependent and post-fire behavior of large-scale steel welded connections exposed to fire temperatures:
- a. Experimental program can be conducted on large-scale welded connections (such as shear tab welded connection, top and seat welded connection, beam-column welded connection, or beam to beam welded connection (splice)) to investigate their time-dependent and post-fire behavior during and after exposed to fire temperatures.
 - b. Experimental program can be conducted to investigate implicitly the creep behavior of the large-scale welded connections by applying different loading rates.
 - c. Experimental program can be conducted to investigate explicitly the creep behavior of the large-scale welded connections. These tests can be performed by applying different constant loads and temperatures and the only variable is time.
 - d. Experimental program can be conducted to investigate the post-fire behavior of the large-scale welded connections after exposed to elevated temperatures. The large-scale welded connection can be exposed to elevated temperatures ranging from 500°C to 900°C and then cooled down to ambient before loading until failure.

BIBLIOGRAPHY

- [1] Kodur VK, Garlock M, Iwankiw N. Structures in fire: state-of-the-art, research and training needs. *Fire Technology*. 2012;48(4):825-839.
- [2] Chicchi R, Varma AH. Research review: Post-earthquake fire assessment of steel buildings in the United States. *Advances in Structural Engineering*. 2018;21(1):138-154.
- [3] National Research Council. Making the nation safe from fire: A path forward in research. National Academies Press; 2003 Sep 15.
- [4] McAllister T, Corley G, editors. World Trade Center Building performance study: Data collection, preliminary observations, and recommendations. Diane Publishing Company; 2002.
- [5] Grosshandler WL, Grosshandler W. Fire resistance determination and performance prediction research needs workshop: proceedings. US Department of Commerce, Technology Administration, National Institute of Standards and Technology; 2002 Sep 1.
- [6] National Institute of Standards, Technology (US). Final report on the collapse of the World Trade Center towers. US Department of Commerce, Technology Administration, National Institute of Standards and Technology; 2005 (Vol.13).
- [7] Wang W, Wang K, Kodur V, Wang B. Mechanical properties of high-strength Q690 steel at elevated temperature. *Journal of Materials in Civil Engineering*. 2018;30(5):04018062.
- [8] Boresi AP, Schmidt RJ. *Advanced Mechanics of Materials*. Wiley, New York, 2003.

- [9] Toric N, Harapin A, Boko I, Peroš B, Ban M. Modelling of the influence of creep strains on the fire response of steel elements. *Applications of Structural Fire Engineering*. 2013.
- [10] European Committee for Standardization (CEN), Eurocode 3: Design of Steel Structures- Part 1–8: Design of Joints and Building Frames, 2005 (BS EN 1993-1-8, Brussels).
- [11] Kirby BR, Preston RR. High temperature properties of hot-rolled, structural steels for use in fire engineering design studies. *Fire safety journal*. 1988;13(1):27-37.
- [12] Cooke GM. An introduction to the mechanical properties of structural steel at elevated temperatures. *Fire safety journal*. 1988;13(1):45-54.
- [13] ANSI/AISC 360 (2016), Specification for structural steel buildings. American Institute of Steel Construction 360-16, Chicago.
- [14] Toric N, Sun RR, Burgess IW. Creep-free fire analysis of steel structures with Eurocode 3 material model. *Journal of Structural Fire Engineering*. 2016;7(3):234-248.
- [15] Daryan AS, Yahyai M. Behaviour of welded top-seat angle connections exposed to fire. *Fire safety journal*. 2009;44(4):603-611.
- [16] Selden KL, Fischer EC, Varma AH. Advanced fire testing of a composite beam with shear tab connections. In *Structures Congress 2014*, 2014 (pp. 1170-1174).
- [17] Hosseini SA, Zeinoddini M, Saedi Daryan A, Rahbari M. Model fire tests on a beam- to- leg connection in an offshore platform topside. *Fire and materials*. 2014;38(5):529-549.
- [18] Latham D J and Kirby BR. Elevated temperature behavior of welded joints in structural steels. Report EUR 17855 EN, European Commission – Technical Steel Research, ECSC Agreement No. 7210.SA/824. 1998.

- [19] Twilt L. The new Eurocode on fire design of steel structures. In Proceedings of the International Seminar on Steel Structures in Fire, Shanghai, People's Republic of China 2001 Nov 1 (pp. 241-54).
- [20] Ufuah E, Ikhayere J. Elevated temperature mechanical properties of butt-welded connections made with high strength steel grades S355 and S460M. In Design, fabrication and economy of metal structures 2013 (pp. 407-412). Springer, Berlin, Heidelberg.
- [21] Rezaeian A, Keshavarz M, Hajjari E. Mechanical properties of steel welds at elevated temperatures. *Journal of Constructional Steel Research*. 2020;167:105853.
- [22] Conlon KA. Strength of transverse fillet welds at elevated and post-elevated temperatures (MSc Dissertation). Lehigh University; 2009 Jun.
- [23] Zhang G, Zhu MC, Kodur V, Li GQ. Behavior of welded connections after exposure to elevated temperature. *Journal of Constructional Steel Research*. 2017;130:88-95.
- [24] Hanus F, Zilli G, Franssen JM. Experimental tests and analytical models for welds and grade 8.8 bolts under heating and subsequent cooling. *Journal of Structural Fire Engineering*. 2011; 2(3):181-194.
- [25] Liu H, Liao X, Chen Z, Huang SS. Post-fire residual mechanical properties of steel butt weld—Experimental study. *Journal of Constructional Steel Research*. 2017;129:156-162.
- [26] Luecke WE, McColskey JD, McCowan CN, Banovic SW, Fields RJ, Foecke T, Siewert TA, Gayle FW. Federal building and fire safety investigation of the world trade center disaster: Mechanical properties of structural steels. Technical Rep. No. NCSTAR 1-3D. Gaithersburg, MD: National Institute of Standards and Technology. 2005.

- [27] Hu G, Morovat MA, Lee J, Schell E, Engelhardt M. Elevated temperature properties of ASTM A992 steel. In Structures Congress 2009: Don't Mess with Structural Engineers: Expanding Our Role 2009 (pp. 1-10).
- [28] Seif M, Choe L, Gross J, Luecke W, Main J, McColskey D, Sadek F, Weigand J, Zhang C. Temperature-dependent material modeling for structural steels: formulation and application. US Department of Commerce, National Institute of Standards and Technology; 2016 Apr 15.
- [29] Harmathy T, Stanzak W. Elevated-temperature tensile and creep properties of some structural and prestressing steels. In Fire test performance 1970 Jan. ASTM International.
- [30] Knight DC, Skinner DH, Lay MG. Prediction of isothermal creep. BHP; 1971.
- [31] Skinner DH. Determination of High-Temperature Properties of Steel. BHP Tech. Bull.. 1972;16(2):10-21.
- [32] Fujimoto M, Furumura F, Ave T, Shinohara Y. Primary creep of structural steel (SS 41) at high temperatures. Transactions of the Architectural Institute of Japan. 1980;296:145-157.
- [33] Fujimoto M, Furumura F, Ave T. Primary creep of structural steel (SM 50 A) at high temperatures. Transactions of the Architectural Institute of Japan. 1981;306:148-156.
- [34] Fujimoto M, Furumura F, Ave T. Primary creep of structural steel (SM 58Q) at high temperatures. Transactions of the Architectural Institute of Japan. 1982;319:147-155.

- [35] Morovat MA, Lee JW, Engelhardt MD, Taleff EM, Helwig TA, Segrest VA. Creep properties of ASTM A992 steel at elevated temperatures. In *Advanced Materials Research 2012* (Vol. 446, pp. 786-792). Trans Tech Publications Ltd.
- [36] Kodur VK, Aziz EM. Effect of temperature on creep in ASTM A572 high-strength low-alloy steels. *Materials and Structures*. 2015;48(6):1669-1677.
- [37] Harmathy TZ. A comprehensive creep model. *Journal of Basic Engineering Trans. ASME* 1967;89(3):496-502.
- [38] Fields BA, Fields RJ. *Elevated Temperature Deformation of Structural Steel: Report NISTIR 88-3899*. NIST, Gaithersburg, MD. 1989.
- [39] Norton FH. *The creep of steel at high temperatures*. McGraw-Hill Book Company, Incorporated; 1929.
- [40] Luecke WE, McColskey JD, McCowan CN, Banovic SW, Fields RJ, Foecke T, Siewert TA, Gayle FW, Gutierrez CM. *Federal building and fire safety investigation of the World Trade Center disaster mechanical properties of structural steels (draft)*. (2005).
- [41] Naumenko K, Altenbach H. *Modeling of creep for structural analysis*. Springer Science & Business Media; 2007 Apr 6.
- [42] ABAQUS version 6.14 [Computer software]. Dassault Systemes, Waltham, MA.
- [43] AWS, *Specification for carbon steel electrodes for shielded metal arc welding, AWS A5.1/A5.1M*, (2012) American Welding Society. Doral, Florida.
- [44] Morovat MA, El Ghor AH, Hantouche EG. Time-dependent response of flush endplate connections to fire temperatures. *Journal of Structural Engineering*. 2018;144(4):04018023.

[45] May DL, Gordon AP, Segletes DS. The application of the Norton-Bailey law for creep prediction through power law regression. In ASME Turbo Expo 2013: Turbine Technical Conference and Exposition 2013 Jun 3. American Society of Mechanical Engineers Digital Collection.

[46] AISC (2011), Steel Construction Manual, 14th Edition, American Institute of Steel Construction, Chicago, IL.

[47] Buchanan AH, Abu AK. Structural design for fire safety. John Wiley & Sons; 2017 Jan 30.

[48] Deng K, Grondin GY, Driver RG. Effect of loading angle on the behavior of fillet welds. Department of Civil and Environmental Engineering, University of Alberta; 2003 Jun.

[49] Aziz EM, Kodur VK. Effect of temperature and cooling regime on mechanical properties of high- strength low- alloy steel. Fire and Materials. 2016;40(7):926-939.

